GEOLOGY OF THE DRIPPING SPRINGS VALLEY CHABAZITE AND RELATED ZEOLITE DEPOSITS, SOUTHEAST ARIZONA AND SOUTHWEST NEW MEXICO

by

Mark R. Bowie

Submitted in Partial Fulfillment of the
Requirements for the Degree of
Master of Science

New Mexico Institute of Mining and Technology
Socorro, New Mexico 87801

May 1985

ABSTRACT

The Dripping Springs Valley (DSV) chabazite deposit is one of several potentially economic zeolite deposits which formed in a series of late Cenozoic closed basins extending from the Tonto Basin in southeast Arizona through Buckhorn in southwest New Mexico. Zeolitization in this system resulted from reaction of vitric ash with saline, alkaline-lake waters. The sedimentologic and mineralogic characteristics of the zeolite deposits at Tonto Basin, Bear Springs, and Bowie, Arizona, and near Buckhorn, New Mexico, are similar to those of DSV.

At least 10 ash-fall tuffs underlie approximately 16.1 km^2 (10 mi^2) of epiclastic-fluvial and lacustrine sediment within DSV, about 37 km (23 mi) south of Globe, Gila County, Arizona. X-ray diffraction (XRD) data indicate at least five of the tuffs have been inhomogeneously altered, predominantly to chabazite. The main zeolite tuff horizon ranges from an unaltered vitric tuff at the north end of the deposit to 90% chabazite at the south end. Scanning electron microscopy reveals that the chabazite occurs as "cubes" or "rhombs" ranging from much less than one micrometer up to two micrometers on a side. The crystals are isolated or occur as intergrown clusters or radial stringers. The tuffs also contain trace to abundant fresh glass, quartz, calcite, dolomite, feldspars, evaporite minerals, mafic minerals, and clay minerals. Southerly- and southeasterly-flowing paleochannels have eroded large portions of the tuffs.

Semi-quantitative XRD analyses of the less-than-two micron size fraction of the DSV lacustrine and alluvial facies indicate that they consist of discrete illite, mixed-layer illite/smectite, chlorite, sodium smectite, and kaolinite, in decreasing order of abundance. The clays are dominantly of detrital origin, but minor discrete illite, mixed-layer illite/smectite, and sodium smectite have formed authigenically.

The DSV ash beds probably are of rhyolitic parentage. X-ray fluorescence spectrometry of bulk zeolitic-tuff samples indicates that zeolitization of fresh rhyolitic tuff resulted in an enrichment of Al_2O_3, MgO, CaO, and H_2O, and a depletion of SiO_2 and K_2O. Na_2O was enriched in some tuffs but depleted in others.

Paragenetic sequences of fresh glass --> chabazite, and fresh glass --> smectite (and/or mixed-layer illite/smectite) --> chabazite are observed in the DSV zeolitic tuffs. The mineralogic similarities of all the tuffs suggest similar geochemical conditions were prevalent throughout their deposition. Chabazite precipitated after dissolution of rhyolitic glass by moderately saline and alkaline pore fluids, presumably when the H^+:alkali ion activity ratio decreased below the level for montmorillonite crystallization. These solutions were relatively silica-poor, had a high activity of H_2O, and a low K^+:$Na^+ + Ca^{+2} + Mg^{+2}$ activity ratio. These conditions favored the formation of chabazite over potassium feldspar as well as other zeolites, such as clinoptilolite, erionite, and analcime.

ACKNOWLEDGMENTS

This study has benefited substantially from advice and materials supplied by others. I wish to thank my advisory committee of Drs. John R. MacMillan and David B. Johnson of the New Mexico Institute of Mining and Technology, and Mr. James M. Barker of the New Mexico Bureau of Mines and Mineral Resources for their guidance and for critically reviewing this paper. I am deeply indebted to Mr. Barker, who gave generously of his time and experience throughout this study.

Sincere thanks to the Anaconda Minerals Company, in particular, employees Mr. Ken Santini and Mr. Mike LeBaron, for supplying their base map, drill hole data, and X-ray diffraction analyses of the Dripping Springs Valley deposit. Mr. Steve Peterson and Mr. Ben Donegan of the Leonard Minerals Company provided data and geologic insight on the Buckhorn clinoptilolite deposit.

The assistance of staff members of the New Mexico Bureau of Mines and Mineral Resources, Dr. Frank E. Kottlowski, Director, is deeply appreciated. Dr. George S. Austin discussed the semi-quantitative analysis of the Dripping Springs Valley basin-fill. Dr. Charles E. Chapin provided insight into tectonic factors influencing the formation of basins in the southern Basin and Range province. Mr. Mark Tuff helped with the X-ray fluorescence analysis. Mr. James Brannan demonstrated drafting techniques. Mrs. Lynne McNeil typed the manuscript.

Mr. James Mabon shot the scanning electron photomicrographs. Mr. Everett A. Bowie of Dean Color Service, gave photographic advice and developed the photomicrograph prints contained in this paper.

TABLE OF CONTENTS

LIST OF TABLES

LIST OF ILLUSTRATIONS

LIST OF ILLUSTRATIONS

LIST OF ILLUSTRATIONS

...

LIST OF ILLUSTRATIONS

INTRODUCTION

Location and Geography

Southeast Arizona and southwest New Mexico lie within the Mexican Highlands physiographic sub-province of the southern Basin and Range province (Shafiqullah and others, 1978). Zeolitization of ash-fall tuffs in a late Cenozoic network of closed basins in this region is postulated to have resulted from reaction of vitric ash with saline, alkaline-lake waters. The ash was ejected into the atmosphere from several possible sources (Scarborough, 1975) during Miocene to Pleistocene time. The Bowie chabazite (Arizona); Bear Springs chabazite (Arizona); Buckhorn clinoptilolite (New Mexico); and Dripping Springs Valley (DSV) chabazite (Arizona) deposits are among the potentially economic zeolite prospects formed in this system (Fig. 1).

Several chabazite-bearing ash-fall tuff horizons underlie approximately 16.1 km^2 (10 mi^2) in epiclastic-fluvial and lacustrine sediment of Dripping Springs Valley, about 37 km (23 mi) south of Globe, Gila County, Arizona. DSV is a narrow, north-northwest-trending, intermontane valley bounded by the Pinal, Mescal, and Dripping Springs Mountains, which rise to the north, north-northeast and southwest respectively (Fig 2). Several peaks in the Mescal Mountains have elevations over 1829 m (6,000 ft) above sea level and altitudes over 1219 m (4,000 ft) are common in the Pinal and Dripping Springs Mountains. Dripping Springs Wash (average elevation about 731 m [2,400 ft] intermittently flows south-

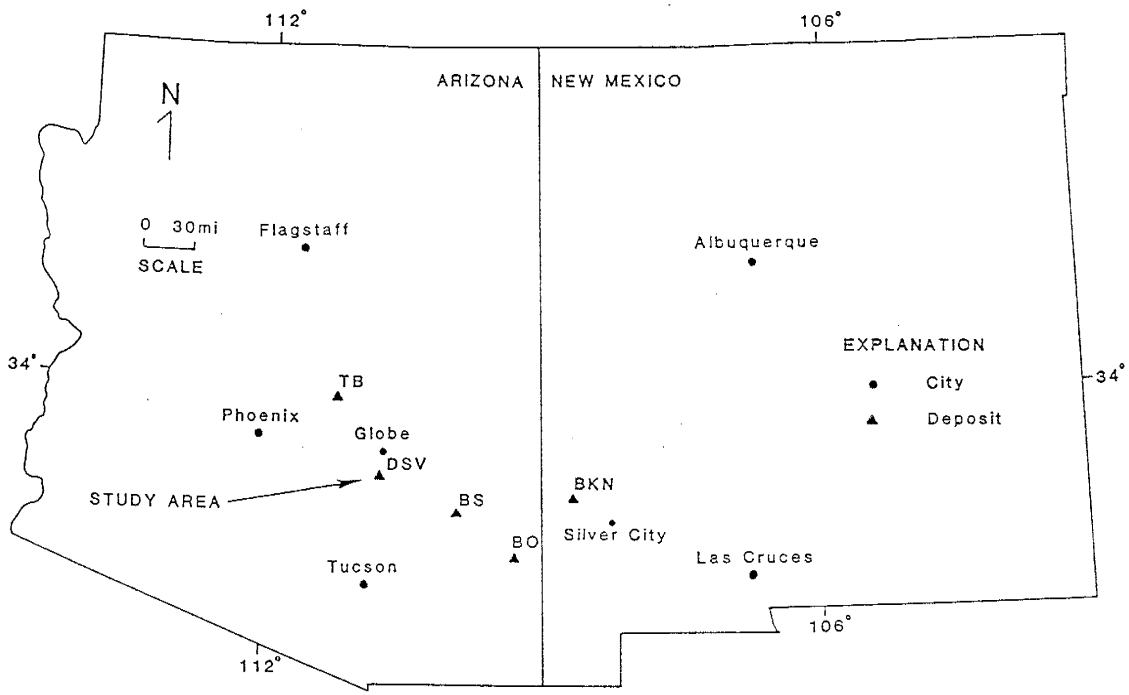

Figure 1. Location map of selected zeolite deposits in Arizona and New Mexico. DSV = Dripping Springs Valley chabazite deposit; TB = Tonto Basin chabazite deposit; BS = Bear Springs chabazite deposits; BO = Bowie chabazite deposit; BKN = Buckhorn clinoptilolite deposit.

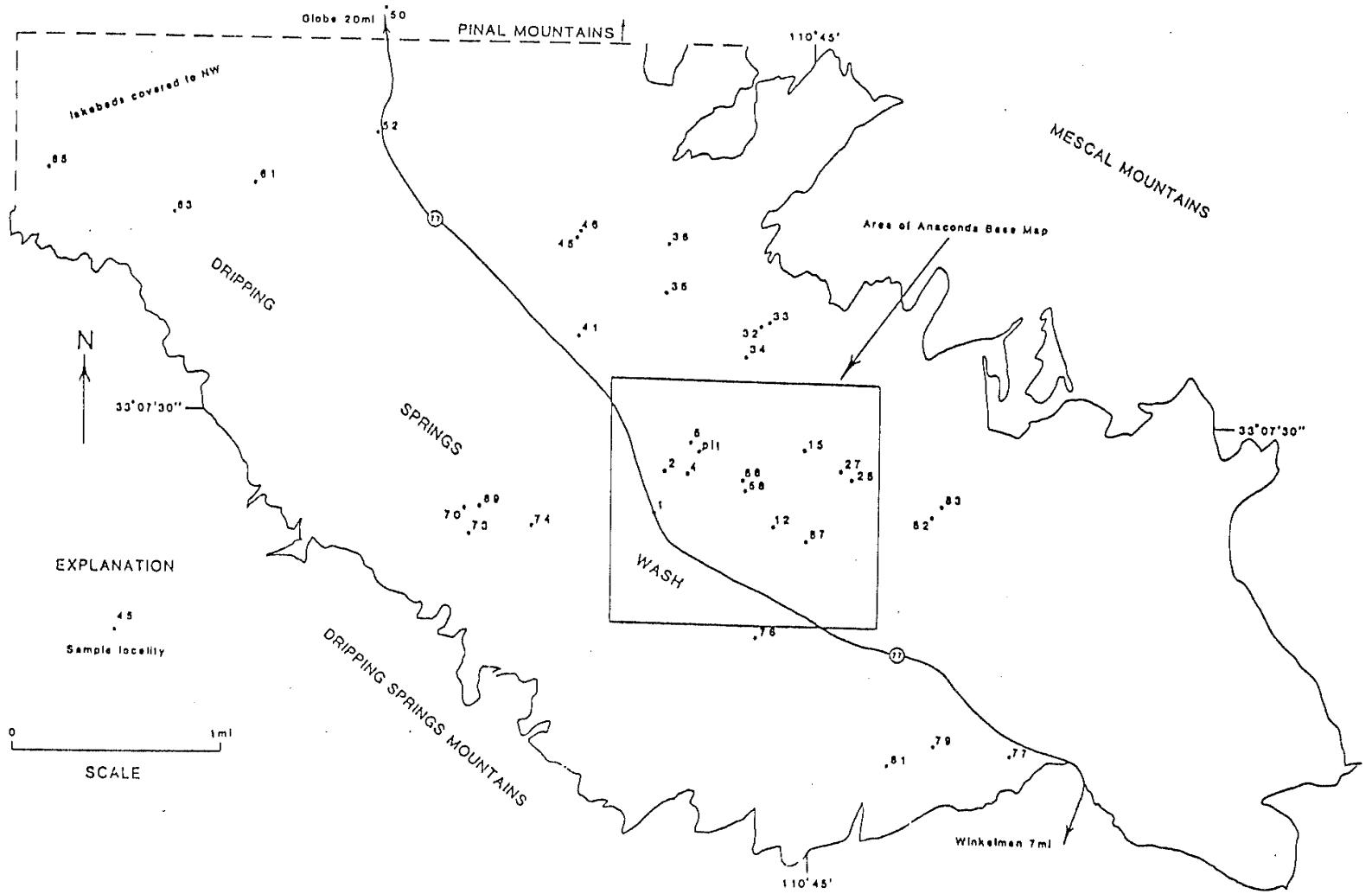

Figure 2. Map of Dripping Springs Valley showing sample localities and area covered by the Anaconda base map.

east through the southwest portion of DSV.

Climate and Vegetation

The southern Basin and Range province has a semiarid climate. DSV generally receives 25.4 to 38.1 cm (10 to 15 in) of precipitation a year. Higher elevations of the Mescal Mountains receive 50.8 to 63.5 cm (20 to 25 in) of precipitation a year (Willden, 1964). U.S. Weather Bureau data (Willden, 1964) indicate the precipitation falls in two main stormy periods: 1) during frontal storms in the winter months of December through March; 2) during summer thunderstorms in July through mid-September. Heavy summer thunderstorms occasionally produce flash floods. Summer midday temperatures often exceed 38°C (100°F) but the wide ranging daily temperatures, with the daily minimum as much as 30°F lower than the maximum (Wilden, 1964), result in mild nights. Midday winter temperatures are generally about 16°C (60°F).

The native vegetation of the southern Basin and Range province varies as influenced by climate, topography, soil, bedrock, and man. The lower elevations, such as DSV, support various combinations of grasses, cacti, mesquite, palo verde, creosote bush, and yucca; the intermediate ones support various grasses, cacti, oak, pinyon, juniper, and chaparral, while the higher elevations are dominated by evergreens (Peirce, 1967).

Land Status, Accessibility, and Nature of Exposures of the Dripping Springs Valley, Arizona Chabazite Prospect

The Anaconda Minerals Company acquired the DSV deposit in 1978 and drilled over 150 exploration holes before abandoning their claims in September, 1983. The prospect has since been claimed by Ted Eyde, a consultant for GSA Resources, Inc. in Cortaro, Arizona.

Modern, paved Arizona State Highway Route 77 borders the southern edge of the deposit and provides good access. To aid their assessment work, Anaconda constructed dirt roads in and around the prospect. These roads are reached via access gates on the north side of Route 77. Although some prospect roads were altered by Anaconda's reclamation efforts, practically all are still accessible to four-wheel drive vehicles. Such vehicles are not a necessity, however, as most lakebed exposures are easily reached on foot, many within short walking distance of Route 77. Improved dirt roads connected to the south side of Route 77 provide further accessibility to the southernmost outcrops of DSV basin-fill.

The upper 680 m (2221 ft) of DSV basin-fill are best exposed in areas of deep dissection. There are abundant outcrops of fluvial and lacustrine facies but exposures of ash-fall tuff horizons are generally sparse, owing to masking by talus and overlying sediments, and erosion by paleochannels. I found only three exposures of the "main" zeolite tuff.

Scope of Investigation

Surficial geologic-mapping is combined with extensive drill-hole data to examine the geology of the DSV basin-fill. The primary purpose of this research is to describe spatial distributions and relationships with respect to mineralogy, chemistry, stratigraphy, and structure of the depositional basin. These characteristics are briefly compared and contrasted with those of other closed-basin zeolite deposits of the southern Basin and Range province of Arizona and New Mexico as described in the geological literature.

X-ray diffraction (XRD) analyses of the zeolite horizons, surrounding lacustrine facies, and overlying fluvial facies are used to describe vertical and lateral mineralogical trends. Scanning electron microscopy of selected lacustrine claystone and altered tuff samples is used to estimate mineral abundance and grain size, and to illustrate morphology, degree of crystallinity, and paragenetic relationships. Major oxide and loss on ignition (LOI) analysis through X-ray fluorescence (XRF) spectrometry methods was conducted to examine gross vertical and lateral chemical trends within the basin. This data helps explain the occurrence and distribution of the authigenic mineral assemblage.

PREVIOUS WORK

The DSV chabazite deposit lies within the U.S. Geological Survey 7 1/2-minute Hayden (Banks and Krieger, 1977) and El Capitan (Cornwall and Krieger, 1978), and the U.S. Geological Survey 15-minute Christmas (Willden, 1964) quadrangle maps. Krieger (1979) has summarized these mapping projects as well as those of the nearby Sonora quadrangle (Cornwall, 1971), Kearny quadrangle (Cornwall and Krieger, 1975), and San Manuel area (Creasey, 1965). The Arizona state geologic map (Wilson and others, 1969) and geologic maps of the Gila (Wilson and others, 1959), Pinal (Wilson and Moore, 1959), Graham and Greenlee (Wilson and Moore, 1958), and Cochise (Arizona Bureau of Mines, 1959) Counties illustrate the location and extent of southeast Arizona basin-fill. The New Mexico state geologic map (Dane and Bachman, 1965) and the surficial geologic map of southwest New Mexico (Hunt, 1978) provide this information for basins in southwest New Mexico.

Several workers indicate zeolites occur in sedimentary rocks of diverse lithology, age, and depositional environment; several classifications of zeolite deposits have been offered (Hay, 1966, 1978; Sheppard, 1971, 1973, 1975; Munson and Sheppard, 1974). One prominent type is the closed-hydrographic basin, or saline, alkaline-lake deposit (Hay, 1966; Sheppard, 1973; Kossovskaya, 1975; Mumpton, 1975; and Surdam, 1977). Lowe (1875) tentatively identified chabazite in a volcanic tuff near Whitlock Cienega, Arizona in what is

believed to be the first published description of a bedded zeolite anywhere in the world. Other initial observations of zeolites in saline, alkaline-lake deposits in the United States were made by Ross (1928) and Bradley (1928), but it was not until the late 1950's when geologists of the Linde Division of the Union Carbide Corporation "rediscovered" the chabazite deposit first described by Lowe, which today is known as the Bowie chabazite deposit. It was during the same exploration program that the DSV chabazite, Bear Springs chabazite, and Buckhorn clinoptilolite deposits were discovered in the Gila and San Simon Valleys in 1960 and 1961.

T. H. Eyde and G. W. Irwin (in Arizona Department of Mineral Resources, 1978) described Arizona zeolites to acquaint prospectors with zeolite minerals, typical occurrences, analytical methods, industrial uses, and potential consumers. They provide brief, descriptive accounts of 47 individual zeolite occurrences in the state, including those at DSV, Bowie, Bear Springs, and Tonto Basin.

Edson (1977) and Sheppard and others (1978) describe the bedded zeolitic tuffs at the Bowie deposit and examine their genesis in a saline, alkaline-lake. Three earlier ground water studies (Schwenneson, 1917; Knetchel, 1938; and Cushman and Jones, 1947) refer to tuff beds in the fluviatile and lacustrine sediments of the San Simon basin, but failed to recognize these as being zeolitically altered.

Little study has been devoted to the zeolitized ashfall tuffs of DSV. Besides the Arizona Department of Miner-

al Resources report (1978), only three other sources acknowledge the presence of zeolitized tuffs in the valley.

Scarborough (1975) attempted to correlate geochronologically Pliocene valley-fill sediments of southern Arizona basins via whole-rock chemical analyses and potassium-argon age dating. Most of his efforts were applied to the air-fall ashes in the Upper and Lower San Pedro Valley, but he did mention the presence of at least four "devitrified" ash beds in DSV. He did not date these beds. Krieger (1979) analyzed DSV tuff samples by XRD and found one to be composed almost entirely of chabazite. Eyde (1982) briefly described two zeolitized horizons and the surrounding lake-bed facies.

Olander (1979) examined authigenic mineral reactions in tuffaceous sediments of the Buckhorn, New Mexico clinoptilolite deposit. He laterally and vertically sampled air-fall tuff samples from the saline, alkaline-lake and lacustrine-fringing environments to characterize the relationships among depositional environments, mineralogy, chemistry, and cation-exchange capacity.

Deffeyes (1959) stressed the abundance of zeolites in tuffaceous sedimentary rocks and described their genesis by the reaction of vitric material and saline, alkaline solutions. Van Houten (1964, 1965) reiterated these ideas by examining zeolite occurrences in Cenozoic rocks of Wyoming and Triassic rocks of the New Jersey Lockatong and associated formations of the Newark Group. Hay (1966) collated

the existing geological, theoretical, and experimental data pertinent to natural zeolites and presented new data on the authigenic mineral assemblages in saline, alkaline-lakes. Sheppard and Gude (1968, 1969, 1973) made initial recognition of a lateral zonation of authigenic zeolite assemblages in saline, alkaline-lake deposits upon studying the mineral distribution and authigenic mineral reactions in closed basins of the western United States. Several workers have since presented a general model of zeolite genesis within these systems (Hay, 1977, 1978; Surdam, 1977; Sheppard and others, 1978; and Surdam and Sheppard, 1978).

METHOD OF STUDY

The geologic maps of the DSV chabazite deposit presented here (Plate 1, 2) are the product of field work conducted over a period of six weeks in the fall of 1983 and spring, summer, and fall of 1984. A base map of the prospect, generously supplied by the Anaconda Minerals Company, and the U.S. Geological Survey 7-1/2 minute El Capitan Mountain (1964), Hayden (1964), Mescal Warm Spring (1968), and Christmas (1968) topographic maps were used to record the geological data. Plate 1 is a modification of maps by Banks and Krieger (1977), Cornwall and Krieger (1978), and Willden (1964), and differentiates the previously undivided Tertiary lakebeds into informal claystone and ash-fall tuff units. The surficial geology of Anaconda's 5.6 km^2 (3.5 mi^2) base map area is recorded on Plate 2.

Anaconda also supplied diamond drill logs with lithologic descriptions for 139 holes drilled for assessment work. These analyses were recorded by three different workers, and consequently, the quality and style of the descriptions vary. Rock and mineral colors were determined by comparison with the Rock-Color Chart (Geological Society of America, 1963). The logs are labeled using English units, and for simplicity, I have left and will report the data in these units. The drill logs were used to construct isopach maps (Figs. 8 through 12) and structure contour maps (Figs. 16 through 20) of the rock units penetrated, and to supplement surficial geologic mapping. Anaconda also provided

powder XRD analyses performed by them in Tucson, Arizona. Samples of the "main" zeolite tuff from 57 holes are reported in relative percent of each mineral (or mineral group) present. These data are plotted on copies of the base map to examine trends in character of mineralization (Figs. 6, 7).

I collected surface grab samples of all the informally- and formally-named rock units within DSV for laboratory analysis. These samples are from the margins through central areas of the depositional basin (Fig. 2).

Oriented clay samples were prepared for XRD analysis by allowing suspensions of the less-than-two micron size fraction to dry at room temperature on glass slides. Clay samples that remained flocculated after several attempts to disperse them by immersion and mixing in distilled water, were treated first by wet grinding with a mortar and pestle. If the sample still did not disperse, it was treated with a few drops of Calgon. If it still remained flocculated, it was treated with four drops of concentrated ammonium hydroxide (NH_4OH) and remixed. All clay samples were dispersed prior to or during this stage of preparation. An eye-dropper was then touched to the surface of the suspension and the drawn sample was transferred to a glass slide.

XRD analysis of clays in the less-than-two micron size fraction was made with a Rigaku Geigerflex diffraction unit using Ni-filtered CuK_α (=1.5418 Å) radiation. All samples were first continuously scanned at 32°2θ/min between 2° and 38°2θ to obtain an overall view of the peak intensi-

ties of the mineral assemblage of the sample, and then continuously scanned at 2°2θ/min between 2° and 38°2θ so that the highest peak was at or near full recorder chart scale. After solvation for at least 24 hours with ethylene glycol, all less-than-two micron size samples were again analyzed by XRD in the manner just described, and with the same machine settings used in the first trace. Glycolation caused complete expansion of the expandable clay minerals and expandable clay mineral layers within mixed-layer clay minerals. A third XRD analysis was made for each slide after the slides were heat-treated at 350° to 400°C for between 30 and 60 minutes in a Blue M Model M15A-1A Lab-Heat Muffle Furnace. Again, the same machine settings used in the first two runs were used. The XRD scan was passed over the 10Å peak while the slide was still hot. Any enhancement of the glycolated 10Å peak by heating was attributed to the collapse of interstratified smectite layers within illite/smectite mixed-layer clay minerals (Austin and Leininger, 1976).

The dropper-on-glass slide mounting technique is inadequate for quantitative analysis (Gibbs, 1965, 1968) due to size segregation of the clay minerals. I have therefore conducted a semi-quantitative analysis of the less-than-two micron size fraction using Austin's (pers. comm., 1984) method. This method is essentially the same as that developed by Walter Parham of the Minnesota Geological Survey who modified the initial technique developed by Johns and

others (1954). Austin's method quantifies the major clay mineral groups to parts in 10, and is based on the heights of certain peaks above background. Austin (pers. comm., 1984) states that this technique is within the range of "acceptable error" of parts in 10, which should not be equated with percentage. Table 1 lists the equations used for my semi-quantitative analysis. No sample of DSV basin-fill had enough illite/smectite to produce a measurable reflection between 33-35° 2θ and Srodon's method (1984) of estimating the ratio of illite-smectite layers and of identifying the type of interstratification in illite/smectite mixed-layer minerals, could not be used.

Selected samples of the fluvial and lacustrine facies (including the ash-fall tuffs) were prepared for semi-quantitative XRD analysis by dry, powder-press methods. The samples were ground to a fine powder with a mortar and pestle and the thoroughly mixed sample was manually pressed flat into the recess of a glass sample holder with a petrographic slide. The sample was then scanned with the diffractometer in the same manner the untreated oriented slides were.

The mineral assemblage in the powder press and sedimented-slide samples was identified from hkl reflections. Clay minerals were identified primarily by 001 reflections. Mixed-layer illite/smectite is indicated by a series of reflections on the low angle side of the 10Å "d"-spacing (Carroll, 1970).

Scanning electron micrographs of selected lacustrine

Table 1. Equations used in the semi-quantitative analysis of clay mineral groups in the less-than-two micron size fraction of DSV basin-fill samples. The calculations are in counts above background. Peaks in the analysis are designated with subscripts to indicate the order (e.g. first order illite is I_1). All traces are run on the same slide and with the same machine settings.

$$\text{Illite} = \frac{I_{1G}}{T} \times 10$$

$$\text{Smectite} = \frac{1/4S_{1G}}{T} \times 10$$

$$\text{Mixed-layer Illite/Smectite} = \text{Heated } 10\text{A}^{\circ} - \frac{[1/4S_1 + I_{1G}]}{T} \times 10$$

$$\text{Kaolinite} = \frac{K_2}{2C_4} \times \frac{C_3}{I_2} \times \frac{I_{1G}}{T} \times 10$$

$$\text{Chlorite} = \frac{C_3}{I_2} \times \frac{I_{1G}}{T} \times 10$$

$$T = I_{1H} + \frac{(C_3)(I_{1G})}{I_2} + \frac{(K_2)(C_3)(I_{1G})}{(2\,C_4)(I_2)}$$

Where, T = total counts
G = glycolated
H = heated
I = illite
S = smectite
K = kaolinite
C = chlorite

---

claystone and ash-fall tuff samples were taken with a Hitachi HHS-2R scanning electron microscope (SEM) at the New Mexico Institute of Mining and Technology. Samples were broken to expose fresh surfaces, and chips about 5 mm (0.20 in) in size were cemented with Duco cement to 14 mm (0.55 in) diameter aluminum pegs and placed in a desiccator overnight. The samples were then coated with a film of gold-palladium alloy to insure electrical conductivity and thus prevent charging effects in the microscope. Images produced by the emission of secondary electrons were viewed on the phosphorescent screen of the instrument and photographed with a Polaroid camera.

XRF spectrographic analysis was conducted to determine the major-oxide chemistry of selected ash-fall tuff and lacustrine claystone samples. Fused discs of these samples were then placed in a Rigaku 3064 Wavelength Dispersive X-ray Fluorescent Spectrometer for the chemical analysis. The results are reported in weight percentage of ten major oxides. Loss on ignition (LOI) was determined at 1000°C.

DEPOSITIONAL HISTORY OF THE DRIPPING SPRINGS VALLEY, ARIZONA CHABAZITE DEPOSIT

Stratigraphy of the Surrounding Highlands

DSV is a north-northwest-trending, normal fault-bounded, intermontane valley with adjacent north-northwest-trending Pinal, Mescal, and Dripping Springs Mountains (Fig. 2). The highlands are composed of Precambrian igneous and metamorphic rocks nonconformably overlain by Precambrian sedimentary rocks, which are unconformably or disconformably overlain by Paleozoic sedimentary rocks. All of these units were intruded by Late Cretaceous quartz diorite and granodiorite plutons, as well as Late Cretaceous or Early Tertiary rhyodacite and quartz latite dikes. Elaboration on the sedimentologic and structural characteristics of these pre-Early Tertiary rock units is not within the scope of this paper. See Darton (1925); Bromfield and Shride (1956); Heindl (1958); Pye (1959); Willden (1964); Krieger and others (1974); Banks and Krieger (1977); and Cornwall and Krieger (1978) for this information.

Dripping Springs Valley Basin-Fill

Immediately prior to basin-fill time, the Pinal and Mescal Mountains area was topographically positive, dipping gently to moderately southwest. To the south, the Dripping Springs Mountains were a broad, open anticline plunging to the southeast (Banks and Krieger, 1977). A major northwest-trending normal fault, downthrown to the northeast and bounding the southwest margin of DSV, was reactivated in

Miocene(?) time, and formed the elongate, asymmetrical, closed basin that was filled with at least 680 m (2221 ft) of Tertiary and Quaternary fluvio-lacustrine deposits. Cornwall and Krieger (1978) note a churn drill hole in Dripping Springs Wash, 1.55 km (0.96 mi) west of the boundary dividing R. 14 E. from R. 15 E, penetrated 448 m (1469.9 ft) of Tertiary conglomerate and did not reach the bottom of the basin even though the older rocks of the basement crop out 300 m (984.3 ft) to the southwest. The exact age of the informally named sedimentary deposits of DSV is uncertain. Banks and Krieger (1977) have tentatively correlated them with the Big Dome Formation (early Miocene) in the Gila River Valley southwest of the Dripping Springs Mountains on the basis of lithology, however, they might be as young as the Quiburis Formation (Miocene or Pliocene) of San Pedro Valley.

Several lines of evidence indicate that lake waters ponded in the closed basin were saline and of moderately high alkalinity. The most obvious indication is the presence of saline minerals, in particular, halite and gypsum. Gypsum fills tiny fractures and forms terrace-like lenses up to a few centimeters thick in the thick deposits of illitic-smectitic lacustrine clay. Halite was detected by XRD analysis of the claystones and observed as macroscopic crystals when laboratory mixtures of the claystones and distilled water were allowed to evaporate to dryness. Zeolitization (as chabazite predominantly) of the ash-fall

tuffs, and the lack of authigenic alkali/alkaline earth carbonates which form at higher salinities and pH values in closed basins, such as nahcolite, pirssonite, gaylussite, and trona, suggest only moderately high alkalinity. The degradation of discrete illite to mixed-layer illite/smectite and a possible basinward conversion of montmorillonite to illite also attest to the moderately high salinity and alkalinity. These clay mineral relationships will be discussed below in the "Clay Mineralogy" section.

If the "chemical delta" model of calichification to be proposed later in this section is valid, it provides indirect evidence of salinity and alkalinity. Carbonates in alluvial fans on the northeast side of the valley are, possibly, precipitates formed where inflowing calcium-bearing "fresh" water mixed with saline, alkaline water.

The sedimentary deposits of DSV consist of a coarse alluvial conglomerate around the margins and fine-grained, laminated clays, silts, and fine sands in the center, separated by a narrow "transition" zone on the southwest side of the basin and by a wide "transition" zone on the northeast side (Plates 1, 2). Walther's Law, coupled with the principle that all lakes are ultimately filled, suggests that the "ideal" lacustrine sequence grades vertically from fine-grained rocks deposited below wave base into coarser marginal and fluvial deposits. The stratigraphic section of DSV has this vertical succession. Quaternary gravels overlie Tertiary lacustrine claystone (Fig. 3, Appendix I). As movement, probably in the Miocene, on the major northwest-

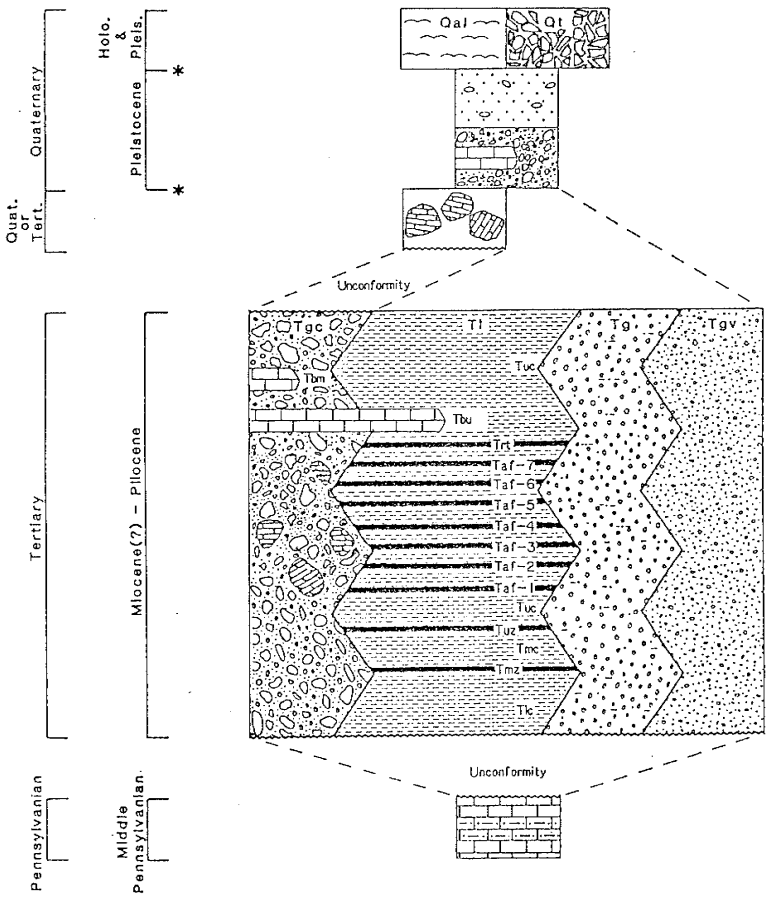

Qal - RECENT ALLUVIUM , Qt - TALUS

Qp - SOIL AND GRAVEL VENEER

Qog - OLDER GRAVELS AND SECONDARY CARBONATES

QTls - LANDSLIDE DEPOSITS

Tbm - MEGABRECCIA, MARTIN LIMESTONE

Tbu - MEGABRECCIA UNDIVIDED

Trt - RHYOLITIC TUFF

Taf 1-7 - ASH-FALL TUFFS ONE THROUGH SEVEN

Tuc - UPPER RED CLAYSTONE

Tuz - UPPER ZEOLITE TUFF HORIZON

Tmc - MIDDLE RED CLAYSTONE

Tmz - MAIN ZEOLITE TUFF HORIZON

Tlc - LOWER RED CLAYSTONE

Tgc - LIMESTONE-DOLOMITE CONGLOMERATE
Tg - CONGLOMERATE
Tgv - VOLCANICLASTIC CONGLOMERATE
Tl - LAKEBEDS UNDIVIDED

Pn - LOWER PART OF NACO LIMESTONE

* - lacunas not shown

Figure 3. Generalized stratigraphy of Dripping Springs Valley. Detailed lithologic descriptions are in Appendix I. Interfingering contacts of Tertiary units are diagrammatic.

trending normal fault formed the DSV depositional basin, penecontemporaneous deposition of alluvial conglomerates (T_g, T_{gv}, T_{gc}), and lacustrine claystones (T_{lc}) began in the closed basin. The lacustrine rocks probably do not extend to the valley floor; alluvial fan deposits and valley-floor alluvium probably underlie them. The T_g conglomerate was derived from erosion of all the surrounding highlands and contains clasts representative of all pre-Miocene rocks in proportions and size that vary with proximity to, and composition of, the adjacent bedrock exposures (Banks and Krieger, 1977). The unit is poorly sorted and bedded near its source bedrock and moderately well sorted and bedded in the transition zone. The T_{gv} conglomerate was derived mainly from erosion of volcanic and intrusive rocks in the Dripping Springs Mountains and is present only on the southwest side of DSV (Plate 1). The facies is dominated by clasts of Williamson Canyon volcanics and Cretaceous and Early Tertiary intrusive rocks. Its greenish-gray, sand-size matrix is composed mainly of decomposed volcanic and intrusive rocks. T_{gc} is a limestone-dolomite conglomerate which was largely derived from weathering of Paleozoic carbonate units in the Pinal and Mescal Mountains. It occurs adjacent to these carbonates along the northeast side of DSV (Plates 1, 2). This conglomerate does not crop out on the southwest side of the valley. Initial deposition of horizontal to gently dipping, very well- to well-sorted, silty to arenaceous, lacustrine claystones was intermittently disrupted by mar-

ginal influx of lenses (observed up to 0.91 m [three ft] thick) of coarser material derived from erosion of the surrounding highlands. Multiple depositional pulses of the coarser material may indicate continued activity along the major northwest-trending normal fault throughout much of lacustrine-fill time. The lacustrine claystones (T_{lc}, T_{mc}, T_{uc}) contain locally, moderately abundant, detrital mafic minerals, including biotite, hornblende, and magnetite.

Lance (1960) studied the general cycle of sedimentation which deposited the late Cenozoic valley-fill sediments in southeast Arizona. He notes a puzzling lack of coarse detritus shed from adjacent mountain blocks in several valleys where fine alluvial and lacustrine silt directly abut mountain fronts. Examples of this include the 111 Ranch lakebeds (Scarborough, 1975) in the San Simon Valley and lakebeds along the southwest edge of DSV. There is insignificant inflow into closed basins and, consequently, shore phases can be muddy. In addition, at DSV, the steepness of the flank of the Dripping Springs Mountains, and recurrent movement along the major northwest-trending normal fault, probably prevented significant lateral accumulation of coarse-grained detritus on the southwest side of the valley. Alternatively, on the opposite side of the basin, the moderately dipping Pinal and Mescal Mountains were eroded to form laterally extensive alluvial fan deposits.

Deposition of the lacustrine claystones (T_{lc}) continued and at least three horizontal, gypsiferous claystone terrace-like lenses formed at the north end of the valley near

and south of SE cor. sec. 35, T. 3 S., R. 15 E. Several other gypsiferous claystone lenses also interfinger with stratigraphically higher lacustrine claystones (T_{mc}, T_{uc}) at the north end of the valley.

Penecontemporaneous deposition of the alluvial conglomerates (T_g, T_{gv}, T_{gc}) and lacustrine claystones continued undisturbed except for intermittent deposition of numerous silicic ash-fall tuffs over the entire valley (Fig. 3). These tuffs are not preserved or observed over the entire valley today due to erosion and exposure, and/or coverage by talus and overlying sediment. Lake bottom currents slightly mixed tuffaceous material and lacustrine sediment as indicated by the tuffaceous content of lacustrine claystones proximal to the tuffs, their gradational contacts with several of the tuffs, and soft sediment deformational features and ripple marks preserved in the tuffs. The stratigraphically lowest tuff exposed in the valley is the main zeolite tuff horizon (T_{mz}). This very fine-grained to fine-grained, very well-sorted tuff conforms to the configuration of the generally flat basin bottom upon which it was deposited, and has an erratic, sharp contact with the underlying claystone. The upper zeolite tuff horizon (T_{uz}) was the next tuff to be deposited. It is separated from the main zeolite tuff horizon by approximately 1.52 m (five ft) of red lacustrine claystone (Figs. 4, 5). This tuff is a very fine-grained, very well-sorted, glassy ash which also conforms to the generally horizontal basin bottom upon which it was depos-

Figure 4. View looking southwest at Anaconda's prospect pit. Main zeolite tuff is piled on the floor along the south side. The middle red claystone lies at the base of the wall. It is overlain by the blocky, resistant upper zeolite tuff. A 0.3 m (one ft) thick layer of white reworked zeolitic material is interbedded with the upper red claystone about 0.5 m (1.5 ft) above the upper zeolite tuff.

Figure 5. View looking northwest at exposures of the T_{mz} and T_{uz} tuffs at locality 86. Geologic hammer rests on the concoidally fractured T_{mz}. Blocks of T_{uz} have fallen down the hillside.

ited. It has an undulatory, gradational contact with the underlying claystone. A series of at least seven, thin, silicic ash-fall tuffs, the stratigraphically lowest of which is separated from the upper zeolite tuff by over 44.2 m (145 ft) of lacustrine claystone, is exposed at the northwest end of the valley. The thickness of the individual tuffs does not exceed 0.91 m (three ft) and averages approximately 0.46 m (1.5 ft). I informally refer to these units as ash-fall tuffs one through seven (T_{af-1} through T_{af-7}) in ascending stratigraphic order (Fig. 3). Some of these tuffs are locally calcified proximal to the basin margin. Calcification probably occurred as calcium-bearing freshwater entered the pore spaces of the tuffs and calcium precipitated out of solution to cement the tuffs. The final preserved ash-fall tuff horizon (T_{rt}) to be deposited overlies and is separated from T_{af-7} by 15.2 m (50 ft) of lacustrine claystone. This fine-grained, locally zeolitically altered ash was partly reworked and waterlain.

Concurrent deposition of the alluvial conglomerates (T_g, T_{gv}, T_{gc}) and lacustrine claystone (T_{uc}) continued after deposition of the final preserved ash-fall tuff. The upper red claystone (T_{uc}) grades southwestward and northeastward away from the basin center into grayish beds containing progressively more silt then progressively more sand, granules, and pebbles. In addition, this unit is locally divisible into three subunits: 1) an arenaceous claystone and argillaceous sandstone overlain by and in sharp contact with, 2) an arenaceous claystone, locally

carbonate-cemented; commonly with lenses of gravels (up to 1.2 m [four ft] thick) which include reworked zeolitically altered tuff, and clay laminae overlain by, and in gradational contact with, 3) a silty to arenaceous claystone and very fine-grained siltstone. Deposition of the upper red claystone, therefore, was intermittently disrupted by influx of coarser material from marginal sources.

As penecontemporaneous deposition of the T_g, T_{gv}, T_{gc}, and T_{uc} units continued, two separate landslide megabreccia blocks slid south off El Capitan Mountain and came to rest along the northeast side of the valley (Fig. 3). The first block is composed predominantly of Mississippian Escabrosa Limestone underlain by Upper Devonian Martin Limestone (T_{bu}). It slid four km (2.49 mi) and was probably one huge slab which was later dissected by several washes. The second block is a one to five m (3.28 to 16.41 ft) thick slab of Martin Limestone (T_{bm}) which slid 0.8 km (0.5 mi) from its source. After cessation of deposition of the T_g, T_{gv}, T_{gc}, and T_{uc} units, jumbled angular blocks of Escabrosa Limestone and some Martin Limestone (QT_{ls}) were eroded from bedrock ledges and slid a short distance down the dip slope of these formations and now rest on the northeast side of the valley.

Post-Miocene uplift of the DSV region drained the lake occupying the closed basin and produced erosion, faulting, development and later dissection of several pediment (terrace) surfaces, and an evolution from the interior paleo-

drainage system to the exterior modern drainage system. Holocene downcutting has been active in a zone concentric with the present Mogollon Rim, an area encompassing the Lower San Pedro Valley, Aravaipa Valley, and DSV (Melton, 1965). Entrenchment dies out southward in the former two valleys. This selective stream incision may indicate localized block faulting is still active (Scarborough, 1975).

Erosion reduced the lacustrine claystones to exposure on a low, hummocky surface near the center of the basin. Where weathered, the claystones have a distinctive "popcorn" surface several centimeters thick. Shoreward, the hummocks become progressively higher and become small buttes capped with gravel which, near the margins of the basin, coalesce to form gravel-capped pediments dissected by steeped-sided washes with gravelly alluvium covering the bottoms. Gravels now partly carbonate-cemented (Q_{og}; Fig. 3) were deposited along but at higher topographic levels than present drainage. The Q_{og} unit is exposed primarily within the transition zone but was deposited on eroded lakebeds and tuff horizons in numerous areas. It contains deposits of several ages and bears clasts from older rocks exposed along adjacent drainages. Included in this unit is a silt- to boulder-size, locally massive, locally laminated, very-poorly- to poorly-sorted, ridgecapping, calcite-cemented conglomerate with abundant clasts of Escabrosa Limestone. This and other carbonate beds (up to 1.5 m [4.9 ft] thick) are abundant in the transition zone on the northeast side of the basin. The origin of these carbonates remains specula-

tive until more detailed mapping and further study is conducted. Several models of secondary carbonate emplacement may explain their genesis: lacustrine "chemical delta", nonpedogenic cement, and pedogenesis.

A lacustrine chemical delta may have formed the conglomeratic freshwater limestone when calcium-charged "freshwater" brought by streams weathering the surrounding Paleozoic limestones mixed with the CO_2-rich saline, alkaline ground and lake waters, precipitating the calcium as calcite. The chemical delta mode of occurrence has been hypothesized for lacustrine deposits by numerous workers (Picard and High, 1972). Smith (1966) proposes a lacustrine origin for the calcium carbonate in the Upper Wisconsin sediments at the inlet to saline Searles Lake, as do Starkey and Blackmon (1979) for the calcite in Pleistocene Lake Tecopa. Hay (1977) observed this phenomenon at modern Mono Lake in California and at Pyramid Lake in Nevada, and Picard (1957) found that limestone in the Green River and Uinta Formations is dominantly of lacustrine origin.

Secondary carbonate deposits may have formed via a nonpedogenic process through introduction of cementing material by lateral groundwater flow (Carlisle and others, 1978). Carbonate-charged waters generated in the Paleozoic limestones of the Pinal and Mescal Mountains flowed over and through alluvial fans into and down the axis of DSV, possibly precipitating calcretes in their paths. This depositional model is analogous, in part, to that which formed the

nonpedogenic calcretes observed in Western Australia by Carlisle and others (1978). Barker (1983) postulates nonpedogenic processes have formed secondary carbonate deposits in sections of the Riley travertine, Socorro County, New Mexico. He also notes nonpedogenic calcrete may be locally indistinguishable, without detailed study, from pedogenic calcrete and from lacustrine or playa limestones.

A pedogenic origin for the DSV carbonate is less probable than the previous two processes offered. This model forms calcretes through soil-forming processes. Carlisle and others (1978) speculate that the calcrete at the Bowie chabazite deposit in the San Simon Valley formed in situ by pedogenic processes.

Pedimentation formed gently sloping Quaternary terrace surfaces (Q_p; Fig. 3) of several ages and developed a reddish-brown soil and gravel veneer with pebble to boulder clasts from older rocks. The pediment surfaces are largely developed on older gravel (Q_{og}) and other conglomeratic units, and lakebeds. The oldest recognizable terraces in the southern Basin and Range province appear to be no older than about three million years (Scarborough, 1975).

Currently, clay, silt, sand, and gravel are being deposited in stream channels and on young low-lying terraces along streams. Erosion of the surrounding highlands continues via the major valley drainage route, the Dripping Springs Wash, and its numerous, intermittent, small tributaries.

DRILL HOLE DATA INTERPRETATIONS

The 139 drill holes and logs supplied by Anaconda cover an area of approximately 1.6 km^2 (one mi^2) (Fig. 2). Three types of maps were constructed from the available drill hole data: 1) relative mineral-percentage, 2) isopach, and 3) structure contour. The maps were contoured by linear interpolation with modifications dictated by current knowledge of geological and sedimentological relationships within the basin. For instance, lakebed unit isopach contour lines were not connected across a major paleochannel separating two ridge-forming lake deposits as much of the lake deposits were eroded prior to deposition of the alluvial gravels. In fact, the paleodrainage has destroyed the lakebeds to the extent that four, essentially separate, lakebed outcrop areas exist in the Anaconda base map area. These areas are hereafter informally referred to as the West Ridge, the Wash Ridge, the Central Ridge, and the East Ridge (Fig. 6). The maps compliment one another in revealing important information on the character of mineralization, basin morphology, and delineation of major paleodrainages and fault traces. Key drill hole cross sections have also been constructed to supplement the data provided in the above maps.

Mineral-Percentage Maps

Relative mineral-percentage maps were constructed from the results of Anaconda's powder XRD analysis of only the main zeolite bed. The most important of these maps is Fig. 6, which shows relative percent chabazite. The values range

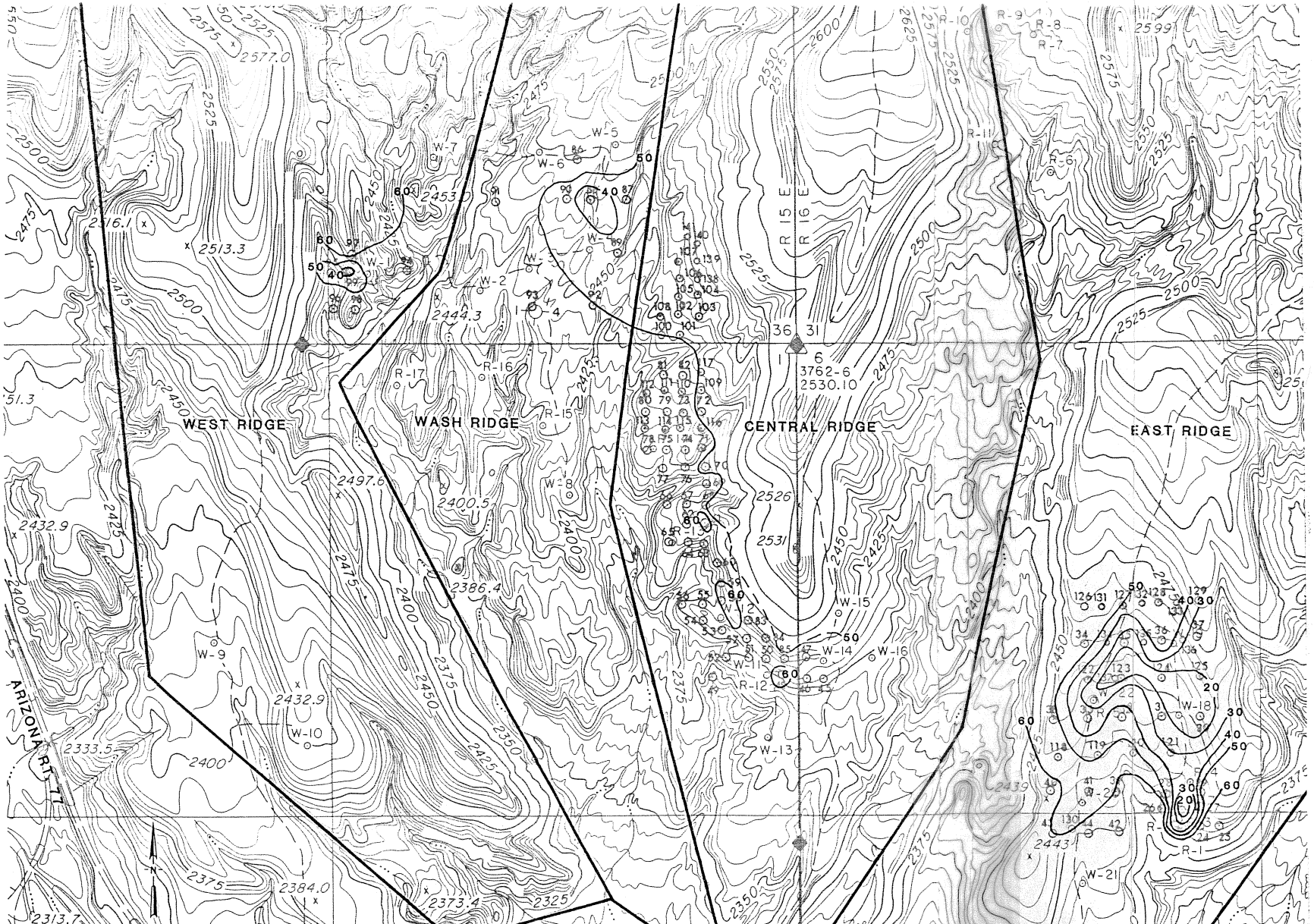
WEST RIDGE
WASH RIDGE
CENTRAL RIDGE
EAST RIDGE
ARIZONA RT. 77
R 15 E
R 16 E
3762-6
2530.10
2513.3
2444.3
2497.6
2400.5
2432.9
2386.4
2333.5
2384.0
2373.4
2313.7
2577.0
2599
2443
W-1
W-2
W-3
W-4
W-5
W-6
W-7
W-8
W-9
W-10
W-11
W-12
W-13
W-14
W-15
W-16
W-18
W-20
W-21
R-1
R-11
R-12
R-15
R-16
R-17

from 0 to 69% chabazite. Eyde (1982) states that sampling done in 1960 indicated the main zeolite horizon grades from clean, unaltered vitric ash at the north end of the deposit to 90% chabazite at the south end.

Krieger (1979) analyzed five ash-fall tuff samples from DSV. These are thought originally to have been of rhyolitic composition based on the 1.495 refractive index of preserved, unaltered glass shards. The five samples are from the transition zone and are vitric, although two have undergone some clay alteration. Krieger speculates that freshwater in the pores and the freshness of subsequent groundwater, prevented zeolitization of the tuffs.

The wide range of values in Fig. 6 illustrates the zeolitic alteration was not homogeneous. An anomalous 97% carbonate value was found for DH W-23. The relatively uniform chabazite values in the Central Ridge are generally higher than the wide ranging values in the East Ridge. The chabazite content increases to the southwest in both ridges. This suggests that the basin center, and its more saline, alkaline conditions, was situated to the southwest while a wide basin margin zone, with greater freshwater influence, was located to the northeast of these sample localities.

Drill holes which penetrated the Q_{al}, Qp, and Qog units, but did not encounter the lakebed facies, help define the distribution of alluvial sediments and delineate major paleodrainage paths. The paleodrainage mirrored the modern drainage, but cut the lakebeds topographically higher.

Major paleochannels flowed south between and to the south of the West and Central Ridges, and between and to the south of the Central and East Ridges. Perhaps if the channels had not eroded the main zeolite bed on the southwest side of the Central Ridge, chabazite values higher than the 60+% observed in this study would be found.

Clinoptilolite and erionite are the only other zeolites identified in DSV. Clinoptilolite was detected in only 17 drill hole samples. Relative-percent values range from 1 to 5% for clinoptilolite while 1% erionite was found in only DH W-41. Clinoptilolite seems to be more concentrated in the Central Ridge than any other ridge.

A lateral zonation of diagenetic mineral assemblages is common in saline, alkaline-lake deposits (Sheppard and Gude, 1968, 1969, 1973; Hay, 1977, 1978; Sheppard, 1973; Sheppard and others, 1978; Surdam, 1977; Surdam and Sheppard, 1978). Generally, a lateral basinward zonation of fresh glass --> alkalic, silicic zeolites --> analcime --> potassium feldspar is noted. Powder XRD analysis of the main zeolite bed at the DSV prospect reveals no such lateral zonation. Instead, the tuffs have been essentially monomineralically altered to chabazite. Genetic reasons for this are proposed under "Model of Zeolitization" below.

Relative percent amorphous material (glass) data are contoured in Fig. 7. The values range from 0 to 71%, are relatively low in the West and Central Ridges, and are highly variable with higher values northeastward in the East Ridge. The amount of glass present in any sample is in-

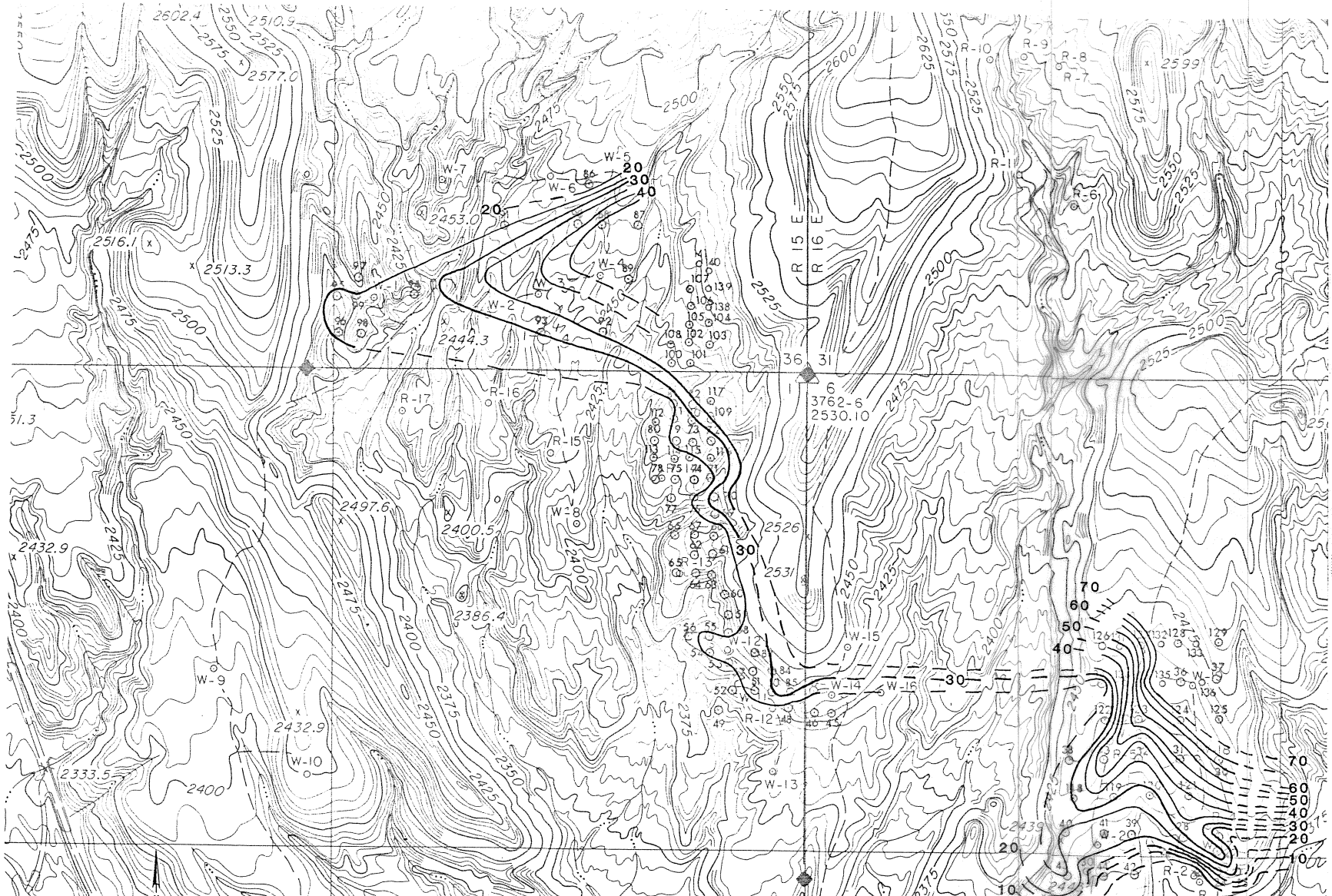
R 15 E
R 16 E
T 1
36
31
6
3762-6
2530.10
2602.4
2577.0
2516.1
2513.3
2453.0
2444.3
2497.6
2400.5
2432.9
2386.4
2333.5
2526
2531
2439
W-1
W-2
W-3
W-4
W-5
W-6
W-7
W-8
W-9
W-10
W-12
W-13
W-14
W-15
W-16
R-1
R-2
R-6
R-7
R-8
R-9
R-10
R-12
R-15
R-16
R-17
20
30
40
50
60
70
10

versely proportional to the degree of authigenic mineralization, particularly from zeolitization. The increasing amounts of glass in a northeasterly trend is correlative with decreasing chabazite content in this direction, again suggesting proximity of the basin margin to the northeast and deepening basin to the southwest of the East Ridge. The inverse relation between glass and zeolite also suggests the glass is the source material of the zeolite.

XRD analysis of drill hole samples of the main zeolite bed also detected minor quartz, feldspar, halite, fluorite, sphalerite, carbonate/calcite, montmorillonite, and amphibole. These minerals were found in only a few widely scattered samples and no lateral mineralization patterns are discernible.

Clay-mica (presumably mixed-layer illite/smectite) was detected in several holes. The content of clay-mica ranges from 0 to 25% with relatively moderate, uniform values slightly increasing to the southwest in the Central Ridge and with a roughly concentric zonation with higher values towards the center in the West and East Ridges.

Isopach Maps

Isopach maps of the alluvial and soil facies (Q_{al}, Q_p, and Q_{og} map units inclusive), upper red claystone, upper zeolite tuff, middle red claystone, and the main zeolite tuff were constructed from drill hole data. The isopach map of the alluvial and soil facies (Fig. 8) supports the hypothesis of southerly flowing paleodrainage between the West

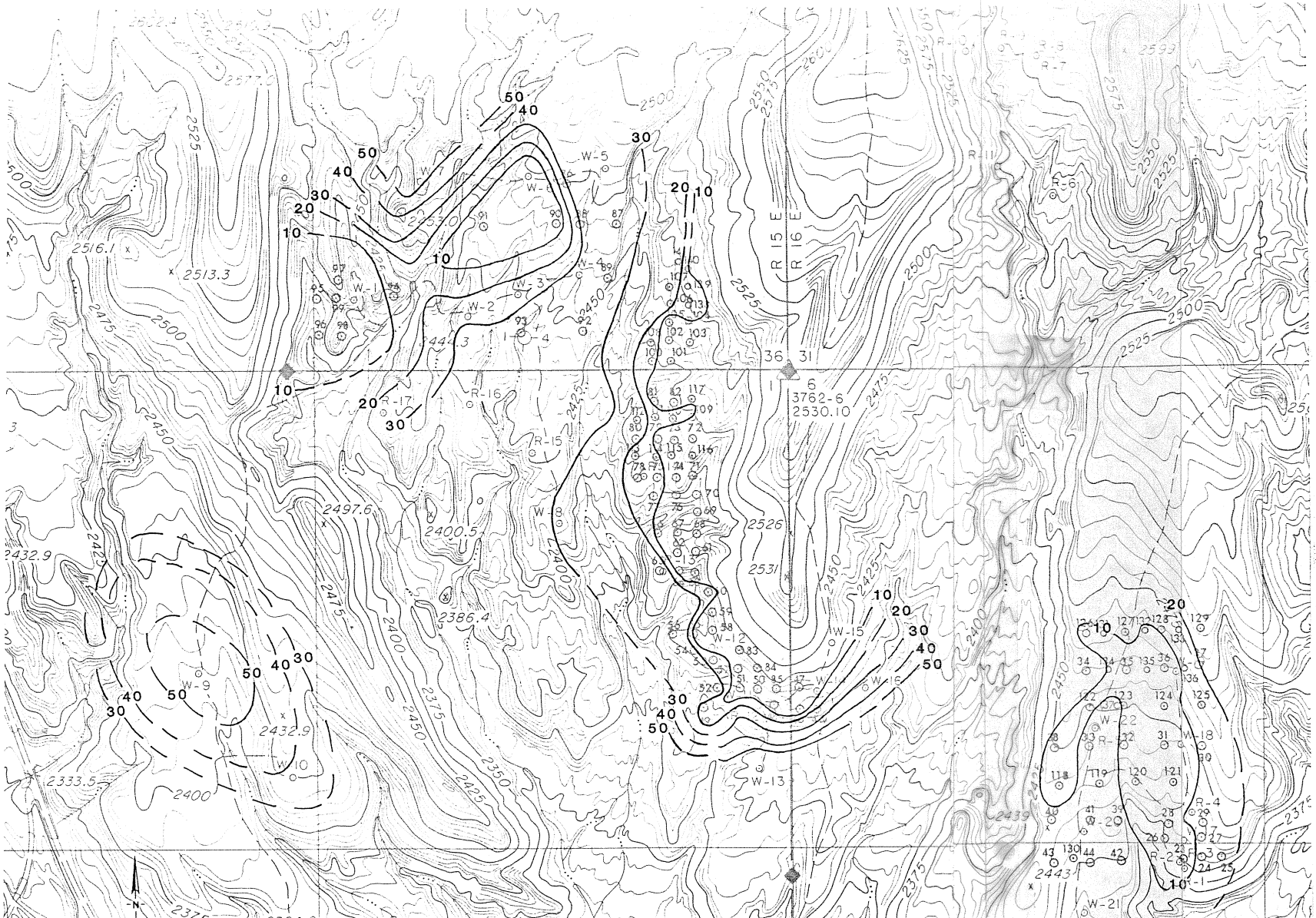
R 15 E
R 16 E
36
31
1
6
3762-6
2530.10
2516.1
2513.3
2497.6
2400.5
2386.4
2432.9
2333.5
2526
2531
2439
2443
W-1
W-2
W-3
W-4
W-5
W-9
W-10
W-12
W-13
W-15
W-16
W-18
W-20
W-21
W-22
R-4
R-6
R-15
R-16
R-17
10
20
30
40
50
2400
2425
2450
2475
2500
2525
2350
2375

and Central, and between the Central and East Ridges. This facies ranges from 0 to 60 ft (18.29 m) thick, is thickest in practically the same positions as the modern drainage, and generally gradually thins updip.

Portions of the lakebed units were eroded prior to deposition of the alluvial facies in many areas, and consequently, the thickness trends of the lakebeds are inversely related to those of the alluvial facies. This is illustrated on Fig. 9, an isopach map of the upper red claystone, whose thickness varies from 0 to 56 ft (17.07 m). The values in the Central Ridge decrease southwestward and southward and those in the East Ridge decrease southward and southeastward, due in part to erosion of the lakebeds prior to deposition of alluvial gravels. The large increase in thickness of the upper red claystone and upper zeolite tuff (Fig. 10) units along the line dividing secs. 1 and 36 on the Central Ridge is probably the result of downdropping on the north along an east-west-trending fault. Structure contour maps also support this conclusion (Figs. 19, 20).

The thickness of the upper zeolite tuff ranges from 0 to 5.5 ft (1.68 m) and averages approximately 1.25 ft (0.38 m) (Fig. 10). Anomalously high values of three to 5.5 ft (0.91 to 1.68 m) are present at the north end of the Central Ridge and the east side of the East Ridge. A 12.5 ft (3.81 m) thick value, measured from DH W-121, is regarded as unreliable. It is difficult to draw conclusions concerning the nature of this bed from its isopach map. It is uniformly

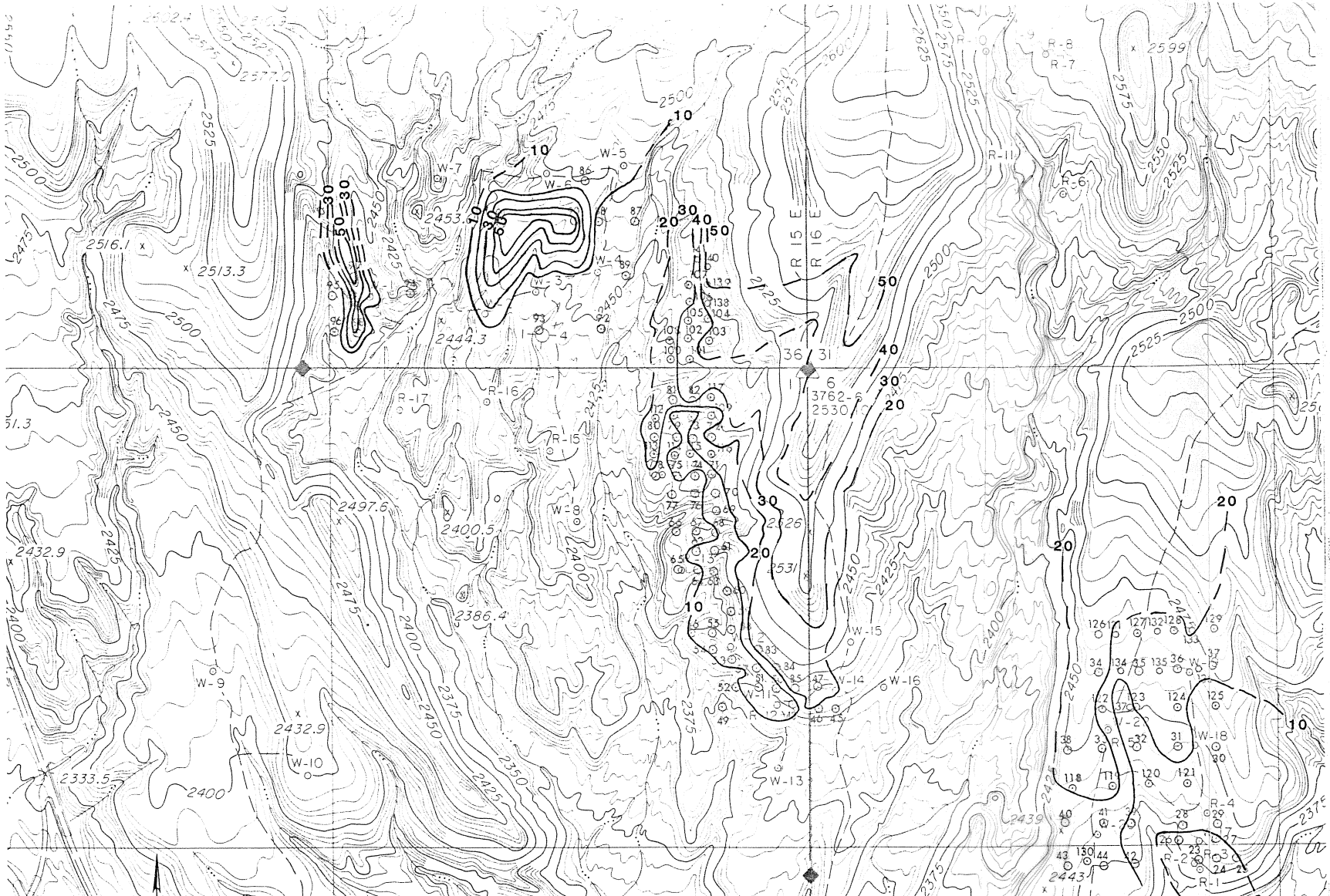
R 15 E
R 16 E
36
31
6
3762-6
2530
2516.1
2513.3
2453.1
2444.3
2497.6
2400.5
2432.9
2386.4
2432.9
2333.5
2531
2626
2439
2443
W-1
W-2
W-3
W-4
W-5
W-6
W-7
W-9
W-10
W-11
W-12
W-13
W-14
W-15
W-16
W-18
R-1
R-2
R-3
R-4
R-5
R-6
R-7
R-8
R-11
R-15
R-16
R-17

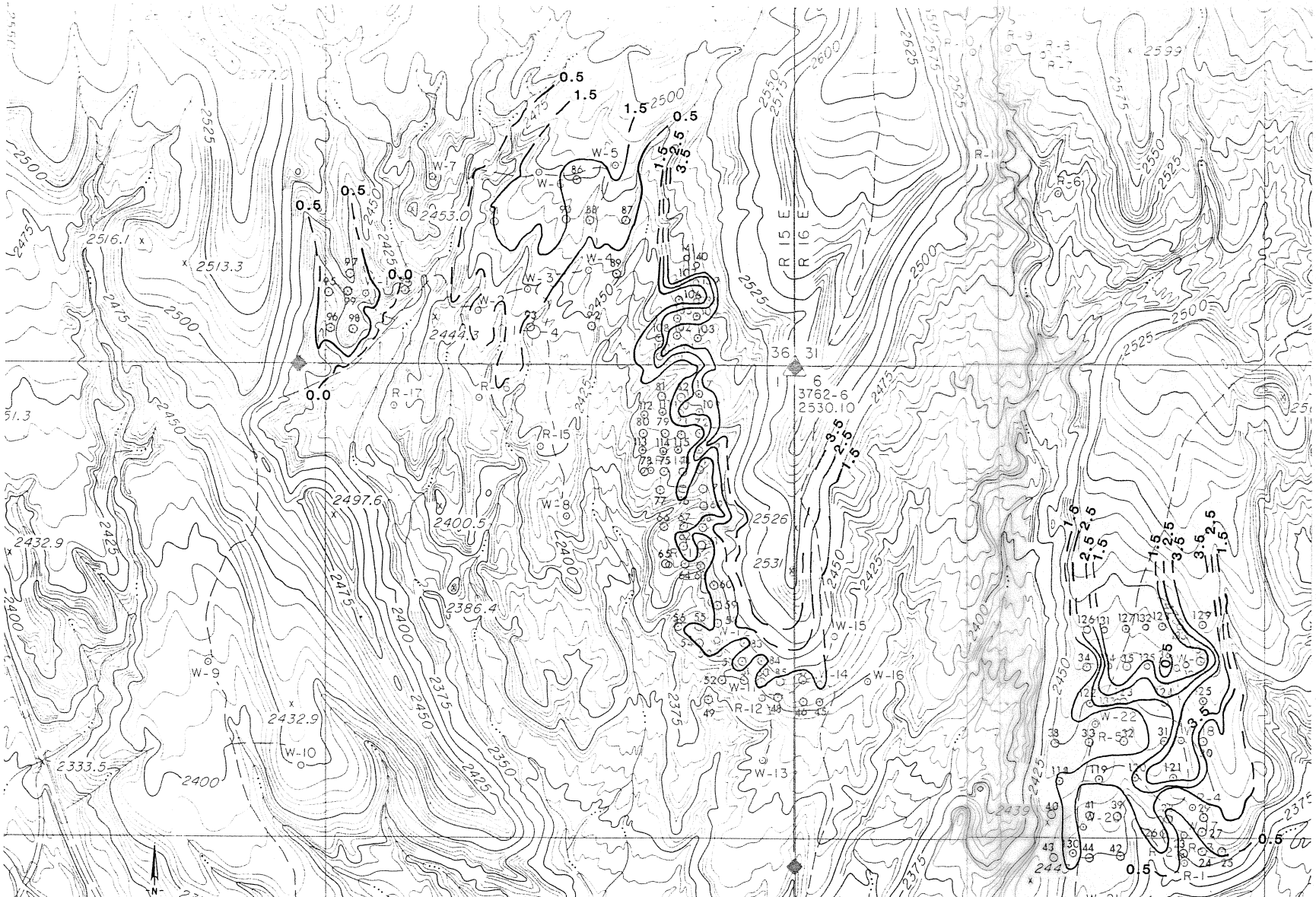
R 15 E
R 16 E
36
31
6
3762-6
2530.10
W-1
W-2
W-3
W-4
W-5
W-6
W-7
W-8
W-9
W-10
W-13
W-14
W-15
W-16
W-20
W-22
R-1
R-5
R-6
R-12
R-15
R-17
2516.1
2513.3
2444.4
2497.6
2400.5
2386.4
2432.9
2333.5
2253.0
2526
2531
2439
2443
0.5
1.5
2.5
3.5
0.0

thin in the West Ridge, increasingly thick northward in the Wash Ridge, increasingly thick northward and northeastward in the Central Ridge, and extremely variable in the East Ridge. Erosion prior to deposition of alluvial gravels, nonuniform deposition of the ash-fall tuff, the irregular basin bottom configuration upon which the tuff was deposited, and/or faulting may account for its inhomogeneous thickness.

The middle red claystone ranges up to 9.5 ft (2.90 m) thick, averages approximately five ft (1.52 m) thick, is of relatively uniform, average thickness in the West Ridge, increasingly thick northward in the Wash Ridge, and increasingly thick northeastward in the Central Ridge (Fig. 11). A concentric pattern with the greater thicknesses in the center is present in the East Ridge. An anomalously high 15.1 ft (4.60 m) thickness, recorded in DH W-122, is regarded as unreliable.

The thickness of the main zeolite tuff ranges from 0.25 to 1.74 ft (0.08 to 0.53 m) and generally mimics the bedding characteristics just described for the middle red claystone (Fig. 12). It is thinner in the East Ridge than elsewhere, most likely due to this ridge's proximity to the basin margin.

In summation, the lakebeds forming the four ridges are generally thicker northeastward away from the main paleodrainage channels. Minor faulting probably caused anomalous increases in the thickness of these beds over very short distances.

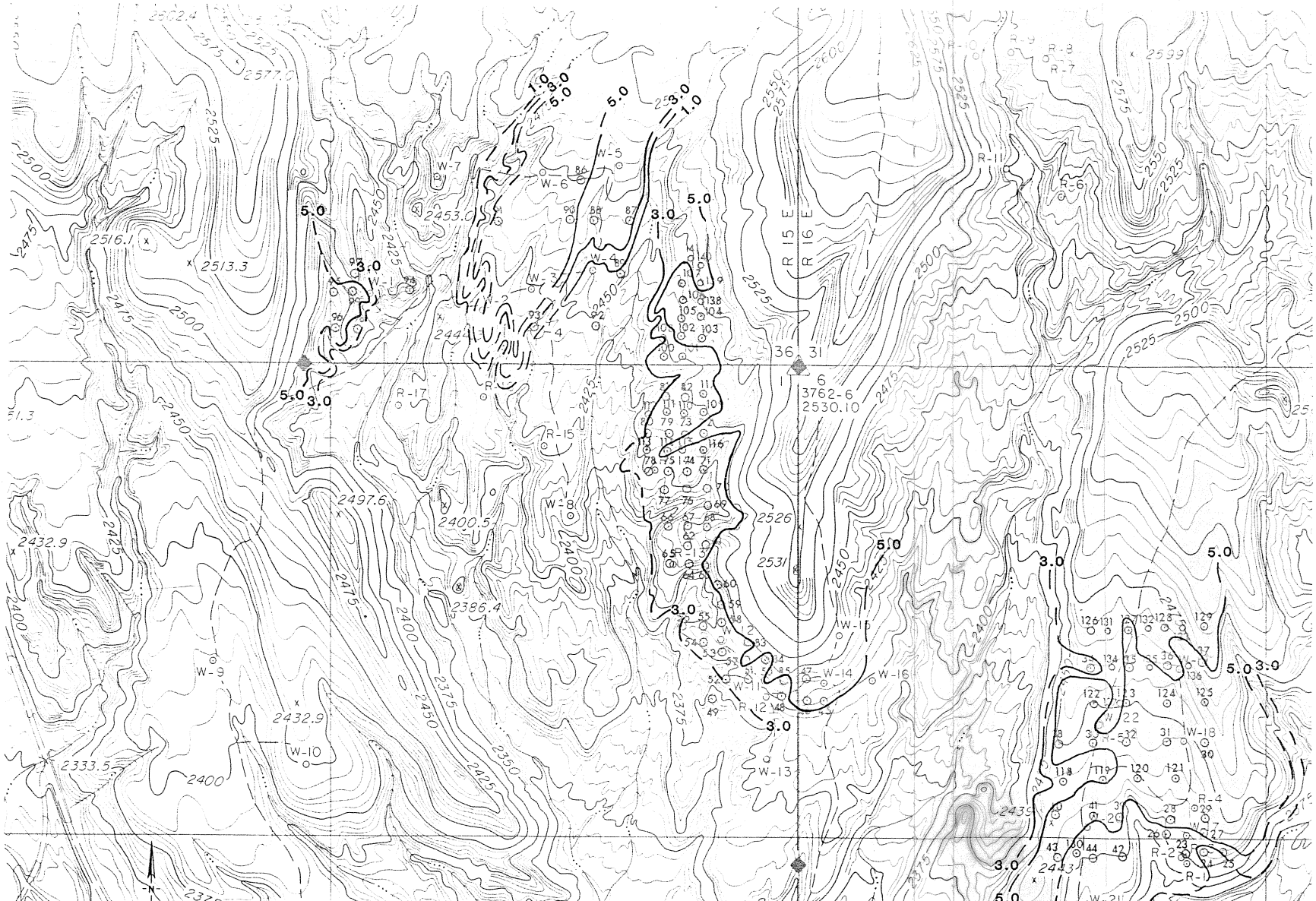
R 15 E
R 16 E
36
31
1
6
3762-6
2530.10
2513.3
2516.1
2497.6
2400.5
2386.4
2432.9
2333.5
2453.0
2526
2531
2435
W-1
W-2
W-3
W-4
W-5
W-6
W-7
W-8
W-9
W-10
W-11
W-12
W-13
W-14
W-15
W-16
W-17
W-18
R-1
R-2
R-3
R-4
R-5
R-6
R-7
R-8
R-9
R-10
R-11
R-12
R-15
R-17
5.0
3.0
1.0

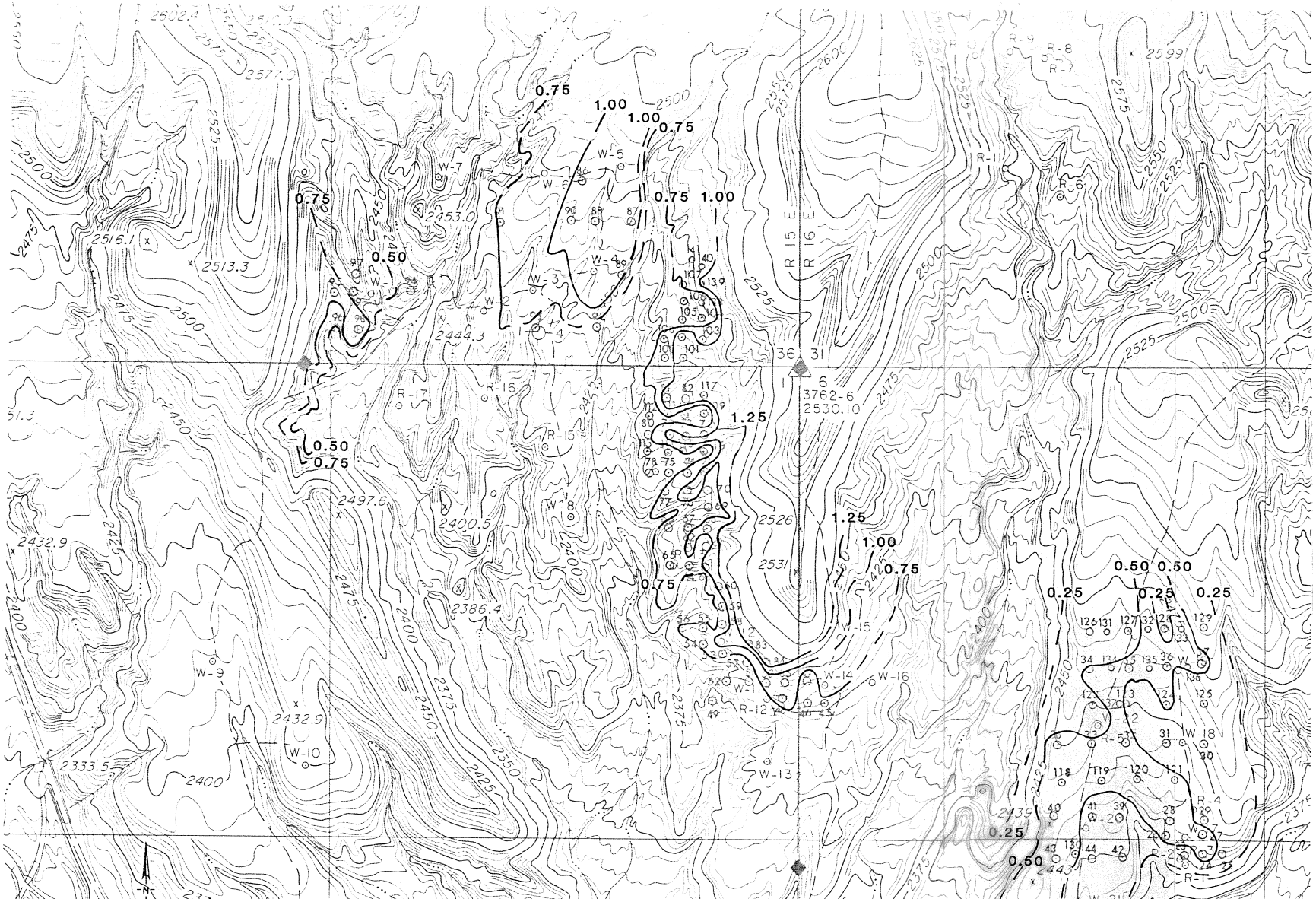
R 15 E
R 16 E
36
31
6
3762-6
2530.10
0.75
1.00
1.00
0.75
0.75
1.00
0.50
0.50
0.75
1.25
1.25
1.00
0.75
0.75
0.50 0.50
0.25
0.25
0.25
0.25
0.50
W-1
W-2
W-3
W-4
W-5
W-6
W-7
W-8
W-9
W-10
W-13
W-14
W-15
W-16
W-18
W-20
R-1
R-4
R-5
R-6
R-7
R-8
R-11
R-12
R-15
R-16
R-17
2516.1
2513.3
2444.3
2453.0
2577.0
2602.4
2497.6
2400.5
2386.4
2432.9
2333.5
2526
2531
2439
2443

Structure Contour Maps and Drill Hole Cross Sections

The structure contour maps constructed from the available drill hole data illustrate the geometry of the DSV sedimentary basin at the time of deposition of various rock units. Datum is mean sea level for all five of these maps. The inexact nature of these maps should be noted. For most drill holes, the collar elevation had to be estimated from the base map, and therefore, the accuracy of the calculations of the elevation of the bottom of the rock units is directly dependent upon the accuracy of the collar elevations, which are accurate to $\pm$ three feet (0.91 m).

Drill hole cross sections have also been constructed from the drill hole data and base map (Figs. 13, 14, 15). Some of the drill holes were moved into the plane of section (by moving them perpendicular to it) in an effort to provide a more detailed view of the basin. Cross sections A-A', B-B', and C-C' illustrate the lakebeds dip very gently basinward (Figs. 13, 14, 15). A fault between holes W-79 and W-113 in the Central Ridge has displaced the lakebeds southwest of the fault downward. Possible faulting between holes W-32 and W-40 may have displaced the sediments encountered by hole W-119 further into the subsurface, and may be responsible for the anomalously great thickness of the T_{uc} unit in DH W-119.

The structure contour map on the bottom of the alluvial and soil facies unit provides further evidence that the paleodrainage was directed the same, but had encroached topographically higher up the lakebed ridges, than present

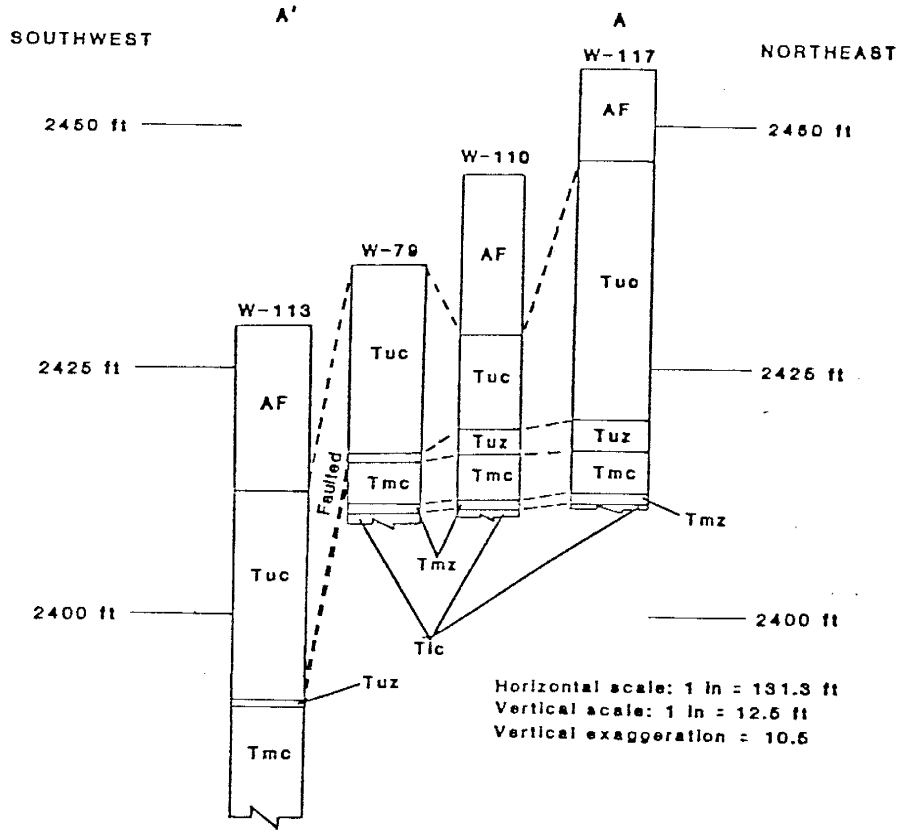

Figure 13. Cross-section through drill holes W-117, W-110, W-79, and W-113 along the Central Ridge.

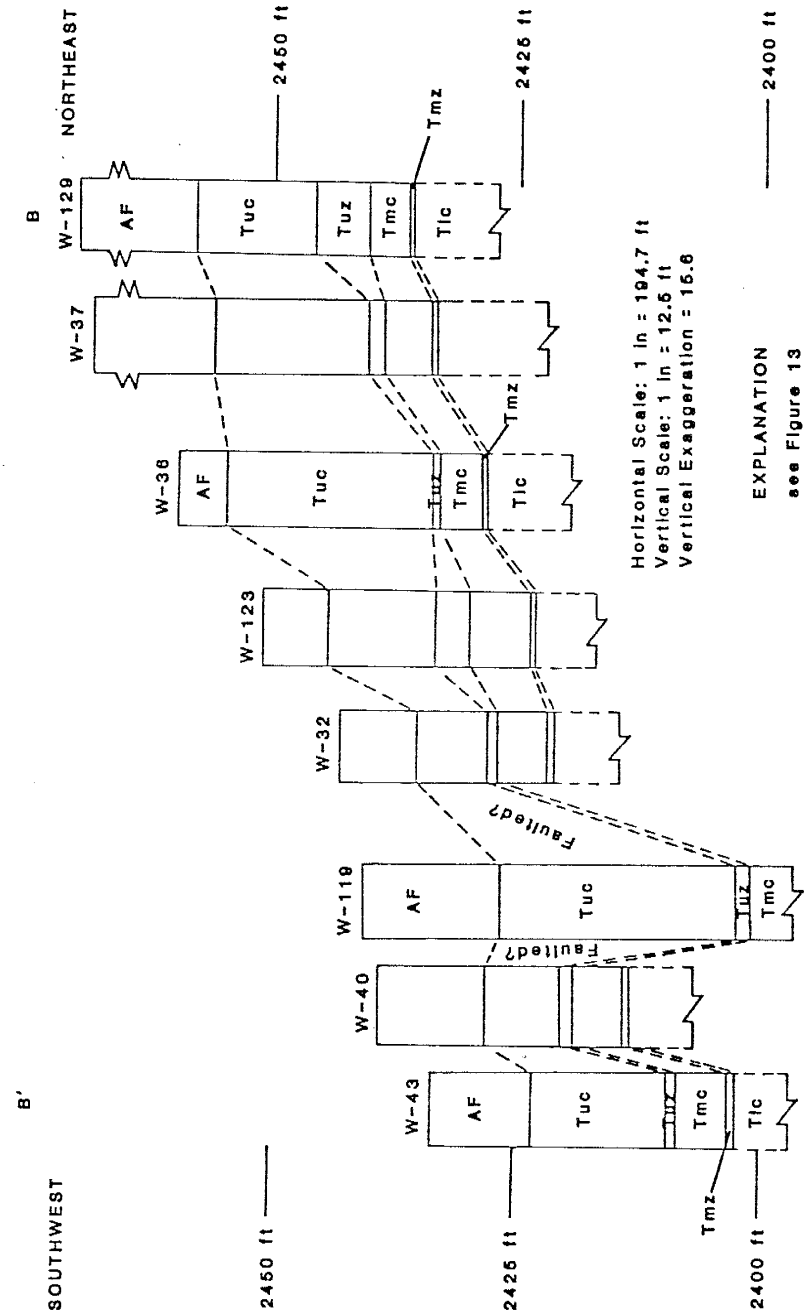

Figure 14. Cross-section along the East Ridge. Holes W-37, W-123, and W-40 have been moved perpendicularly into the plane of the section.

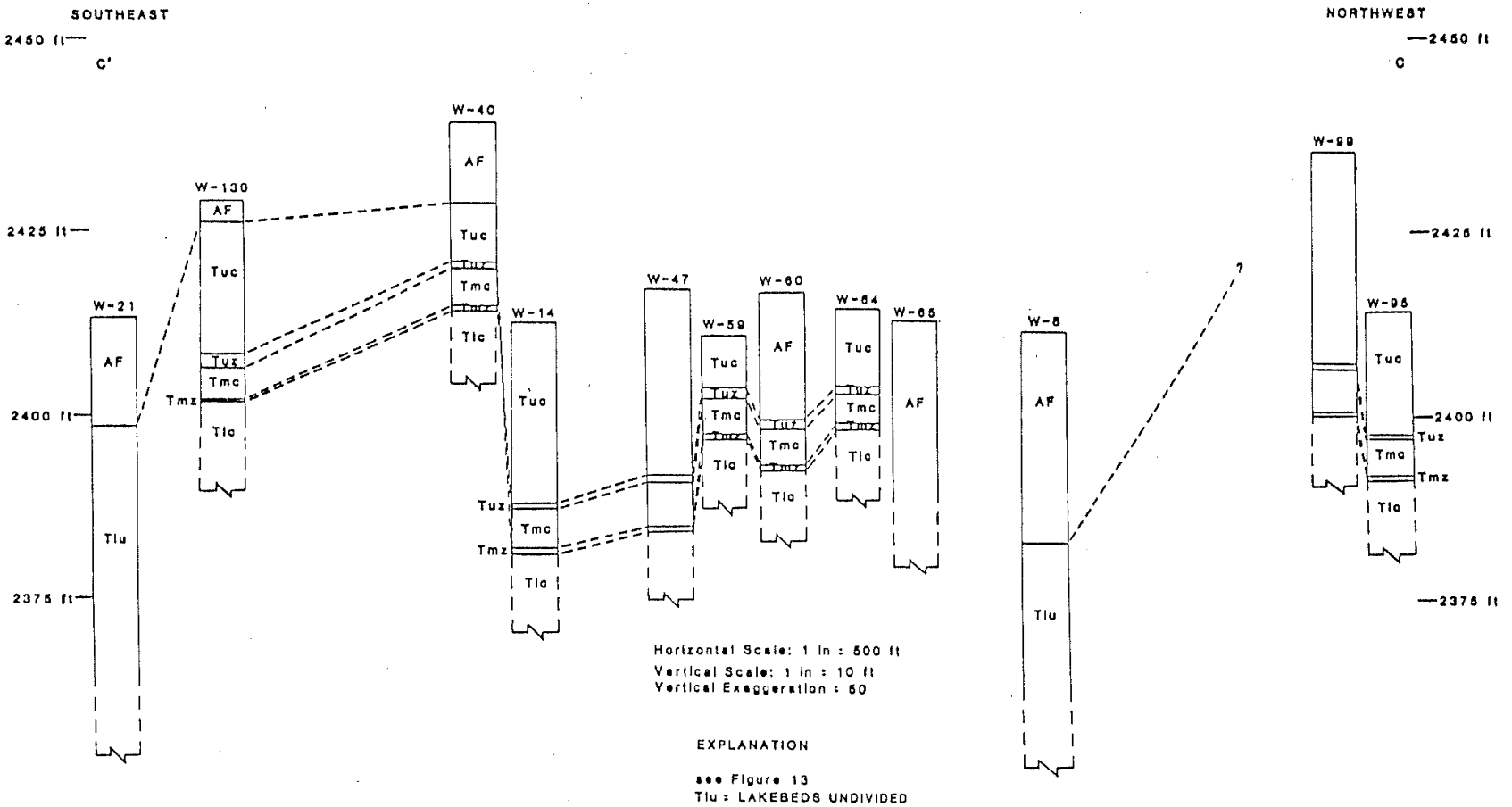

Figure 16. Cross-section C-C' through the Anaconda base map area. Holes W-99, W-8, W-64, W-60, W-14, W-40, and W-21 have been moved perpendicularly into the plane of the section.

drainage (Fig. 16). The elevation of the bottom of the alluvial and soil facies unit decreases southward off the ridges, suggesting that these ridges are the remnant of a surface which was topographically positive and sloped gently south so that the paleodrainage flowed south over it towards the deeper parts of the basin.

The structure contour maps on the bottom of the upper red claystone (Fig. 17), the bottom of the upper zeolite tuff (Fig. 18), the bottom of the middle red claystone (Fig. 19), and the bottom of the main zeolite tuff (Fig. 20) also illustrate that the ridges were higher than the basin to the southwest during deposition of these units. The elevations in question increase northward into the ridges (closer to the basin margin) and decrease southward towards the basin center.

The isopach maps of the upper red claystone and upper zeolite tuff suggest a generally east-west-trending fault, downthrown on the north side, along the line dividing secs. 1 and 36 on the Central Ridge. Structure contour mapping on the bottom of the middle red claystone and main zeolite tuff also indicates a fault there. The elevations of the bottoms of the units north of the fault average four feet (1.22 m) less than those south of the fault.

The structure contour maps on the middle red claystone and main zeolite tuff provide a valuable tool for future exploration of the DSV chabazite prospect. The drill hole data reveal the main zeolite bed is present between the

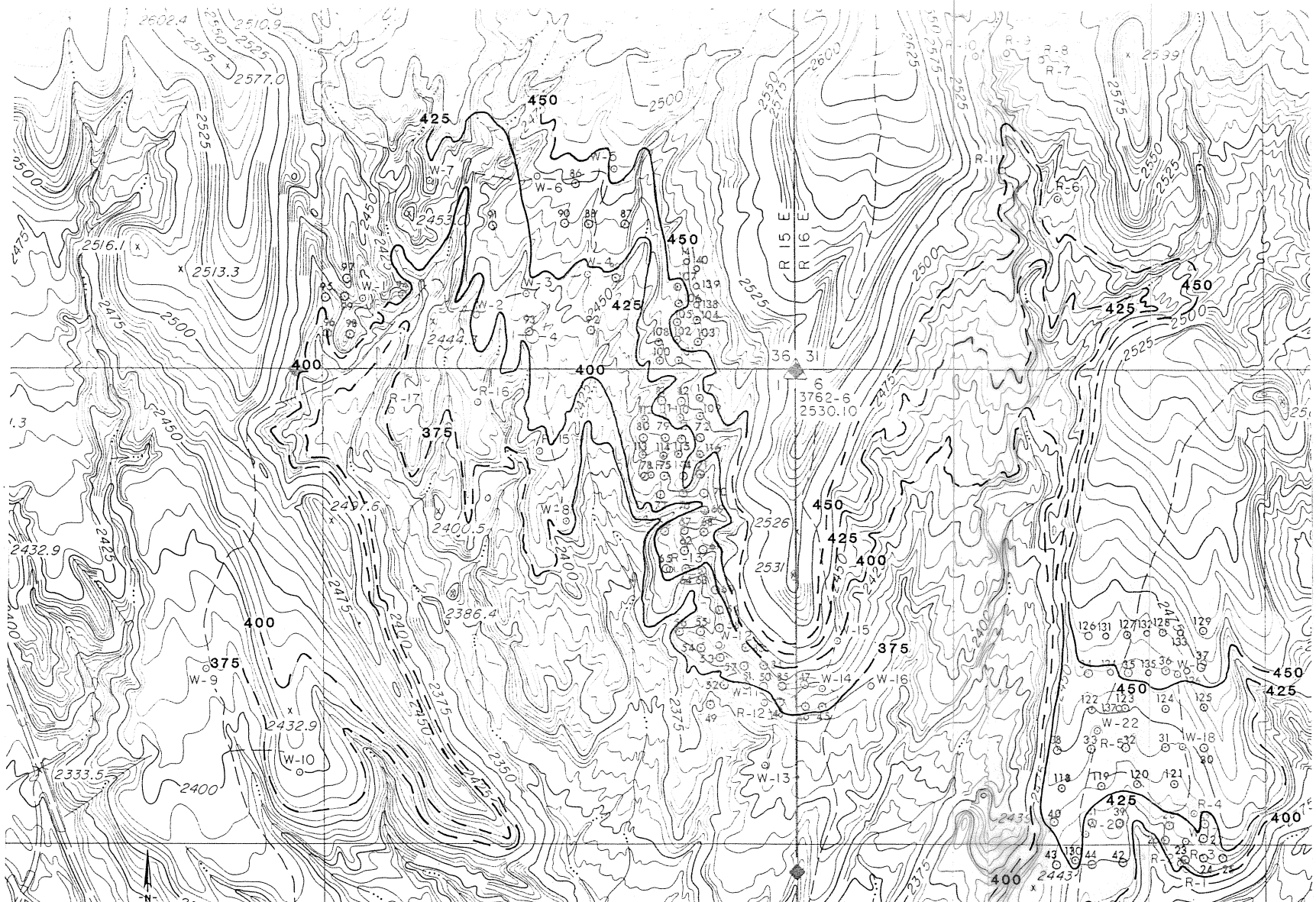
R 15 E
R 16 E
36
31
6
3762-6
2530.10
W-1
W-2
W-3
W-4
W-5
W-6
W-7
W-8
W-9
W-10
W-11
W-12
W-13
W-14
W-15
W-16
W-18
W-20
W-22
R-1
R-2
R-3
R-4
R-5
R-6
R-7
R-8
R-10
R-11
R-12
R-15
R-16
R-17
2577.0
2516.1
2513.3
2453.0
2444.7
2432.9
2333.5
2386.4
2400.5
2526
2531
2439
2443
450
425
400
375
2500
2525
2550
2575
2600
2625
2475
2450
2425
2400
2375
2350

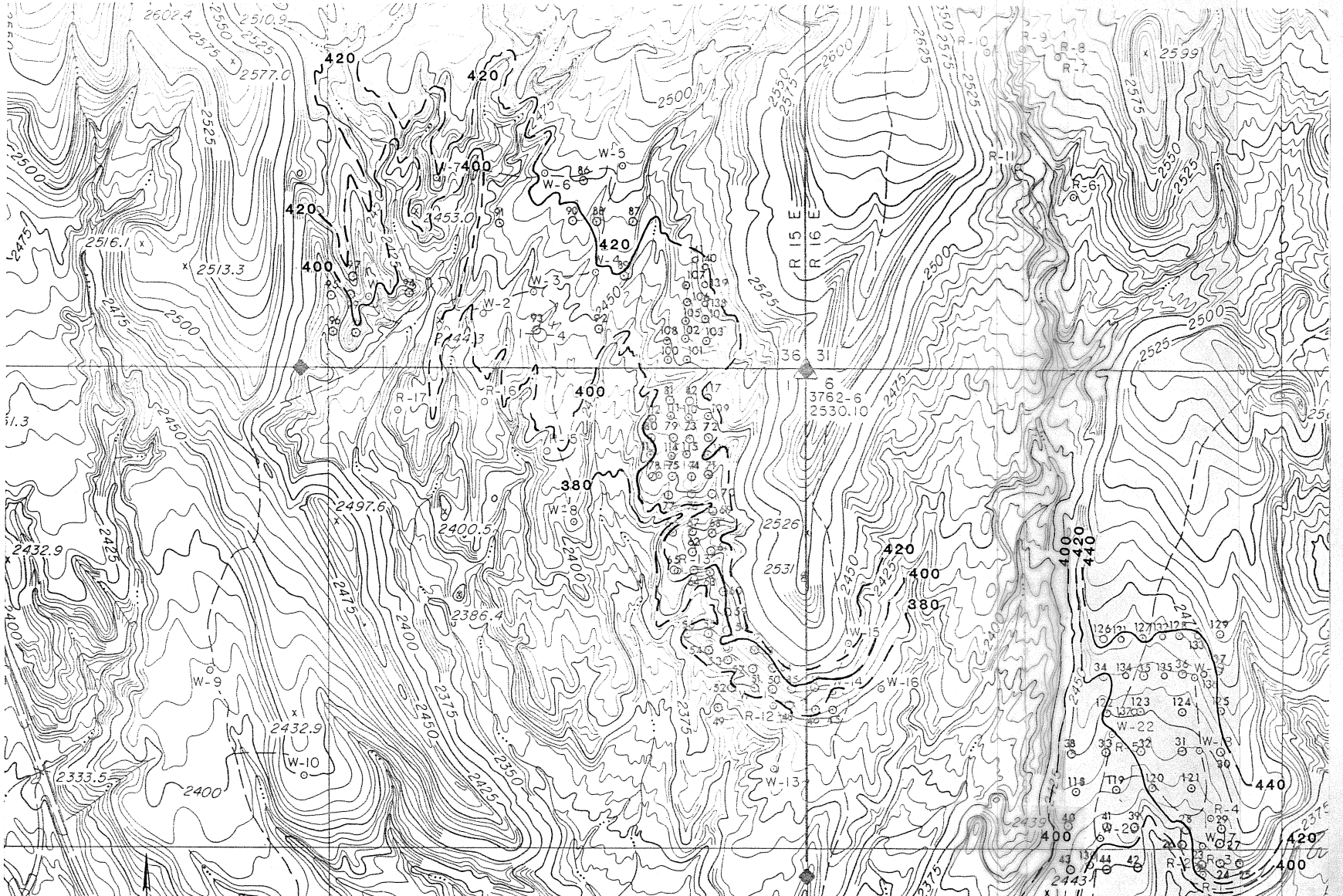
R 15 E
R 16 E
36
31
6
3762-6
2530.10
W-1
W-2
W-3
W-4
W-5
W-6
W-7
W-9
W-10
W-13
W-15
W-16
W-20
W-22
R-1
R-2
R-3
R-4
R-5
R-6
R-7
R-8
R-9
R-10
R-11
R-12
R-16
R-17
2602.4
2577.0
2516.1
2513.3
2497.6
2400.5
2432.9
2386.4
2333.5
2453.0
2526
2531
2599
2439
2443
420
400
380
440

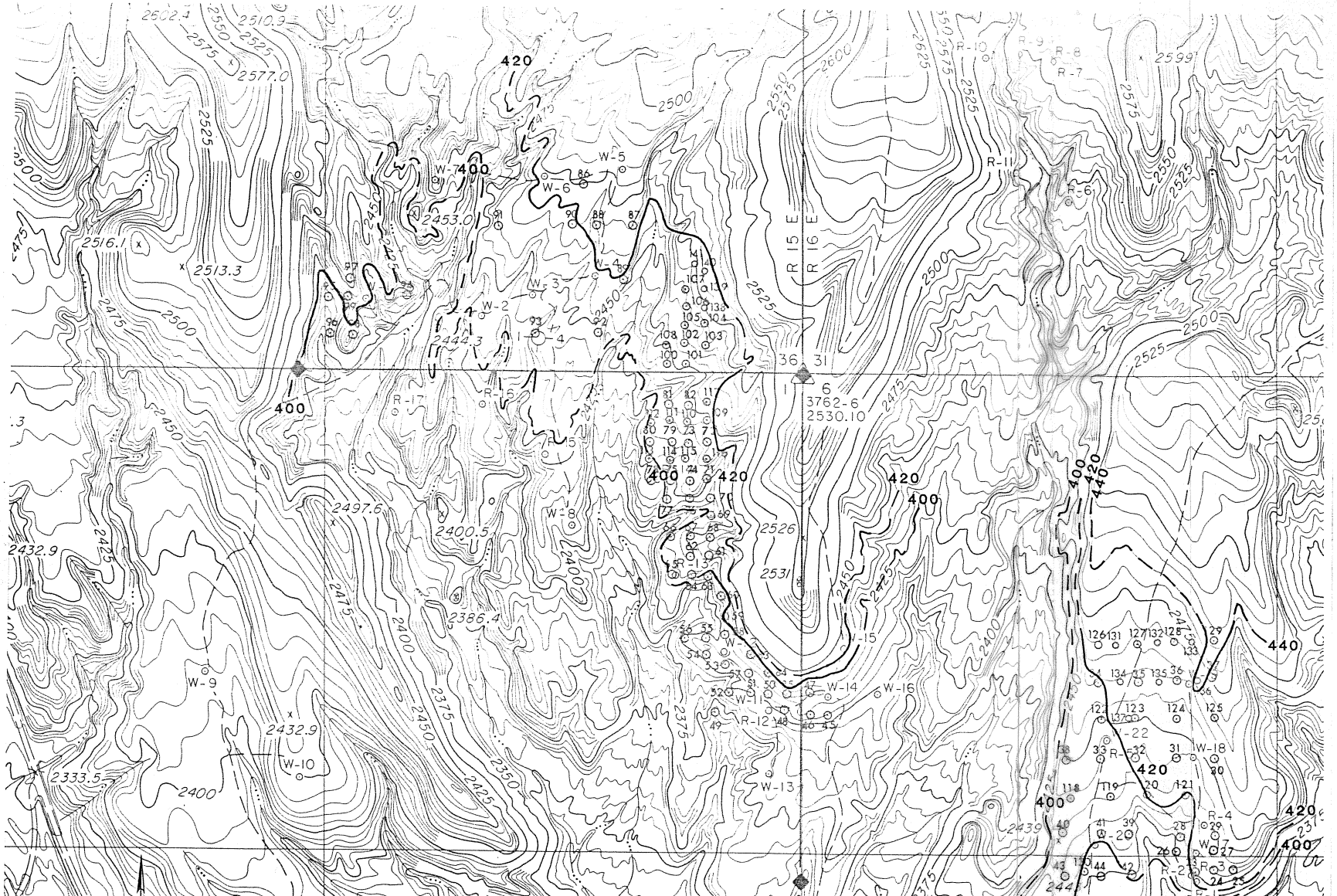
R 15 E
R 16 E
T 36
T 31
6
3762-6
2530.10
W-1
W-2
W-3
W-4
W-5
W-6
W-7
W-8
W-9
W-10
W-11
W-12
W-13
W-14
W-15
W-16
W-18
W-20
W-22
R-1
R-2
R-3
R-4
R-5
R-6
R-7
R-8
R-9
R-10
R-11
R-12
R-15
R-16
R-17
R-19
R-20
R-22
2577.0
2513.3
2516.1
2453.0
2444.3
2497.6
2400.5
2386.4
2432.9
2333.5
2439
2526
2531
2599
400
420
440

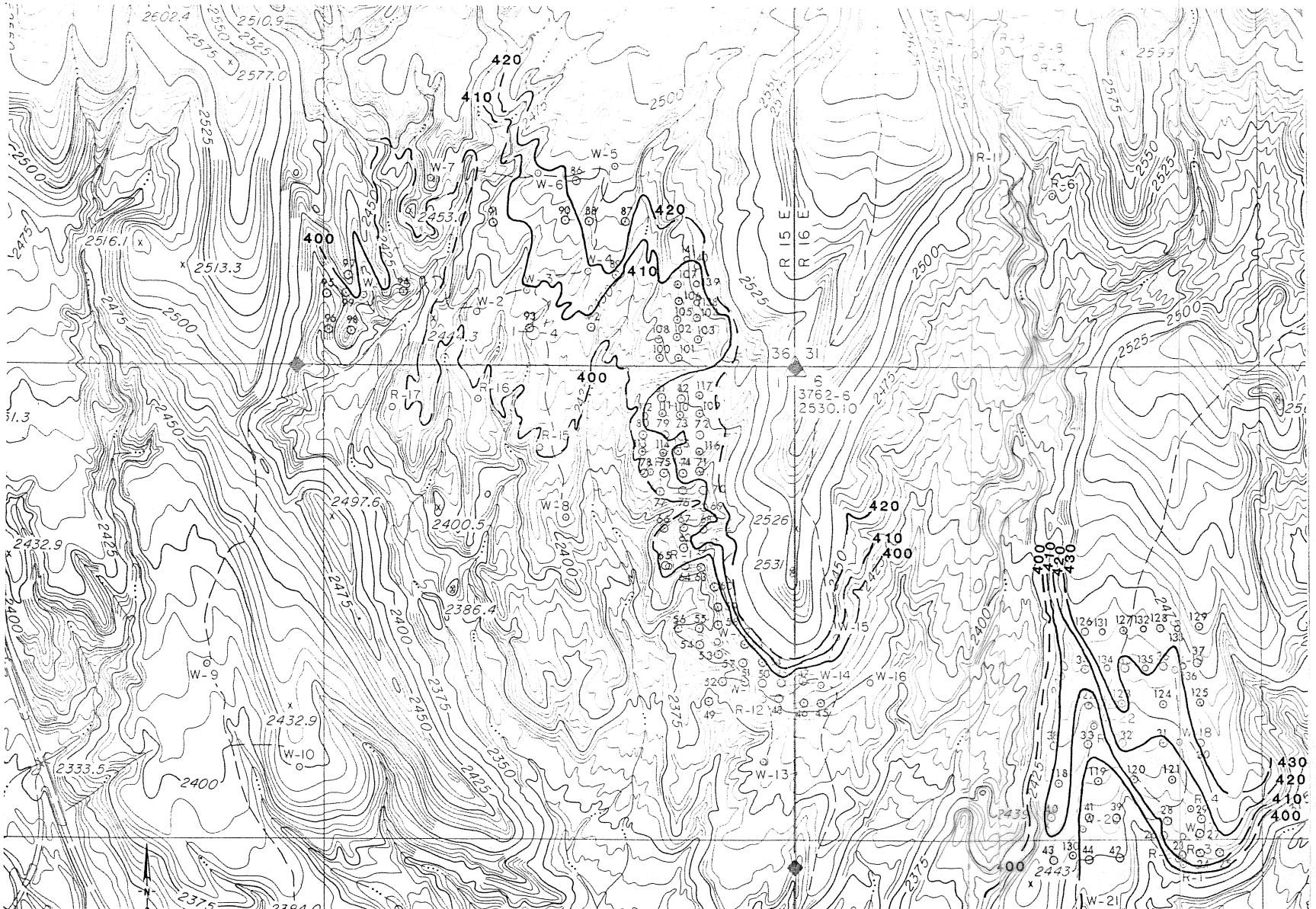
R 15 E
R 16 E
36
31
6
3762-6
2530.10
W-1
W-2
W-3
W-4
W-5
W-6
W-7
W-8
W-9
W-10
W-11
W-12
W-13
W-14
W-15
W-16
W-17
W-18
W-19
W-20
W-21
R-1
R-2
R-3
R-4
R-5
R-6
R-7
R-8
R-9
R-10
R-11
R-12
R-13
R-14
R-15
R-16
R-17
2516.1
2513.3
2577.0
2510.9
2453.1
2497.6
2400.5
2386.4
2432.9
2333.5
2526
2531
2443
400
410
420
430
2500
2525
2550
2575
2475
2450
2425
2400
2375
N

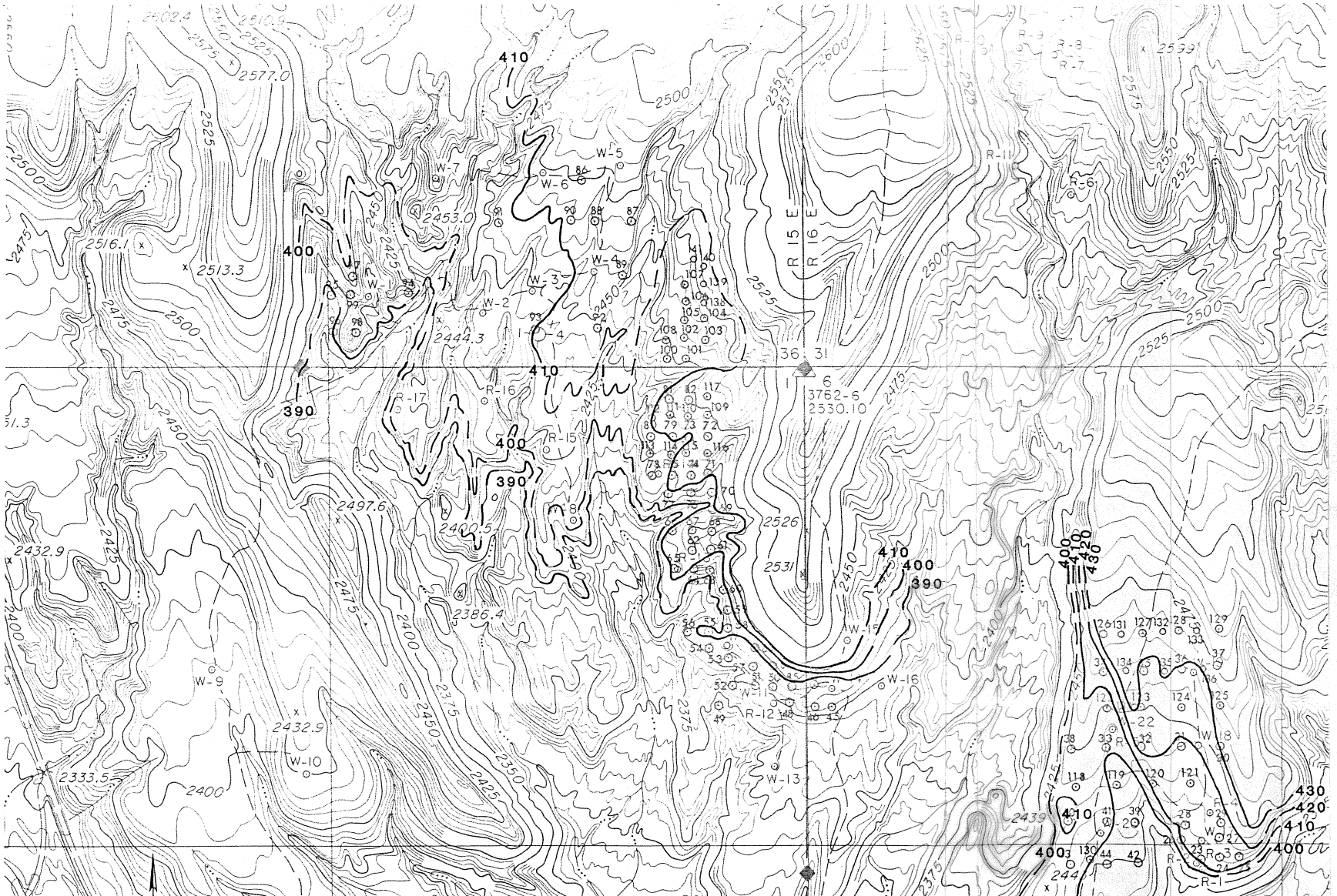
R 15 E
R 16 E
36
31
6
3762-6
2530.10
W-1
W-2
W-3
W-4
W-5
W-6
W-7
W-9
W-10
W-11
W-12
W-13
W-15
W-16
R-11
R-12
R-13
R-15
R-16
R-17
2602.4
2577.0
2516.1
2513.3
2453.0
2444.3
2497.6
2432.9
2432.9
2386.4
2333.5
2526
2531
2439
410
400
390
430
420

elevations of 2380 to 2436 ft (725.4 to 742.5 m). Faulting may have expanded the range of elevations at which the bed is present in some as yet unexplored areas. Knowledge of the configuration of the basin bottom, the relative positions and movements of faults, and delineation of paleochannels that have removed portions of the tuffs, will aid future targeting of the zeolite resource.

CLAY MINERALOGY

Results of Semi-Quantitative XRD Analysis

Semi-quantitative XRD analysis of the less-than-two micron size fraction was undertaken to examine lateral and vertical mineralogical trends in the DSV sedimentary suite. Discrete illite, mixed-layer illite/smectite, chlorite, sodium smectite (montmorillonite), and kaolinite, in decreasing order of relative abundance, are present in the clay size fraction of the lacustrine and alluvial facies (Table 2). These five clay mineral groups were also detected by XRD semi-quantitative analysis of bulk, powder-press samples in trace to minor amounts. Subordinate quartz, calcite, dolomite, halite, gypsum, orthoclase and plagioclase feldspar, chabazite, clinoptilolite, and pyrite were also detected. Although sepiolite and attapulgite frequently occur in saline, alkaline-lacustrine deposits, these minerals were not detected in the lakebeds of DSV.

Scanning electron micrographs of the middle red claystone (T_{mc}) from locality 1 (Figs. 21, 22, 23, 24) illustrate the unit is illitic, and also contains chlorite, smectite, chabazite, iron oxide(?), unaltered glass, and detrital quartz and/or calcite. These are the only minerals identifiable from the microanalysis of this claystone.

Diagenetic illite occurs as pore-lining, elongate spines or fibers up to approximately two micrometers long (Figs. 21, 23, 24). It appears to be coating detrital glass or, less probably, quartz grains. Chlorite occurs primarily

Table 2. Clay mineral group composition of DSV lacustrine and alluvial facies samples as determined by XRD semi-quantitative analysis of the less-than-two micron size fraction. Results reported in parts in 10. Rounding of figures has produced deviations from the ideal sum of 10 parts in 10 for individual samples. I = illite, S = sodium montmorillonite (smectite), I/S = mixed-layer illite-smectite, K = kaolinite, C = chlorite.

Rock Unit	Sample	Locality	I	S	I/S	K	C
T_{lc}	040584-2	86	2	1	4	1	2
	101084-1	82	3	1	3	1	2
	100984-4	79	3	4	4	0	0
		Average in unit	3	2	4	1	1
T_{mc}	111383-1	1	3	0	3	1	2
	111383-14	2	4	1	5	0	1
	111483-2	4	3	2	5	0	1
	111483-14	5	2	0	2	1	4
	040584-4	86	3	0	2	3	3
	101084-4 (T_{mc}?)	83	2	1	3	1	3
		Average in unit	3	1	3	1	2
T_{uc}	080584-16	61	0	10	0	0	0
	080384-11	46	3	1	1	2	3
	111383-6	1	6	0	1	1	2
	111383-8	1	4	0	2	1	2
	111383-9	1	4	1	4	1	3
	111383-10	1	2	1	5	1	2
	111383-11	1	2	1	7	0	0
	111383-18	2	3	2	4	1	1
	111383-19	2	3	1	3	1	3
	111383-21	2	4	1	3	1	2
	111483-8 (T_{uc}?)	4	3	0	1	2	4
	111483-13	5	4	2	4	0	1
	111483-15	5	3	2	5	1	1
	040584-7	86	4	1	4	1	1
		Average in unit	3	2	3	1	2
T_{lu}	080884-2	70	6	1	3	0	1
	080884-6	74	5	1	3	0	1
	080984-2	76	1	1	1	2	6
	080984-5	76	2	3	1	1	3
		Average in unit	3	1	2	1	3

Table 2 (con't)

			I	S	I/S	K	C
Average in the above 27 claystone samples			3	1	3	1	2
Q_{og}	111383-12	1	4	0	5	0	1
	111383-13	1	4	0	2	1	2
	111383-22	2	3	1	1	2	4
	111483-7	4	5	1	3	1	3
	111483-10	4	4	0	4	1	1
	080984-7	76	2	3	1	1	3
Average in unit			4	1	3	1	2

	Sample	Rock Unit	I	S	I/S	K	C
Vertical Section at Locality 1	111383-1	T_{mc}	3	0	3	1	2
	111383-6	T_{uc}	6	0	1	1	2
	111383-8	T_{uc}	4	0	2	1	2
	111383-9	T_{uc}	4	1	4	1	3
	111383-10	T_{uc}	2	1	5	1	2
	111383-11	T_{uc}	2	1	7	0	0
	111383-12	Q_{og}	4	0	5	0	1
	111383-13	Q_{og}	4	0	2	1	2
Average in section			4	1	4	1	2
Vertical Section at Locality 4	111483-2	T_{mc}	3	2	5	0	1
	111483-8	T_{uc}(?)	3	0	1	2	4
	111483-7	Q_{og}	5	1	3	1	3
	111483-10	Q_{og}	4	0	4	1	1
Average in section			4	1	3	1	2
Vertical Section at Locality 86	040584-2	T_{lc}	2	1	4	1	2
	040584-4	T_{mc}	3	0	2	3	3
	040584-7	T_{uc}	4	1	4	1	1
Average in section			3	1	3	1	2
Vertical Section at Locality 76	080984-2	T_{lu}	1	1	1	2	6
	080984-5	T_{lu}	2	2	2	2	3
	080984-7	Q_{og}	2	3	1	1	3
Average in section			2	2	1	2	4

Figure 21. Scanning electron micrograph of the middle red claystone from locality 1. Pore-lining, diagenetic illite elongate spines or fibers appear to be coating a glass or quartz grain. Pseudohexagonal chlorite platelets and isolated chabazite "cubes" or "rhombs" are also present. (Sample 111383-1).

Figure 22. Scanning electron micrograph of the middle red claystone from locality 1. At least two ovoid packets of flakes, which are most likely iron oxide particles, are readily visible in the center. Pseudohexagonal chlorite plates are also present. (Sample 111383-1).

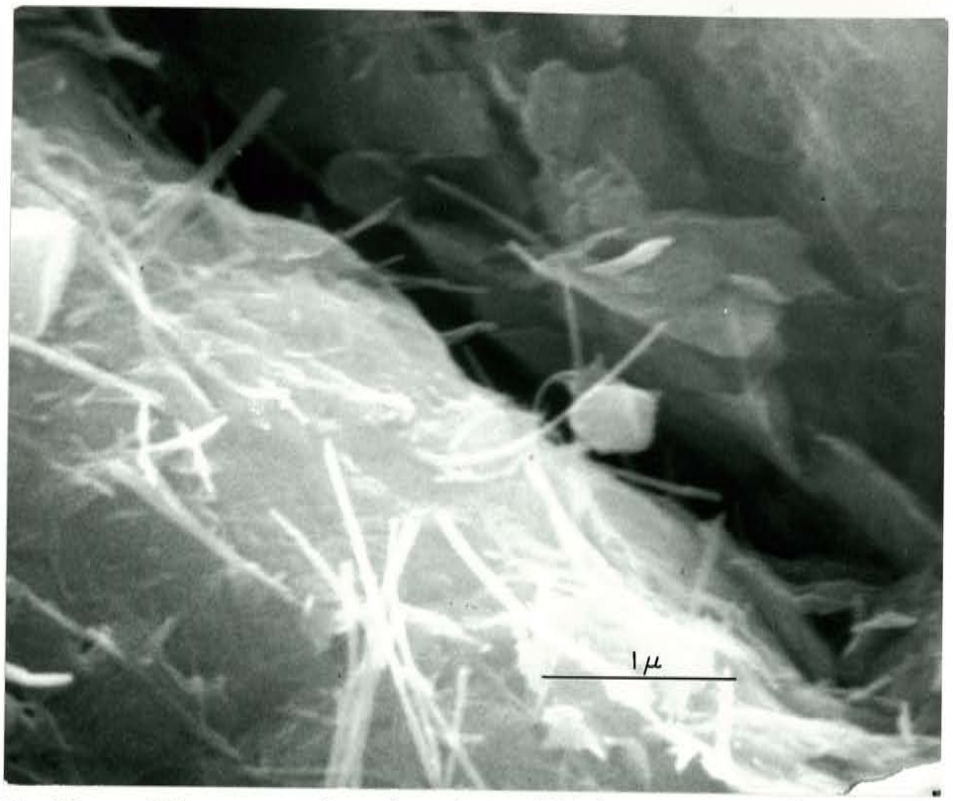

Figure 21. Micrograph showing illite, chlorite, and chabazite.

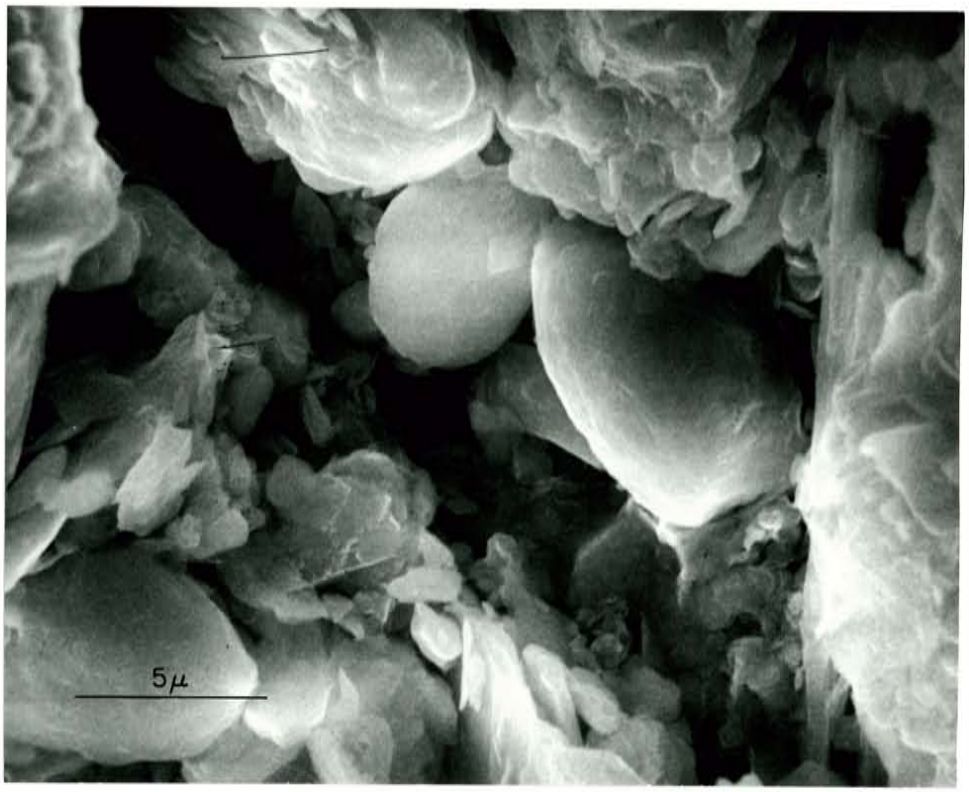

Figure 22. Micrograph showing probable iron oxide packets and chlorite plates.

Figure 23. Scanning electron micrograph of the middle red claystone from locality 1. Abundant, elongate spines of diagenetic illite coat detrital glass(?) grains. Thin, pseudohexagonal, "two-dimensional" cardhouse structure chlorite plates are interspersed through the picture area. (Sample 111383-1).

Figure 24. Scanning electron micrograph of the middle red claystone from locality 1. Diagenetic illite fibers and leafy smectite coat detrital glass(?) grains. Pseudohexagonal chlorite plates are also present. (Sample 111383-1).

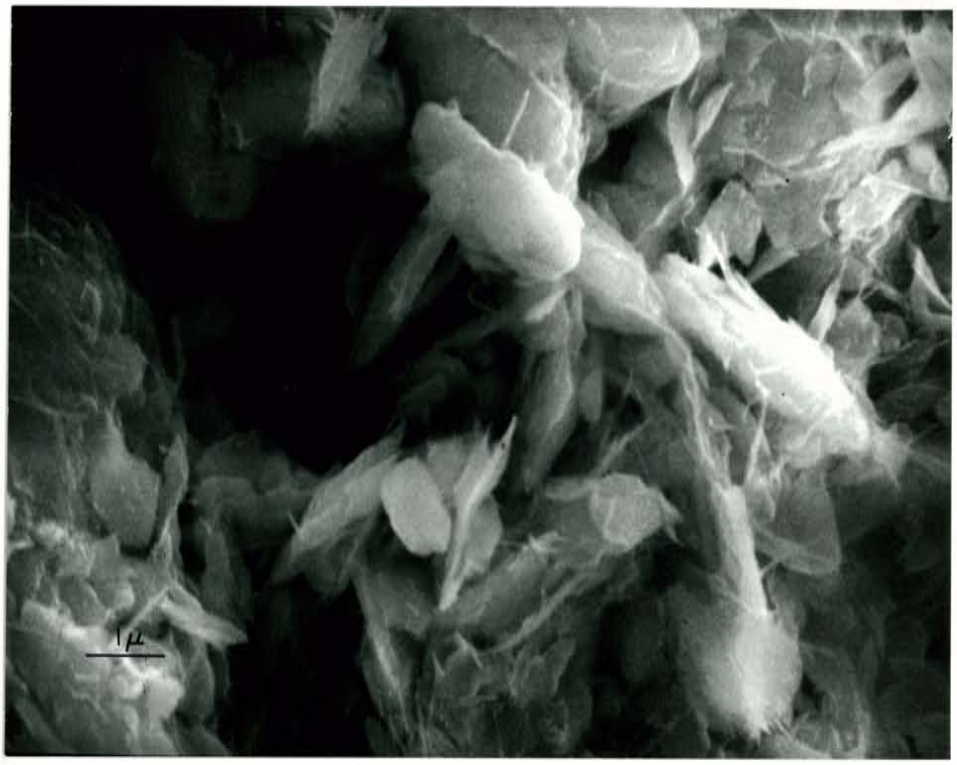

Figure 23. Illite, glass(?), and chlorite.

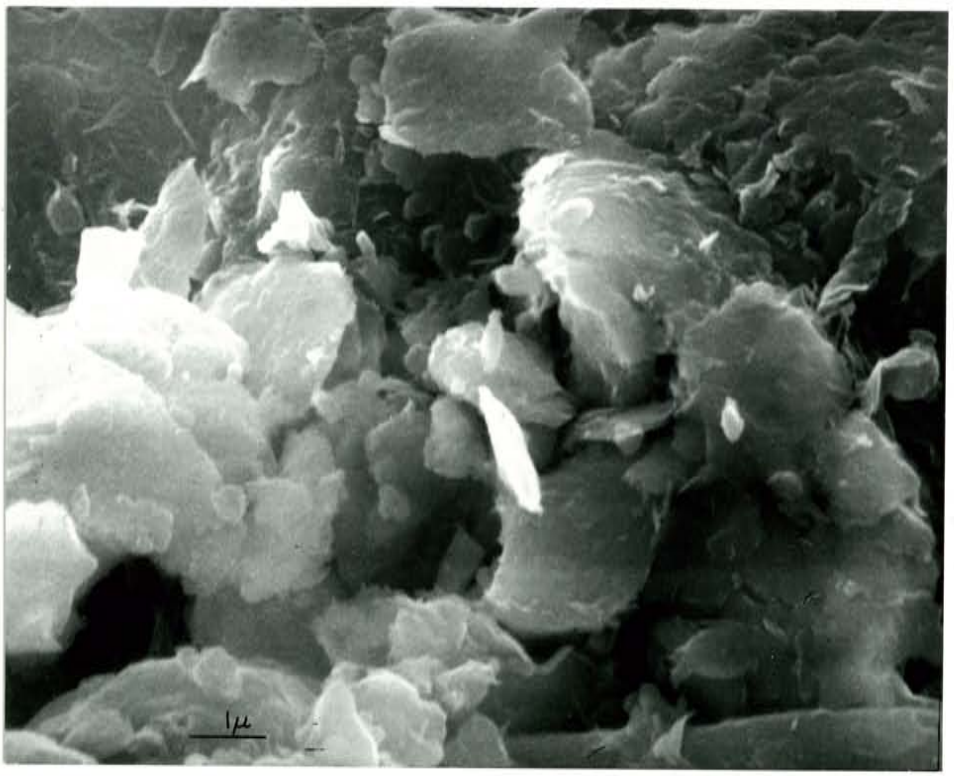

Figure 24. Illite, smectite, and chlorite.

Figure 25. Scanning electron micrograph of the upper red claystone from locality 1. Abundant, leafy smectite and mixed-layer illite/smectite coat an etched, detrital glass grain. Clusters of chabazite "cubes" or "rhombs" are also pseudomorphic after the glass. (Sample 111383-6).

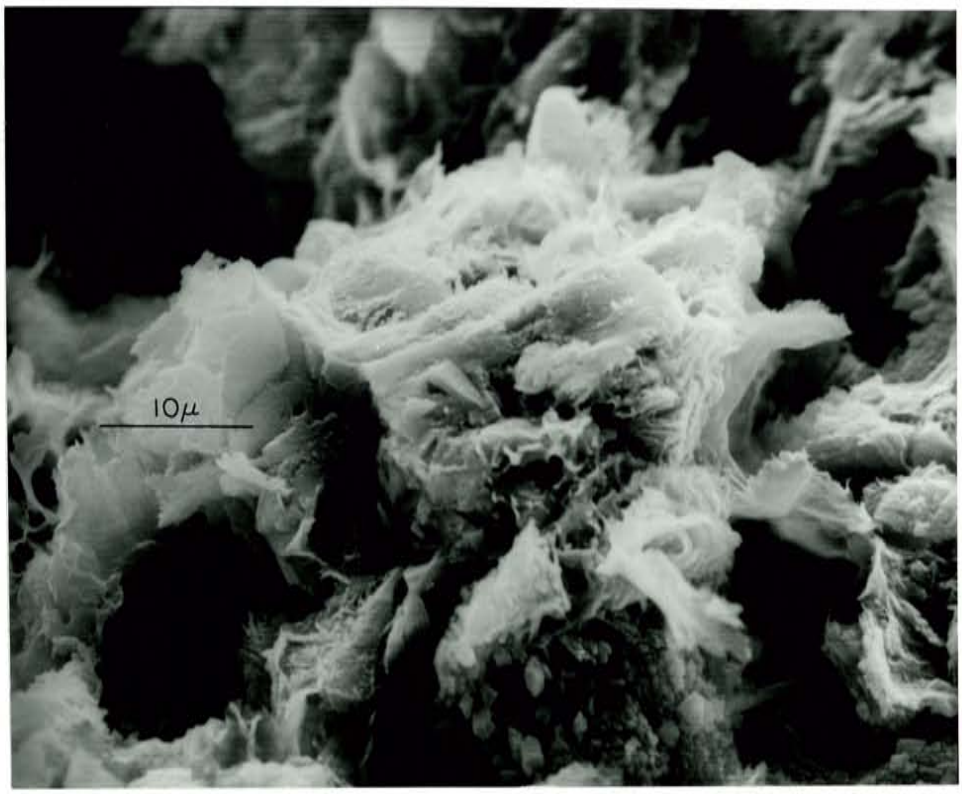

Figure 25. Smectite, illite/smectite, and chabazite in the upper red claystone.

as pseudohexagonal plates, with its characteristic two-dimensional cardhouse structure, up to about three micrometers long in the maximum dimension (Figs. 22, 23, 24). Minor smectite is present with its pore-lining, leafy habit. Isolated subhedral chabazite "cubes" or "rhombs" occur up to 0.5 micrometers on a side in Fig. 21. Chabazite probably occurs in this unit due to reworking of the main zeolite tuff. Two isolated, three to seven micrometer-long, ovoid grains, probably of iron oxide, are shown in Fig. 22. These particles are rounded packets of slightly warped flakes. This morphology is similar to that of kaolinite, which was detected by XRD of this sample, but not identified positively with the SEM.

A scanning electron micrograph of the upper red claystone from locality 1 illustrates smectite, illite/smectite, and chabazite pseudomorphic after a reworked volcanic glass grain (Fig. 25). The illite/smectite has a ragged, leafy appearance. The chabazite "cubes" or "rhombs" are up to one micrometer on a side and occur in clusters or stringers.

Picard and High (1972) examined the clay mineral assemblage of forty, mostly Recent, lakes and found that lacustrine deposits are characterized by diverse clay mineral assemblages that reflect source materials and climate. These associations are generally dominated by discrete illite, illite/smectite, and smectite, with subordinate chlorite, chlorite/smectite, kaolinite, vermiculite, and sepiolite (Picard and High, 1972; Srodon, 1984). Several saline, alkaline-lake deposits have clay mineral assemblages similar

to that of DSV. Pleistocene Lake Tecopa contains abundant montmorillonite and illite, and local trace to minor illite/smectite, chlorite, vermiculite, and lithian saponite (Sheppard and Gude, 1968; Starkey and Blackmon, 1979). Jones and Weir (1983) found that the clay size fraction of saline, alkaline Lake Abert, in Oregon, showed a dominance of expandable layer silicates, with lesser plagioclase, zeolites, mica, and kaolinite. The lacustrine mudstones of the Buckhorn, New Mexico clinoptilolite deposit consist of major smectite, zeolite, quartz, and calcite, with minor to trace illite, plagioclase, and secondary gypsum (Sheppard and Mumpton, 1984).

Droste (1961a, 1961b) conducted investigations of the clay mineral assemblage of playa sediments of the Mojave Desert and Owens, China, Searles, and other lake basins in California. His results are similar to those reported here (Table 2). Of the 45 playas studied in the Mojave Desert, montmorillonite and illite were found in each one and composed at least 70% of the clay minerals present. Chlorite and kaolinite were in the sediments of less than half the playas studied and accounted for generally less than 30% of the clay minerals present. Sepiolite-like clay minerals were not found in any of the samples studied. At Owens Lake, the ratio of clay minerals in detritus entering the basin is 2:7:1 for montmorillonite:illite:chlorite and/or kaolinite. The ratio of montmorillonite:illite:kaolinite in the Q_{og} conglomerate at DSV averages approximately 2:7:2,

and that for montmorillonite:illite:chlorite is about 2:7:5.

Droste (1961a, b) notes that the clay mineral composition of desert saline sediments in southern California is controlled almost entirely by the composition of the source rocks surrounding the basins, and that there is little evidence that any of the clays are unstable in the sodic and calcic saline-lake environment. In the Mojave Desert, no clay mineral present in the detritus carried into the playas disappeared in the lake environment. Clay mineral stability in the lacustrine complex at DSV can be inferred in a similar manner. The clay minerals brought into the lake as detritus from the drainage area were affected only slightly by diagenesis. Few mineralogical differences can be detected between the clay minerals of the lacustrine claystones and those of the overlying alluvial conglomerates. This evidence, in conjunction with the fact that all these minerals are found areally throughout, and at all observed stratigraphic levels of the basin-fill and surrounding drainage area, supports a predominantly detrital origin for them. The minerals of authigenic origin include chabazite, clinoptilolite, much of the calcite, the saline minerals, and some montmorillonite, illite, and illite/smectite.

Lateral clay mineralogical trends are difficult to discern from my semi-quantitative XRD analysis (Table 2). Variations in relative abundances of clay mineral groups for individual lacustrine claystone samples from the average of all lacustrine claystone samples analyzed, can be attributed to normal sedimentary dispersal patterns. For instance, the

anomalously high chlorite values for some claystones and conglomerates sampled along the south side of the valley are most likely due to weathering and degrading of abundant volcanic rocks in the Dripping Springs Mountains.

The less-than-two micron size fraction was extensively studied in vertical sections at localities 1, 4, 86, and 76 to note trends in clay mineralogy (Table 2). The relative abundances of the five clay mineral groups identified display only one discernible vertical mineralogical trend; generally, the relative abundances of discrete illite and illite/smectite vary inversely in the vertical sections. The uniformity of values is support for the predominantly detrital origin of the clay mineral suite. The average abundance of illite/smectite is less than that of discrete illite in the Q_{og} alluvial conglomerate while the relative abundance of illite/smectite equals that of illite in the lacustrine claystones. This is predictable, as illite/smectite is a weathering product of discrete illite and, consequently, forms at the expense of it. Carroll (1970) states that mixed layering in clays is a two part adjustment to an environment: 1) degradation in weathering rocks and soils, and 2) diagenesis in deposits of detrital materials. The illite/smectite of the DSV basin-fill is regarded dominantly as the result of the former process but minor amounts of it have formed authigenically by reaction of saline, alkaline solutions with discrete illite.

Provenance

The clay minerals of the DSV basin-fill are dominantly of detrital origin. Minor amounts of them formed authigenically though, by reaction of saline, alkaline-lake waters with volcanic ash and precursor, detrital clay minerals.

Authigenic montmorillonite can form from the hydrolysis of intermediate to calc-mafic volcanic ash by saline, alkaline solutions (Sheppard and Gude, 1964, 1965; Hay, 1966; Carroll, 1970; Keller, 1970; Janders, 1978; Starkey and Blackmon, 1979; Jones and Weir, 1983) in environments conducive to the retention of $Me^{+,2+}$ (except K^+) and H_4SiO_4 (Papke, 1969). The altered tuffs in DSV were probably originally of rhyolitic composition and are located in a semi-arid climate where leaching has been ineffective. Sheppard and Gude (1968) observed montmorillonite occurring in the matrix and as a thin film coating glass shards which had been altered to zeolites in Pleistocene Lake Tecopa. This montmorillonite is areally restricted and composes only a small portion of the total clay mineral content. Starkey and Blackmon (1979) speculate the reason for the small amount of this authigenic montmorillonite is that it formed immediately after deposition of the ash when the H^+:$Na^+ + K^+$ activity ratio was high. In addition, the hydrolysis reaction altering silica glass to montmorillonite (Hay, 1963) releases silica and alkali ions into solution, raising the pH, and producing chemical conditions more favorable for the formation of zeolites than for more mont-

morillonite.

Diagenetic illitization and chloritization can occur when volcanic ash reacts with saline, alkaline solutions of sufficient K^+ and Mg^{+2} concentration (Keller, 1970). Illitization/chloritization of detrital smectite can also occur with concomitant uptake of K, Mg, and Si in these chemical environments (Droste, 1961b; Janders, 1978; Jones and Weir, 1983). Tank (1971) noted a basinward alteration of montmorillonite probably to illite in the alkaline-lake deposits of the Green River Formation. This conversion occurred in response to the high cation exchange capacity of montmorillonite and the high-potassium pore-fluid concentration in the central part of the basin. A similar process may have occurred in DSV. Semi-quantitative XRD analysis of the lower and middle red claystones (T_{lc} and T_{mc}) indicates the relative abundances of illite and sodium smectite (montmorillonite) generally vary inversely and that the discrete illite:montmorillonite ratio increases basinward (Table 2).

Essentially all of the kaolinite in DSV is of detrital origin. Primary kaolinization typically occurs under acidic, leaching conditions where $Me^{+,2+}$ are removed and H^+ added to the system, but can also occur in closed-hydrographic basins where the concentration of dissolved Al is high or where H^+ ions displace M ions. There is little evidence of authigenic kaolinite in DSV. Authigenic kaolinite would be expected to have a high degree of crystallinity and subsequently produce sharp, well-defined reflections on XRD charts of oriented slide samples. The kaolinite peaks

of DSV basin-fill samples are generally broad and diffuse. In addition, kaolinite was not detected by scanning electron microscopy.

Biotite was detected in all the informal lacustrine and most of the ash-fall tuff units in the basin. It is of primary origin in the ash beds and, in addition to its detrital origin, its presence in the claystones is attributed to weathering and reworking of the tuffs.

ASH-FALL TUFFS OF DRIPPING SPRINGS VALLEY

Interbedded ash-fall tuffs are most prominent north of Dripping Springs Wash. The tuffs are not sufficiently exposed on the southwest side of DSV to be delineated on my geologic maps. Several possible phenomena may be responsible for the apparent absence of tuff in this area: 1) nondeposition, possibly, although not very likely, owing to a shadow effect of the Dripping Springs Mountains on ash-fall tuff deposition from a prevailing southwesterly wind source; or, 2) poor preservation due to erosion caused by the steep slope, or uplift along the large, range-bounding normal fault, of the northeast flank of the Dripping Springs Mountains; 3) subsidiary faulting adjacent to the range-bounding normal fault which displaced at least the stratigraphically lowest tuff horizons into the subsurface; 4) masking by talus and overlying sediments; and 5) erosion during paleochannel formation.

The age of the alteration of the tuffs is not known, except within broad limits. Preservation of original vitroclastic textures and sedimentary structures in the tuffs indicates alteration occurred after burial. Clasts of altered tuff in the Q_{og} conglomerate indicate alteration occurred before their erosion and later incorporation in the gravel.

Main Zeolite Tuff

The main zeolite tuff horizon (T_{mz}) now underlies at least 1.6 km^2 (one mi^2) of basin-fill. It ranges from 0.076

to 0.530 m (0.25 to 1.74 ft) thick and consists of three distinct lithologies: a lower bed 0.046 to 0.265 m (0.15 to 0.87 ft) thick consisting of zeolitically altered ash and approximately 10% detrital matter (Eyde, 1982). An overlying bed 0.043 to 0.061 m (0.14 to 0.20 ft) thick consists of a laminated, thin-bedded, zeolitically altered ash with traces of detrital matter, detrital and authigenic clay, and calcite (Eyde, 1982). A stratigraphically highest, massive bed 0.091 to 0.204 m (0.30 to 0.67 ft) thick consists of zeolitically altered ash (Eyde, 1982; Appendix I). Clay laminae deposited between the three ash lithologies suggest they accumulated from more than one ash fall event, or that sedimentation and reworking were active in the basin during deposition of the ash. It is possible that the lower bed represents ash initially deposited in the lake, and that the middle and upper beds represent ash that was originally deposited on the surrounding lakescape and later washed or blown into the lake.

The main zeolite tuff horizon ranges from reddish-orange to very light gray to white. The color intensity commonly increases with depth. The unit is also denser with more glass near the base. Alteration, therefore, has been more complete in the upper part of the unit where the lake waters had easier access to the vitric component; although the original vitroclastic texture of the ash is preserved.

Sedimentary structures, although not abundant, indicate that the tuff was partially reworked and disturbed by lake

bottom currents and bioturbation. These structures include ripple marks exposed on laminae partings, soft-sediment deformation, and calcified root impressions.

The main zeolite tuff horizon has been inhomogeneously altered to chabazite. Scanning electron micrographs of the middle massive bed in the Anaconda prospect pit (Figs. 26, 27, 28, 29, 30) show chabazite and smectite are pseudomorphic after glass shards. The vitroclastic texture is well preserved. These observations are direct evidence that volcanic glass was the primary material from which the zeolite formed. Chabazite and erionite were the only zeolites observed in the microanalysis of this bed, although clinoptilolite was detected by XRD. A bundle of erionite rods was seen once, but no photomicrographs were taken of it. Chabazite occurs as subhedral to euhedral "cubes" or "rhombs" varying in size from much less than one micrometer to two micrometers on a side. The crystals are commonly intergrown, forming clusters or radial stringers (resembling a fan made from folded paper) a few micrometers long (Figs. 26, 28, 30). The cube-like habit and extremely fine grain size are typical of lacustrine chabazite (Sheppard and Gude, 1975; Mumpton and Ormsby, 1978).

Smectite and illite/smectite are pseudomorphic after glass shards as pore-filling and pore-lining, leafy, interconnected ridges (Figs. 26, 28, 29, 30) much less than one micrometer wide and up to several micrometers long. Authigenic illite/smectite appears to take on the physical characteristics of the participating minerals (Wilson and Pitt-

Figure 26. Scanning electron micrograph of the middle massive bed of the main zeolite horizon in the Anaconda prospect pit. Extremely fine-grained chabazite "cubes" or "rhombs" are intergrown, forming radial stringers a few micrometers long. The bright, wispy, leafy material in the upper left is smectite. Minute chabazite crystals have grown on the smectite. (Sample 080984-1).

Figure 27. Scanning electron micrograph of the middle massive bed of the main zeolite horizon in the Anaconda prospect pit. Subhedral to euhedral chabazite "cubes" or "rhombs" and leafy smectite are pseudomorphic after the volcanic glass matrix. (Sample 080984-1).

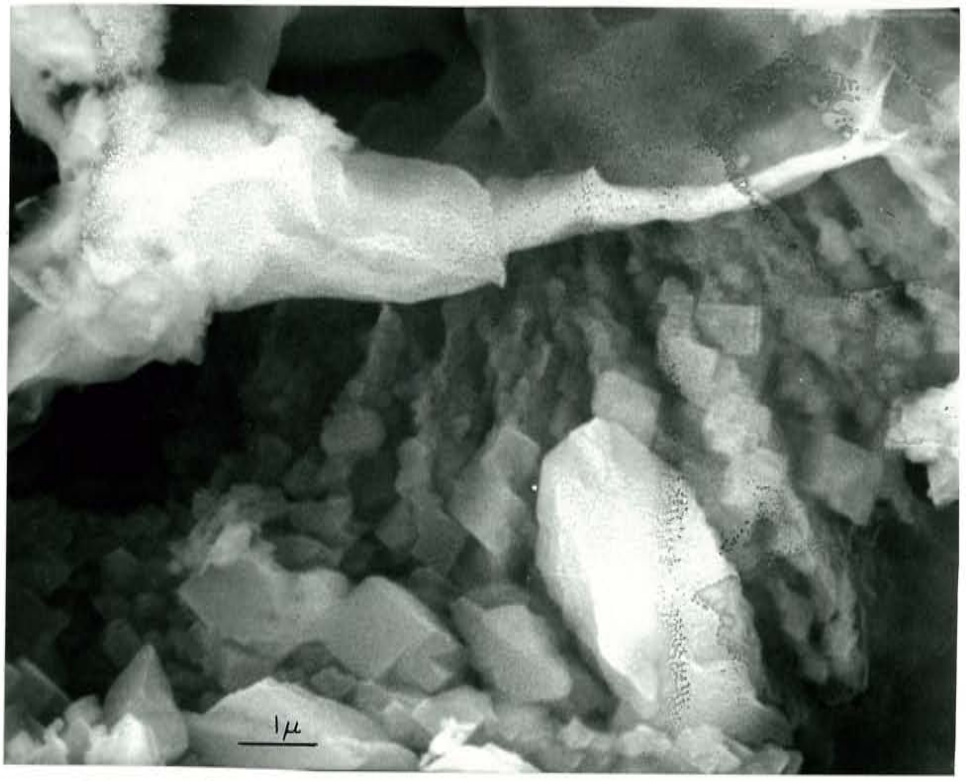

Figure 26. Micrograph of chabazite and smectite.

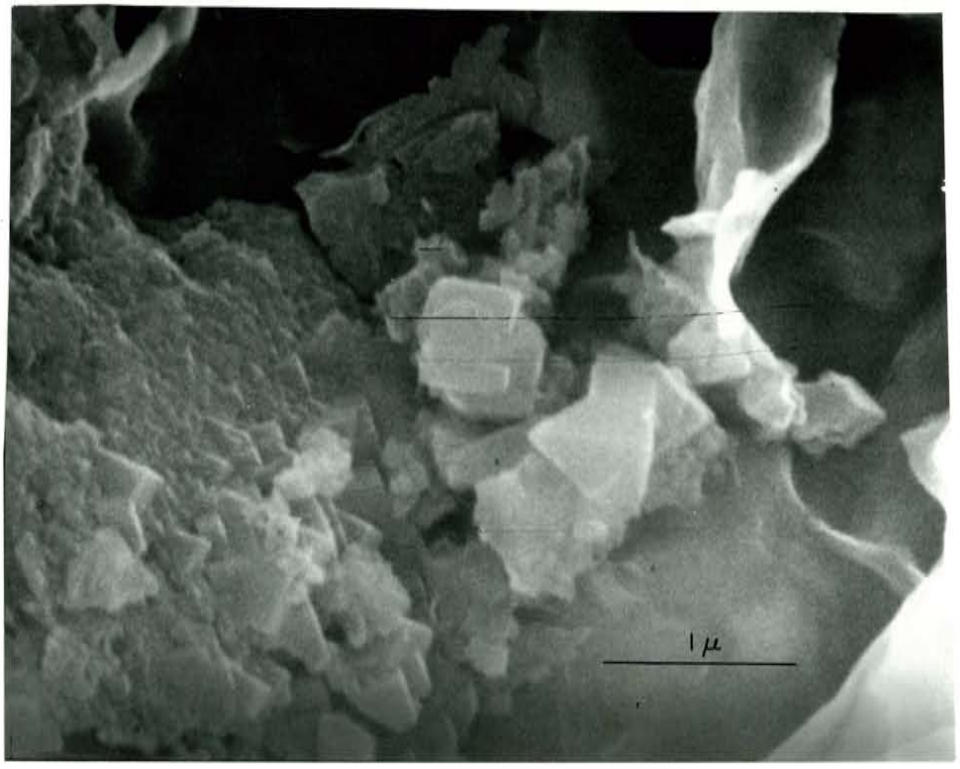

Figure 27. Chabazite and smectite pseudomorphic after volcanic glass.

Figure 28. Scanning electron micrograph of the middle massive bed of the main zeolite horizon in the Anaconda prospect pit. Subhedral to euhedral chabazite "cubes" or "rhombs" form stacked radial stringers on the volcanic glass substrate. Leafy smectite is also pseudomorphic after the glass. Tiny chabazite crystals appear to have formed on the smectite in the upper left corner. (Sample 080984-1).

Figure 29. Scanning electron micrograph of the middle massive bed of the main zeolite horizon in the Anaconda prospect pit. Wispy, leafy smectite and/or illite/smectite has grown from the etched volcanic glass matrix. The "honeycomb" or "corn flake" texture is characteristic of many smectites. Illite/smectite often takes on a more ragged honeycomb habit. (Sample 080984-1).

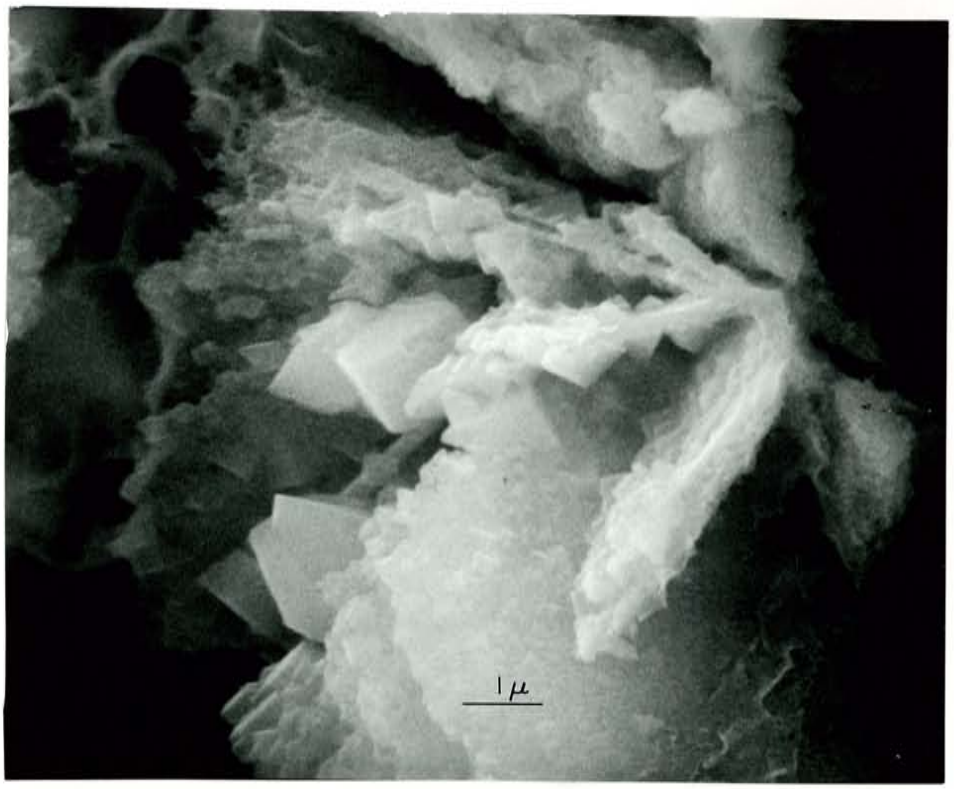

Figure 28. Stacked radial stringers of chabazite.

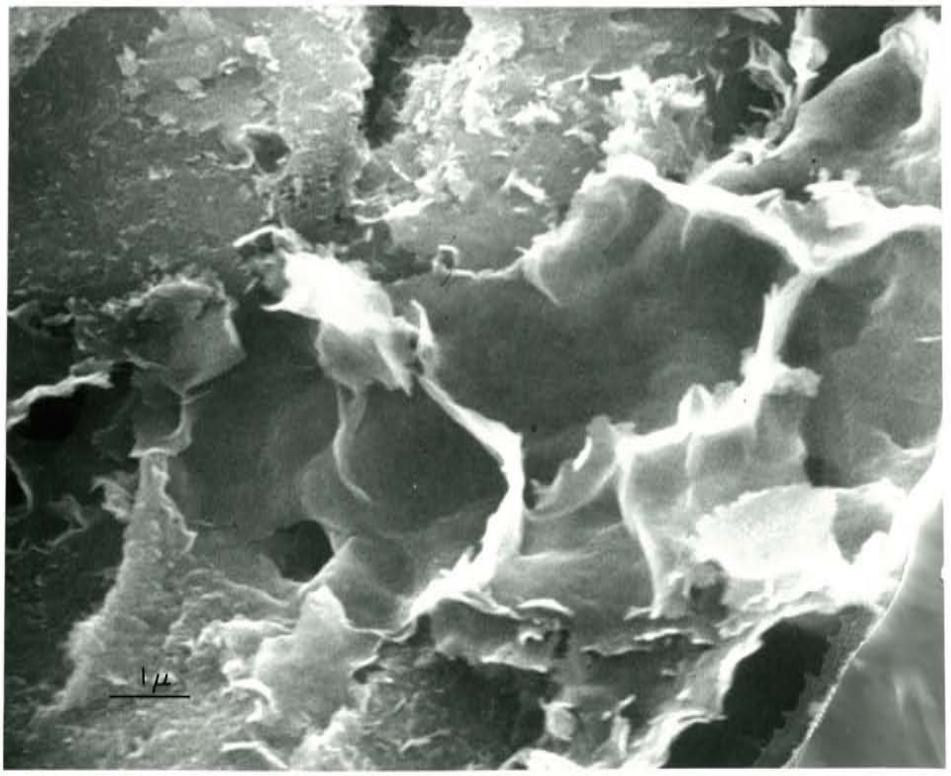

Figure 29. Smectite and/or illite/smectite growing from volcanic glass.

Figure 30. Scanning electron micrograph of the middle massive bed of the main zeolite horizon in the Anaconda prospect pit. Subhedral to euhedral chabazite "cubes" or "rhombs" are intergrown, forming stringers and clusters several micrometers long. Chabazite may have grown from leafy smectite on the right side of the photograph. (Sample 080984-1).

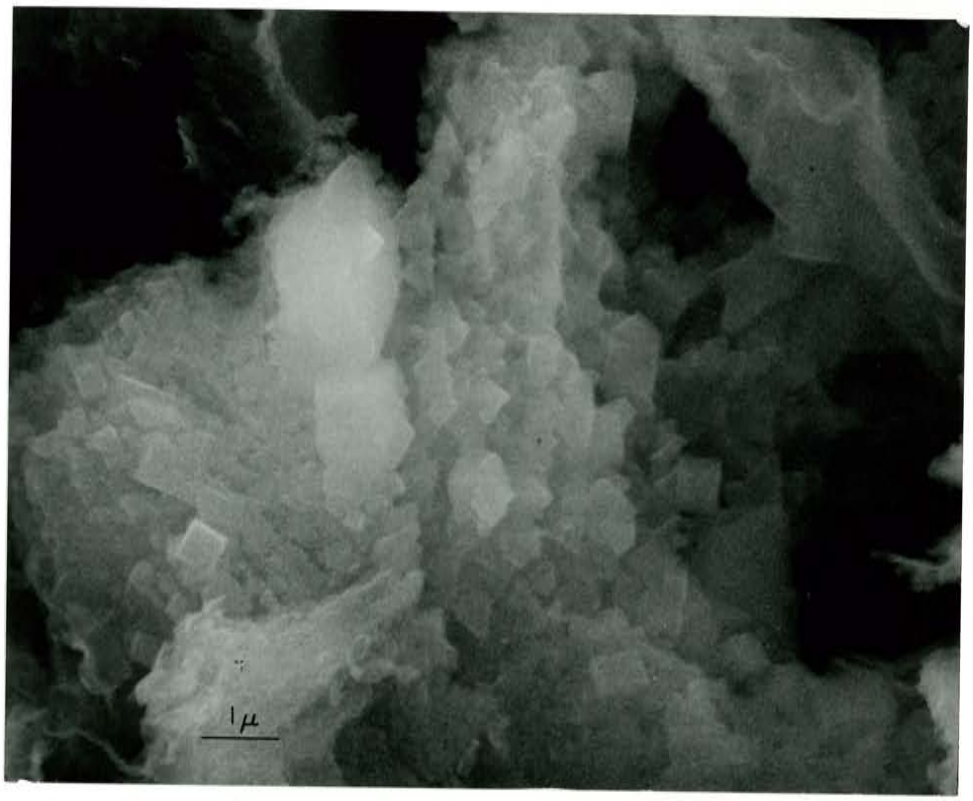

Figure 30. Stringers and clusters of chabazite.

Figure 31. Scanning electron micrograph of the upper zeolite tuff from locality 86. Glass shards occur as irregular, angular masses and platelets. The Y-shaped material in the upper left is glass. Leafy smectite coats some glass shards. Two bundles of possible erionite (or an iron oxide) rods are in the center of the photograph. Minute chabazite "cubes" or "rhombs" are pseudomorphic after glass shards. Charging effects in the instrument are responsible for the very bright rims of the glass, especially noticeable on the left side of the photograph. The white horizontal streaks were also produced by charging. (Sample 040584-5).

Figure 32. Scanning electron micrograph of the upper zeolite tuff from locality 86. Glass shards dominate the photograph, occurring as irregular, angular masses locally coated with leafy smectite. Minute chabazite crystals have grown on the glass shards at the lower left. The three horizontal lines on the right were produced by charging effects in the instrument. (Sample 040584-5).

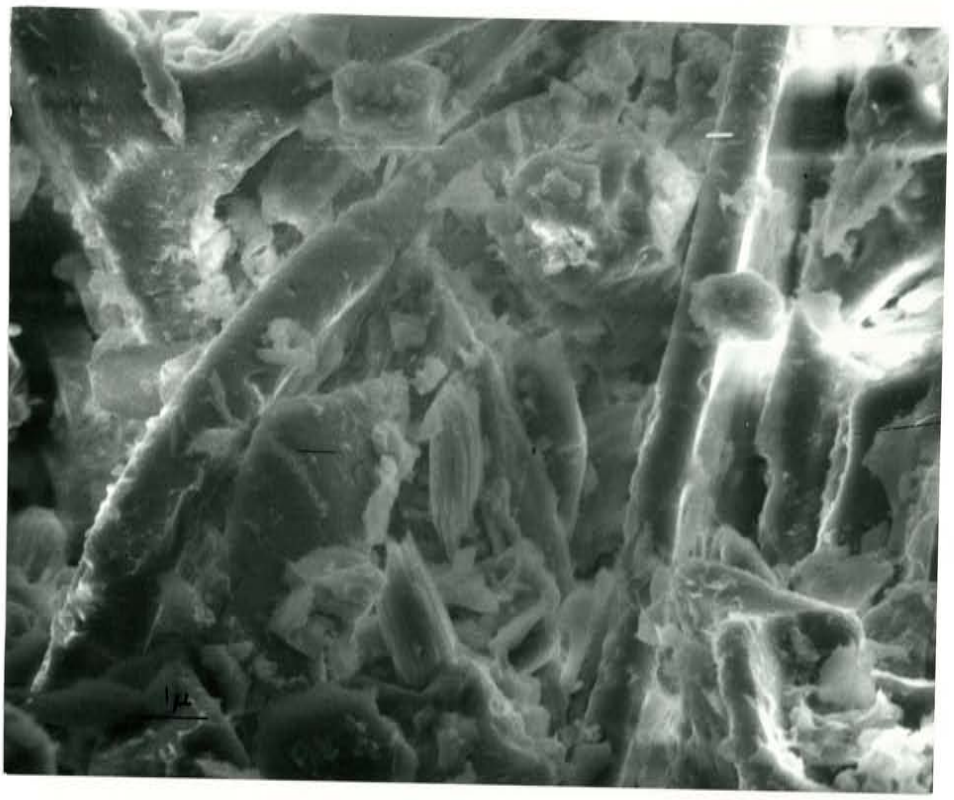

Figure 31. Micrograph showing glass, smectite, and chabazite.

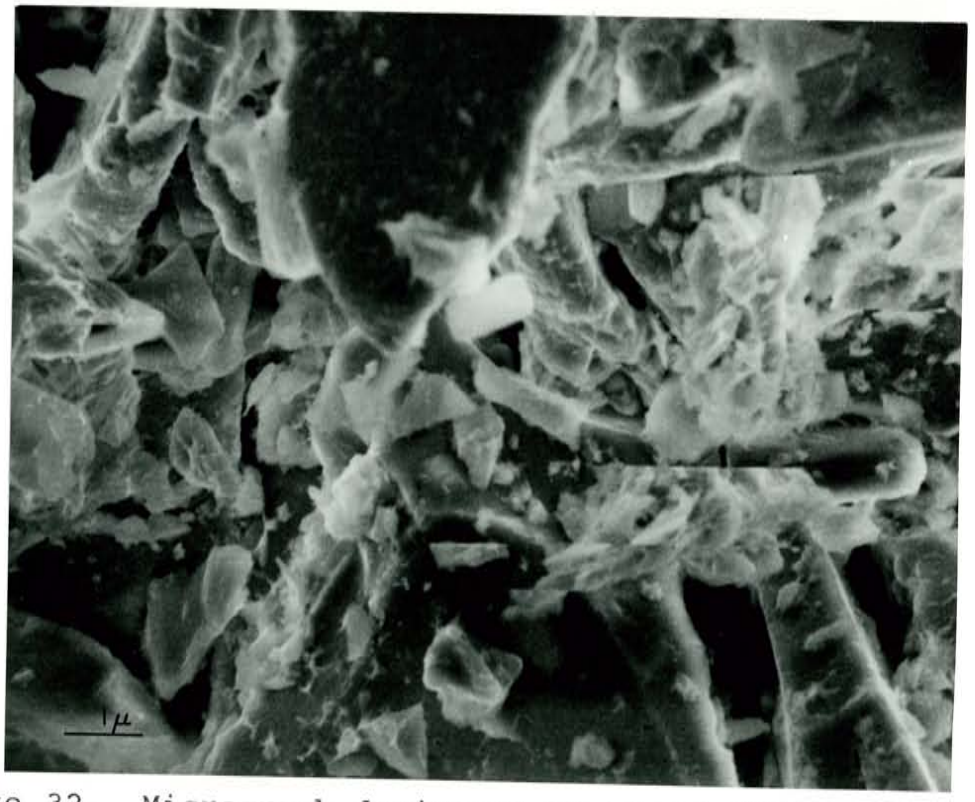

Figure 32. Micrograph dominated by glass shards.

Figure 33. Scanning electron micrograph of the upper zeolite tuff from locality 1. The glass matrix is severely etched and, locally, coated with leafy smectite and minute chabazite "cubes" or "rhombs". The large particle in the center is etched and cracked. Although difficult to determine, it is probably glass. (Sample 111383-4).

Figure 34. Scanning electron micrograph of the upper zeolite tuff from locality 86. Wispy, leafy smectite and/or illite/smectite has grown on the glass shard matrix. A bundle of erionite rods occupies the center of the photograph. It is difficult to decipher the age relationships between the erionite and glass, and erionite and smectite, although it appears the erionite is pseudomorphic after the glass substrate. (Sample 040584-5).

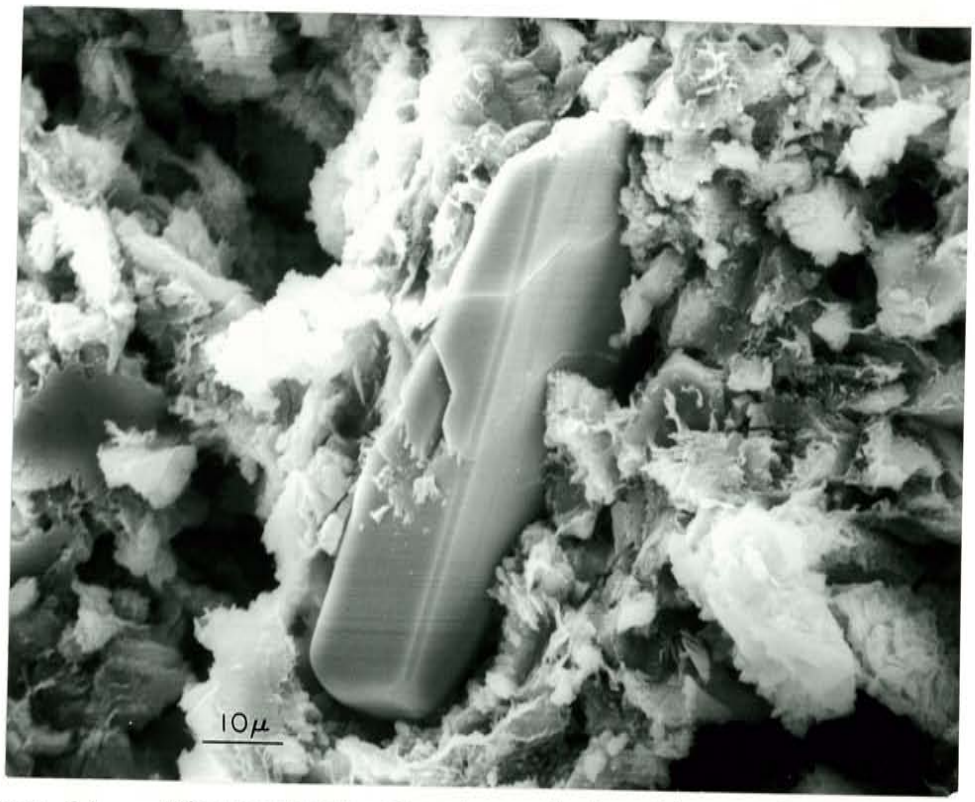

Figure 33. Micrograph showing chabazite and etched glass.

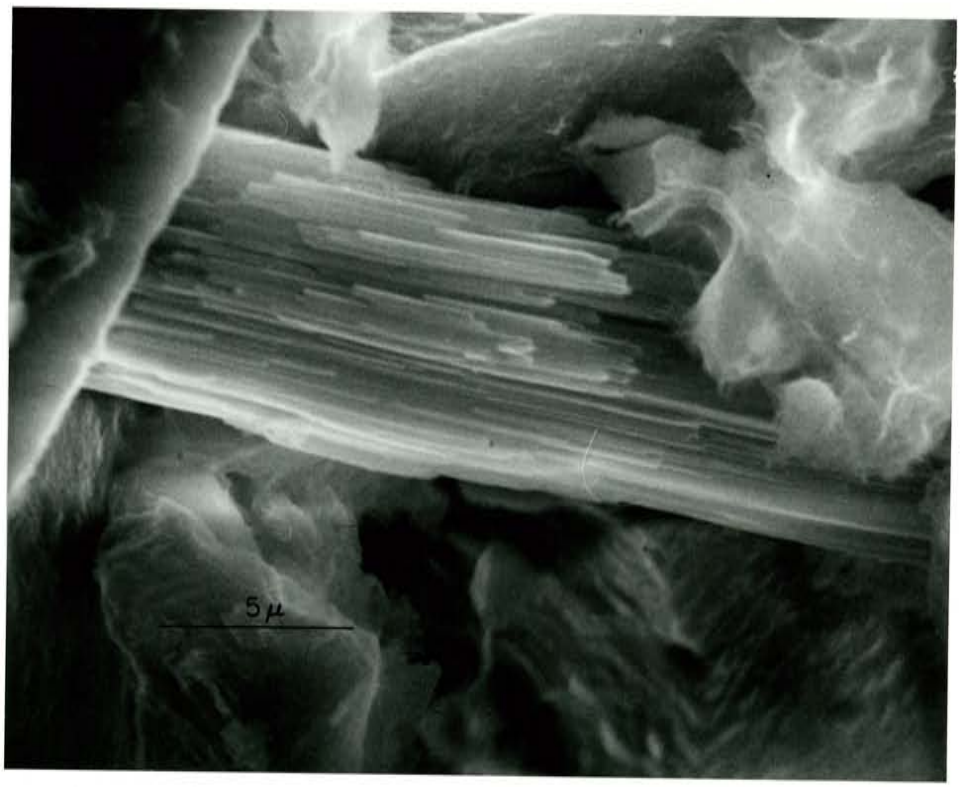

Figure 34. Micrograph of erionite.

Figure 35. Scanning electron micrograph of the middle massive bed of the rhyolitic tuff (T_{rt}) from locality 45. The glass shard matrix consists of irregular, angular masses and plates, severely etched, and, locally coated with wispy, leafy smectite and tiny chabazite "cubes" or "rhombs". (Sample 080384-7).

Figure 36. Scanning electron micrograph of the middle massive bed of the rhyolitic tuff (T_{rt}) from locality 45. The volcanic glass shard matrix consists of etched and cracked, irregular, angular masses and plates. Leafy smectite as well as minute chabazite "cubes" and "rhombs" are pseudomorphic after the glass shards. (Sample 080384-7).

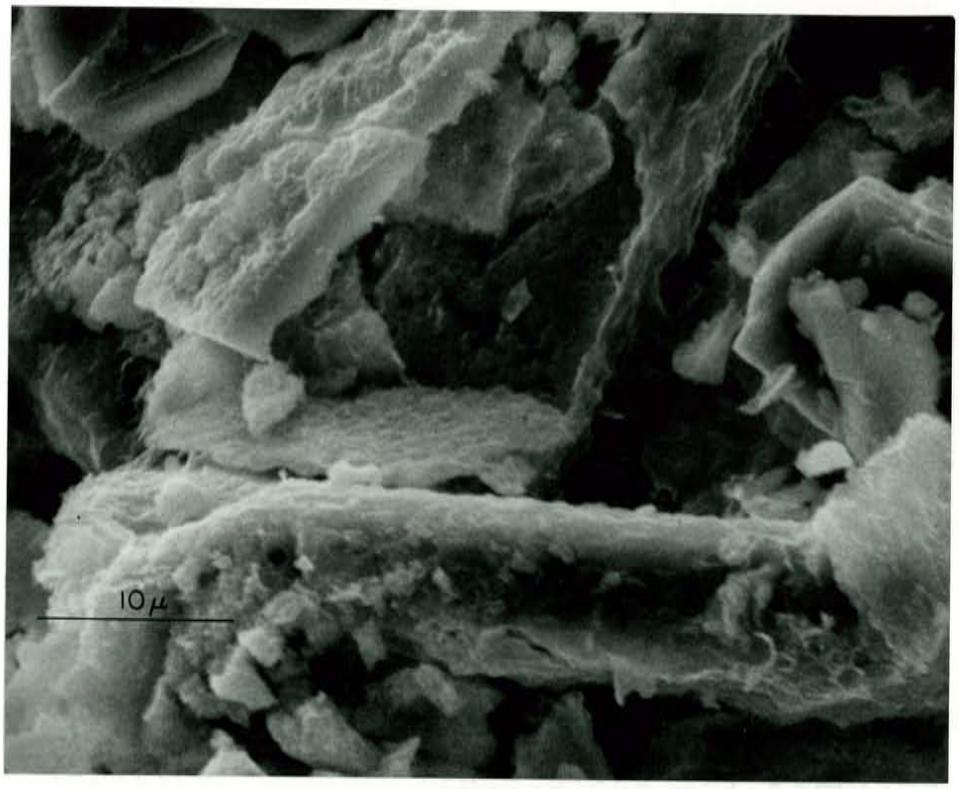

Figure 35. Glass shards of the rhyolitic tuff (Trt).

Figure 36. Smectite and chabazite pseudomorphic after volcanic glass.

man, 1977), therefore, distinguishing mixed-layer illite/smectite from discrete smectite may be difficult with the SEM. Mixed-layer illite/smectite sometimes forms a ragged honeycomb structure. Figs. 26 and 28 reveal the smectite is sometimes an intermediate phase between the volcanic glass and chabazite, as chabazite has grown on the smectite. The volcanic glass matrix is etched to varying degrees, due most likely to various stages of pore-water dissolution (Figs. 27, 29).

Scanning electron microscopy of the main zeolite tuff, therefore, reveals two paragenetic sequences: 1) fresh glass --> chabazite, and 2) fresh glass --> smectite (and/or illite/smectite)--> chabazite. The latter sequence does not always evolve past the smectite phase to the formation of chabazite. Fresh glass, smectite, illite/smectite, chabazite, and rare erionite were the only materials observed in the electron microanalysis of this tuff, although trace to minor quartz, calcite, gypsum, orthoclase and plagioclase feldspar, and non-smectitic clay minerals were detected by XRD of bulk, powder-press samples.

Upper Zeolite Tuff

The upper zeolite tuff horizon (T_{uz}) now underlies at least 4.8 km^2 (three mi^2) of basin-fill. It is up to 1.68 m (5.5 ft) thick and consists of three ash lithologies: a lower thin-bedded to platy bed, a middle massive bed, and an upper thin-bedded to platy bed (Eyde, 1982; Appendix I). The lower and middle beds are often separated by approxi-

mately 2.5 cm (one in) of clay laminae. The contacts between the different lithologies are usually sharp.

Like the main zeolite tuff horizon, sedimentary structures in the upper zeolite tuff horizon indicate the unit has been reworked and disturbed by lake bottom currents and burrowing organisms. Ripple marks, small-scale crossbeds, soft-sediment deformation features, and burrow trails are infrequently present.

The upper zeolite tuff has been inhomogeneously altered to chabazite. The original vitroclastic texture is preserved, and, where alteration is incomplete, glass shards are preserved. Scanning electron micrographs of sample 111383-4 from locality 1 and sample 040584-5 from locality 86, show the glass occurs as a matrix of platelets and irregular, angular masses (Figs. 31, 32, 33). The platelets are 0.5 to one micrometer wide and more than nine micrometers long (Fig. 31). The maximum dimension of the masses can be greater than 15 micrometers. The glass has been subjected to various stages of dissolution.

Scanning electron microscopy reveals that smectite (and/or illite/smectite), chabazite, and erionite (?, or an iron oxide) are pseudomorphic after the glass shards in the upper zeolite tuff. Trace to abundant quartz, calcite, dolomite, halite, gypsum, orthoclase and plagioclase feldspar, illite, chlorite, and kaolinite were detected by XRD but were not identified by the microscopy. Smectite occurs with its characteristic leafy habit (Figs. 31, 33). Chaba-

zite occurs as subhedral to euhedral "cubes" or "rhombs" 0.5 to 1.5 micrometers on a side (Figs. 32, 33), and possibly as poorly-crystallized, nodular clusters. Fig. 34 reveals a bundle of erionite rods 7.5 by greater than 20 micrometers. The width of the individual rods is much less than one micrometer. Although difficult to tell, it appears the erionite has grown from parent glass. Bundles of erionite rods may also be present in the lower central area of Fig. 31.

Ash-Fall Tuffs One through Seven

Seven thin, silicic, ash-fall tuffs now underlie approximately 6.4 km^2 (four mi^2) of basin-fill at the north end of the valley. Each averages about 0.46 m (1.5 ft) thick (Appendix I). The tuffs have been locally calcified along the lake margin. Powder-press XRD analysis of these tuffs indicates some are locally altered to chabazite. They also contain trace to abundant quartz, dolomite, halite, gypsum, potassium and orthoclase feldspar, magnetite, pyrite, and glass. Trace to minor illite, illite/smectite, smectite, kaolinite, and chlorite were also detected.

Rhyolitic Tuff

A rhyolitic tuff (T_{rt}) now underlies approximately 0.40 km^2 (0.25 mi^2) of basin-fill at the north end of the valley. This light- to medium-gray and brownish-gray tuff was partly reworked and waterlain. It is locally altered to chabazite, but where alteration is incomplete, unaltered glass shards

are common (Appendix I). Cornwall and Krieger (1978) determined the refractive index of the glass to be 1.496, indicative of an original rhyolitic composition for the tuff. The original vitroclastic texture of the tuff is preserved. The unit consists of three lithologies: a lower, thin-bedded to platy bed up to 12.7 cm (five in) thick, a middle massive bed up to 64 cm (25 in) thick, and an upper, thin-bedded to platy bed up to 12.7 cm (five in) thick.

Scanning electron micrographs of sample 080384-7 of the middle massive bed of T_{rt} from locality 45 reveal a glass matrix of plates and irregular, angular masses with maximum dimensions up to 100 micrometers (Figs. 35, 36). The glass is etched, suggesting it has been subjected to various degrees of dissolution, probably by pore waters. It also contains cracks two micrometers wide by up to 50 micrometers long (Fig. 36). Subhedral to euhedral chabazite "cubes" or "rhombs" from one to ten micrometers on a side occur as single crystals or intergrown clusters pseudomorphic after the glass. Leafy smectite has also grown from parental glass. Although trace to minor quartz, calcite, gypsum, feldspar, and non-smectitic clay minerals, and abundant pyrite, were detected by XRD of this tuff, these were not observed by electron microscopy.

SEMI-QUANTITATIVE ANALYSIS OF BULK, POWDER-PRESS SAMPLES BY XRD

Selected DSV tuff, lacustrine, and fluvial samples were prepared for semi-quantitative analysis via a bulk, dry, powder-press method. The data derived from this analysis is presented in Table 3. When interpreting XRD charts, peak heights above background do not necessarily correspond to mineral abundance in an individual sample. Peak heights are also a function of grain size, degree of crystallinity, and orientation. Therefore, instead of comparing mineral abundance amongst different samples by comparing peak heights, the ratios of peak heights above background for various minerals were compared between samples to examine trends in mineralization.

All mineral peak-height ratios calculated for the lacustrine claystones (T_{lc}, T_{mc}, T_{uc}) vary only slightly, except the chabazite/calcite and calcite/potassium feldspar ratios (Table 3). This uniformity suggests a predominantly detrital origin for the quartz and the potassium and plagioclase feldspars. Chabazite/calcite generally increases basinward, as the saline, alkaline conditions increasingly favored chabazite formation basinward. No discernible mineralization trends are apparent from the wide-ranging calcite/potassium feldspar ratios.

Two dissimilar trends in chabazite mineralization are apparent for the main zeolite and upper zeolite tuff horizons. Progressively higher chabazite ratios are found from east to west in the main zeolite horizon while the opposite

Table 3. Bulk, powder-press semi-quantitative analysis of DSV ash-fall tuff and alluvial conglomerate facies samples. Results reported in ratios of mineral reflection peak heights above background. The following reflections (in "d"-spacings) were used for the calculations: chabazite - 2.925, quartz - 4.26, calcite - 3.86, halite - 2.821, gypsum - 7.56, potassium feldspar - 3.22, plagioclase feldspar - 3.02. Cb = chabazite, Qtz = quartz, Calc = calcite, Hal = halite, Gyp = gypsum, Kspar = potassium feldspar, Plag = plagioclase feldspar. Samples are arranged by localities, in descending order from northwest to southeast for each rock unit. Blank spaces indicate the peak height ratio could not be determined due to the absence of one of the minerals in the sample.

Rock Unit and Sample Number	Locality	Cb/ Qtz	Cb/ Calc	Cb/ Kspar	Cb/ Plag	Qtz/ Hal+Gyp	Calc/ Hal+Gyp	Qtz/ Kspar	Qtz/ Plag	Calc/ Kspar	Calc/ Plag	Plag/ Kspar	Kspar/ Hal+Gyp	Plag/ Hal+Gyp
T_{lc}'														
040584-2	86	0.23	0.43	0.15	0.15			0.65	0.65	0.35	0.35	1.00		
101084-1	82	0.17	0.42	0.13	0.10			0.75	0.58	0.30	0.23	1.30		
T_{mc}'														
040484-6	58													
040584-4	86	0.19	0.67	0.13	0.08			0.82	0.45	0.12	0.07	1.82		
								0.66	0.40	0.19	0.12	1.63		
T_{uc}'														
080584-16	61	0.05	0.67	0.04	0.03									
080284-1	35	0.83	2.50					0.86	0.62	0.06	0.04	1.39		
080284-1	35	0.20	1.50	0.16	0.08									
080184-1	34	0.12	0.38	0.05	0.03			0.79	0.43	0.10	0.06	1.86		
111383-9	1	0.46	2.00	0.17	0.13			0.38	0.23	0.12	0.07	1.68		
111383-20	2	0.73	0.62	0.22	0.19			0.36	0.29	0.08	0.07	1.25		
111483-9	4	0.79	3.67					0.31	0.21	0.36	0.25	1.47		
072584-1	15					5.50	12.00							
072584-1	15	0.03	0.50	0.02	0.02			0.65	0.33	1.41	0.73	1.94	8.50	16.50
072984-3	27	0.57	0.18	0.17	0.04			0.70	0.53	0.04	0.03	1.32		
								0.30	0.07	0.96	0.23	4.22		
T_{mz}'														
080984-1	pit		5.40	5.40	6.75		5.00							
040584-3	86			4.80	2.82					1.00	1.25	0.80	5.00	4.00
101083-2(T_{mz}?)	83	3.11	1.22	2.55	0.52			0.82	0.17	2.09	0.43	1.70 4.91		
T_{uz}'														
111483-3	4	3.39	4.00	1.69	1.63									
111383-17	1		6.75	0.19				0.50	0.48	0.42	0.41	1.04		
111483-6	4	3.96	2.72	1.93	1.98					0.29				
111383-4	1		6.00					0.49	0.50	0.71	0.73	0.98		
111483-5	4		5.36		4.21		1.22							
040784-3	87		5.44	6.13	5.44						0.79			1.56
072984-4	28					0.67								
101084-5 (T_{uz}?)	83							1.60	1.04	0.47	0.30	1.53		

Sample and Rock Unit	Location	Cb/ Qtz	Cb/ Calc	Cb/ Kspar	Cb/ Plag	Qtz/ Hal+Gyp	Calc/ Hal+Gyp	Qtz/ Kspar	Qtz/ Plag	Calc/ Kspar	Calc/ Plag	Plag/ Kspar	Kspar/ Hal+Gyp	Plag/ Hal+Gyp
T_{af-1}														
080384-1	41		4.44	5.33	5.33		1.80			1.20	1.20	1.00	1.50	1.50
080284-2	35								1.67		1.00			
073184-1	32							0.36	0.29	2.55	2.00	1.27		
073184-3	33					1.50	16.00	0.60	0.30	6.40	3.20	2.00	2.50	5.00
T_{af-2}														
080384-2	41			3.36	2.47							1.36	1.40	1.90
073184-2	32					3.00	13.50	0.55	0.35	2.46	1.59	1.55	5.50	8.50
T_{af-3}														
080284-3	36					2.67	10.00		0.44		1.67			6.00
T_{af-4}														
080284-4	36								0.26		0.83			
T_{af-5}														
080284-5	36								0.20		5.80			
T_{rt}														
080384-6(lower)	45					2.00	15.50		0.50		3.88			4.00
080384-7(middle)	45					1.33	1.67							
080384-8(upper)	45							1.50		1.50				
T_g														
080584-1	50	0.13	1.33	0.54	0.06			0.43	0.51	0.04	0.05	0.85		
080584-3	52	0.11	2.00	0.11	0.06	27.00	1.67	1.00	0.57	0.06	0.03	1.76	27.00	47.50
080584-20	65	0.16	0.50	0.07	0.07			0.40	0.43	0.13	0.14	0.92		
080884-5	73	0.23	0.21	0.07	0.08	2.17	2.33	0.30	0.33	0.33	0.36	0.91	7.17	6.50
100984-6	81	0.06	2.00	0.26	0.07			0.58	0.16	0.13	0.04	3.68		
Q_{og}														
080884-1	69							0.43	4.90			0.09		
100984-1	77	0.17	3.00	0.07	0.07	17.67	1.00	0.43	0.40	0.02	0.02	1.08	41.33	44.67
040584-2	4	0.23	0.43	0.15	0.15			0.65	0.65	0.35	0.35	1.00		

is apparent for the upper zeolite tuff horizon.

Few mineralization trends can be distinguished from the sparse data for T_{af-1} through T_{af-7}, but a difference in lake-water composition is suggested between locality 41 and localities 33 and 32 (Fig. 2) at the time of deposition of T_{af-1} and T_{af-2} (Table 3). The lake waters were more saline at locality 41 as indicated by the drastically lower calcite/halite + gypsum, potassium feldspar/halite + gypsum, and plagioclase/halite + gypsum ratios at locality 41 than those at locality 33 for T_{af-1}. The same relationship is suggested by the plagioclase/halite + gypsum ratios for T_{af-2} between localities 41 and 32.

One vertical mineralization trend is based on sparse data from the three lithologies of the rhyolite tuff (T_{rt}) at locality 45. More saline lake-water conditions are suggested here by the lower calcite/halite + gypsum ratios during deposition of the middle massive bed than during deposition of the lower platy bed.

Mineral peak-height ratios remain relatively uniform for the alluvial conglomerate units (T_g, Q_{og}) at the sampled localities. This suggests that all the analyzed minerals are predominantly detrital in these units. Chabazite was reworked from the previously deposited ash-fall tuffs and incorporated in these units.

MODEL OF ZEOLITIZATION AT DRIPPING SPRINGS VALLEY

Zeolite Chemistry and Structure

Zeolites are hydrated aluminosilicates of the alkali and alkaline earth metals. They are tectosilicates made up of an infinitely extended three-dimensional framework that encloses cavities interconnected by channelways. The structure consists of SiO_4^{-4} tetrahedra wherein all four corner oxygen ions of each tetrahedra are shared with adjacent tetrahedra. This arrangement of silica tetrahedra implies an overall Si:O ratio of 1:2, and if silicon is the central cation of each tetrahedron, the structure is electrically neutral. However, replacement of the quadrivalent silicon by trivalent aluminum gives rise to a net negative charge. The charge is balanced by the addition of the monovalent or divalent cations Na^+, K^+, Ca^{+2}, or Mg^{+2} elsewhere in the structure. The empirical formula of a zeolite can be expressed as:

$$M_{2/n}O \cdot Al_2O_3 \cdot xSiO_2 \cdot yH_2O$$

where M is any alkali or alkaline earth cation, n is the valence of that cation, x is a number from two to approximately ten, and y is a number from two to seven (Mumpton, 1977). The zeolite structure may be divided into three components: 1) the structural cations of the aluminosilicate framework; 2) interconnected void spaces in the framework, containing the exchangeable alkali and alkaline earth cations; and 3) water molecules present as an occluded phase,

held only in the channels of the structure. The exchangeable cations and water molecules are loosely bound and can be easily removed or replaced in most zeolites without disrupting the framework (Hay, 1966). The positions and loose bonding of cations and water molecules makes possible continuous and, in part, reversible changes in hydration state and cation exchange (Hay, 1966). However, the base to alumina ratio always equals unity, and the (Al + Si) :O ratio is always 1:2.

Chabazite has an ideal formula of $(Ca, Na_2)Al_2Si_4O_{12} \cdot 6H_2O$, but natural chabazites show considerable variation in cation content, Si:Al ratio, and water content. This variation causes the index of refraction, specific gravity, unit cell dimension, and other physical properties also to vary. Calcium and sodium are the dominant cations in the chabazite structure; the $Si:Al+Fe^{+3}$ ratio ranges from 1.7 to 3.8. Loosely bound water ranges from 10 to 20% (Mumpton, 1977) of the dehydrated phase of chabazite. In comparison with other calcic zeolites and calcium-aluminum silicates, formation of chabazite is more favored by a silica-poor environment (Deer and others, 1966).

Major-Oxide Chemistry of Zeolitic Tuffs and Lacustrine Claystones in Dripping Springs Valley

The major-oxide chemistry of selected zeolitic tuff and lacustrine claystone samples was determined by XRF spectrographic analyses. Results of the analyses are presented in

Table 4 in weight percent of the oxides. Loss on ignition (LOI) was determined at 1000°C. The LOI is due chiefly to water, but also to other volatile components, particularly CO_2. Samples containing abundant carbonate material have notably high LOI values.

In addition to chabazite, the tuffs analyzed contain varying amounts of impurities, such as clay minerals, quartz, calcite, and feldspars. Thus, these analyses, although they may resemble analyses of the constituent chabazite, are in fact analyses of rocks, as are the analyses of the lacustrine claystones. Regardless, several generalizations of the basin geochemistry can be made from these data.

Only three outcrops of the main zeolite horizon (T_{mz}) were positively identified in DSV. A tuff (sample 101084-2) exposed at locality 83, suspected of being a fourth outcrop (Table 4), is calcified, and consequently, has a higher LOI than that of the two other T_{mz} samples analyzed.

Ideal chabazite has a Si:Al ratio of 2, but chabazite from sedimentary environments is more siliceous and has a Si:Al ratio ranging from 3.0-4.1 (Sheppard and Gude, 1975). The SiO_2:Al_2O_3 ratio for samples 080984-1 and 040584-3 is relatively constant, 3.543 and 3.600, respectively (Table 4). The calcium and sodium oxide concentrations vary inversely, while magnesium and potassium oxides are covariant. In zeolites, the Si:Al+Fe^{+3} ratio is constant, and the monovalent and divalent exchangeable cation concentrations are inversely proportional because charge balance must be maintained. The fact that magnesium and potassium oxides

Table 4. Major-oxide chemical analysis of DSV bulk ash-fall tuff and lacustrine claystone samples as determined by XRF spectrometry. Results reported in weight percent. LOI determined at 1000°C. H_2O^- determined at 100°C.

Sample No.	080984 -1	040584 -3	101084 -2	111383 -4	040584 -5	080384 -1	080384 -7	040684 -3	040584 -2	101084 -1	111383 -1	040584 -4	101084 -4	080584 -19	080384 -9	111383 -6	040584 -7
Rock Unit	T_{mz}	T_{mz}	T_{mz}?	T_{uz}	T_{uz}	T_{af-1}	T_{rt}	T_{lc}	T_{lc}	T_{lc}	T_{mc}	T_{mc}	T_{mc}?	T_{uc}	T_{uc}	T_{uc}	T_{uc}
Locality	pit	86	83	1	86	41	45	12	86	82	1	86	83	63	45	1	86
Oxides																	
SiO_2	54.174	54.103	36.735	53.555	72.766	52.695	69.906	44.732	46.643	44.075	50.808	51.693	41.125	59.437	46.932	51.028	43.122
Al_2O_3	15.290	15.040	9.705	15.029	11.939	16.143	12.045	12.082	13.638	10.130	14.992	14.388	9.381	12.399	10.592	15.337	12.501
Fe_2O_3	2.086	1.565	1.669	1.837	1.518	1.321	1.762	4.483	5.945	3.764	6.047	5.121	3.288	5.985	3.840	4.658	4.841
MgO	2.799	2.118	3.144	2.294	0.120	1.211	1.040	4.181	5.861	2.456	5.948	4.920	4.222	2.609	5.319	3.473	5.373
CaO	2.504	2.399	21.461	3.087	0.510	1.576	0.929	13.024	7.975	18.405	4.427	6.773	18.488	5.055	12.336	3.473	11.818
Na_2O	2.184	3.481	1.120	3.301	3.807	5.888	3.206	0.953	0.980	1.701	1.859	1.381	0.678	1.538	1.424	2.180	0.656
K_2O	1.959	1.893	1.378	1.335	3.001	1.335	3.408	2.541	2.872	2.135	3.159	3.168	1.802	2.158	2.579	2.538	2.740
TiO_2	0.365	0.330	0.293	0.350	0.273	0.287	0.213	0.567	0.624	0.642	0.684	0.613	0.508	0.978	0.612	0.533	0.559
P_2O_5	0.059	0.054	0.067	0.062	0.022	0.013	0.012	0.186	0.225	0.168	0.209	0.211	0.163	0.168	0.156	0.124	0.192
MnO	0.018	0.017	0.031	0.016	0.035	0.016	0.034	0.075	0.078	0.063	0.098	0.100	0.044	0.084	0.047	0.048	0.087
LOI	18.789	18.438	25.583	19.218	5.969	18.827	7.354	16.869	14.701	16.471	11.527	11.854	20.618	8.131	15.816	15.238	17.649
H_2O^-	0.909	0.018	0.038	0.737	0.484	0.054	0.328	0.515	0.818	0.000	1.056	0.465	1.132	0.595	0.383	0.968	0.664
Total	100.220	99.436	101.185	100.083	99.959	99.333	99.908	99.693	99.543	100.010	99.759	100.222	100.316	98.540	99.651	98.630	99.538

seem to be covariant may be a statistical accident due to the small number of T_{mz} samples analyzed.

Two samples of the upper zeolite tuff (T_{uz}) were chemically analyzed (Table 4). The $CaO:Na_2O$ and $SiO_2:Al_2O_3$ ratios of sample 111383-4 are consistent with those of the T_{mz} samples. XRD bulk, powder-press analysis of sample 040584-5 reveals it is vitric, with minor quartz and plagioclase impurities. The SiO_2 content of this sample is greater than that of zeolitically altered T_{mz} and T_{uz} samples analyzed. Sodium, potassium, and manganese oxide concentrations of the vitric sample are also greater than those of the zeolitically altered samples. All other oxides analyzed for the vitric tuff sample are less abundant than those of the zeolitically altered T_{mz} and T_{uz} samples.

Sample 080384-1 is from the zeolitically altered T_{af-1}. Its $SiO_2:Al_2O_3$ ratio of 3.264 is somewhat lower than that calculated for the zeolitically altered T_{mz} and T_{uz} samples. The $CaO:Na_2O$ ratio of this sample is much lower than that of the zeolitically altered samples. This may be due to variations in chabazite composition. The more sodic variety may have formed in the stratigraphically higher tuff, as this tuff probably was subjected to more saline conditions prevalent in the evaporating lake.

Sample 080384-7 is rhyolitic tuff (T_{rt}). It is vitric and contains minor quartz, calcite, gypsum, dolomite(?), and clay mineral accessories. Like the vitric T_{uz} sample 040584-5, it has a higher SiO_2, Na_2O, K_2O, and MnO content,

and lower Fe_2O_3, MgO, and CaO content than the zeolitically altered tuffs.

The ash-fall tuff chemical analyses presented in Table 4 are easily summarized. SiO_2:Al_2O_3 and CaO:Na_2O ratios are consistent among the zeolitically altered tuffs. This is mainly due to uniform chabazite metasomatism as saline, alkaline-lake waters reacted with the fresh ash-fall tuffs. All the ash-fall tuffs of DSV presumably had a rhyolitic parent composition. Approximate changes in chemical composition from fresh to altered tuff can be inferred by comparing the chemical analyses of the altered tuffs with those of the predominantly vitric samples 040584-5 and 080384-7. Zeolitization of fresh rhyolitic tuff produced an enrichment of Al_2O_3, MgO, CaO, TiO_2, P_2O_5, and H_2O, and a depletion of SiO_2, K_2O, and MnO. Na_2O was enriched in some tuffs but depleted in others. Krieger's (1979) conclusions on the metasomatic changes of fresh ash upon zeolitization of the Tuz at DSV coincide with mine in suggesting that zeolitization of fresh ash produced gains in CaO, MgO, Na_2O, and H_2O, and losses in SiO_2 and K_2O. Edson (1977) reports metasomatic changes accompanying the alteration of volcanic glass to zeolites at the Bowie deposit include enrichment of MgO and depletion of K_2O. A lateral chemical gradation of bulk, zeolitic-tuff samples of increasing CaO:Na_2O and SiO_2:Al_2O_3 ratios correlative with increasing salinity has been reported for the Bowie chabazite deposit (Sand and Regis, 1967; Edson, 1977; Sheppard and others, 1978). No such gradation is apparent from the chemical analyses of

bulk, zeolitic tuffs at DSV reported here.

LOI values for the zeolitically altered tuffs are much greater than those of the predominantly vitric tuffs, suggesting zeolitization produced an enrichment in H_2O. Fe_2O_3 and H_2O^- content are variable in a seemingly random manner.

Several generalizations on basin geochemistry can also be made from the chemical analyses of lacustrine claystones (Table 4). The SiO_2:Al_2O_3 ratio increases from west to east in the T_{lc} and T_{mc} units but generally decreases in this direction in the T_{uc} unit. Further analyses of the claystones are needed to determine if there is a true, lateral, SiO_2:Al_2O_3-mineralogical trend.

The CaO:Na_2O ratio is relatively high for all analyzed claystones. This is to be expected because all samples but one are from the northeast side of the basin where extensive weathering of Paleozoic carbonates from the Pinal and Mescal Mountains has contributed large amounts of calcium to the lake. Drill hole data suggest the southeastern portion of the basin was deeper, and probably more saline, than the northern and northwestern parts of the basin. Further chemical analyses of the claystones, especially from the southeastern portion of the basin, could help confirm this supposition.

Magnesium and potassium concentrations are covariant in the T_{lc} and T_{mc} units. They generally decrease from west to east. The potassium concentration generally increases from west to east in the T_{uc} unit. Magnesium content exhibits no

real areal pattern in the T_{uc} unit, but is anomalously high where the unit is strongly calcified. The magnesium content is somewhat higher for the claystones than the tuffs, due chiefly to its accumulation in the structures of illite, montmorillonite, and chlorite.

Iron oxide concentrations vary in a nonsystematic manner in the tuff and claystone units, however, the iron content of the claystones is consistently two to five times that of the altered tuffs. This may be attributable to the iron present in detrital minerals, such as biotite, magnetite, pyrite, illite, and chlorite, in the claystones.

The concentrations of TiO_2, P_2O_5, and MnO in the claystones are relatively constant. An anomalously high TiO_2 content in the T_{uc} unit at locality 63 may be attributable to weathering of igneous rocks from the Dripping Springs Mountains.

LOI values are essentially constant within each claystone unit. These range from approximately 11 to 18%, which is slightly lower than those determined for the altered tuffs. H_2O^- values vary randomly in the tuff and claystone units.

Genesis of the Dripping Springs Valley Chabazite Deposit

The DSV chabazite deposit is young (Miocene(?)-Pleistocene) and has undergone shallow burial. It has therefore remained under near-surface conditions of temperature and pressure. The tuffs are interbedded with relatively impermeable claystones. After deposition, the tuffs probably

behaved as closed systems consisting of rhyolitic glass and interstitial water. Thus, the occurrence and distribution of authigenic silicates in the tuffs reflect the chemistry of the interstitial fluids present during diagenesis.

Chabazite precipitated via solution of the rhyolitic glass by moderately saline and alkaline connate water. Deffeyes (1959) stressed that zeolites form during diagenesis by solution of glass shards and subsequent precipitation of zeolite from the solution, rather than by devitrification. This process is supported by SEM studies by Mumpton (1973) and by experimental studies of glass hydration by Colella and others (1978). Dissolution of the shards is dependent upon the size (and surface area) of the shard. Scanning electron micrographs of the DSV tuffs illustrate some chabazite precipitated in cavitites formed by complete solution of shards, while some chabazite apparently formed concurrently with solution of the shards (Fig. 27). Solution of the shards is commonly incomplete and chabazite consistently occurs adjacent to relict glass, especially near the margins of the basin. This relationship is typical of chabazite in saline, alkaline-lacustrine environments.

Several parameters influence whether clay minerals, zeolites, or feldspars will precipitate when pore solutions react with vitric ash. These include: 1) salinity, 2) pH, 3) relative proportions of the alkali and alkaline earth cations, in particular, Na^{+}, K^{+}, Ca^{2+}, and Mg^{+2}, 4) activities of dissolved species such as H^{+}, H_4SiO_4, and SiO_2, and

5) activity of H_2O (Hay, 1966; Sheppard and Gude, 1968; Surdam, 1977; Ratterman and Surdam, 1981). Precipitation of phyllosilicates is generally favored by high activities of Mg^{+2} and by high ratios of H^+ to base cations (Surdam, 1977). Sheppard and Gude (1968) and Starkey and Blackmon (1979) speculate that early formation of the small amounts of montmorillonite in the tuffs of Lake Tecopa occurred immediately after deposition of the ash when the H^+:Na^++K^+ activity ratio was high. This mechanism of montmorillonite formation is also inferred for the tuffs in DSV.

Surdam (1977) outlined the chemical parameters which affect zeolite paragenesis in saline, alkaline-lake environments. In general, an ideal lateral basinward zonation of fresh glass ---> alkalic, silicic zeolites ---> analcime --> K-feldspar will develop should the appropriate chemical and kinetic conditions exist. The most common alkalic, silicic zeolites in saline, alkaline-lake deposits are clinoptilolite, chabazite, erionite, phillipsite, and mordenite.

The species of zeolite which crystallizes is dependent upon temperature, pressure, and the chemical activities of base cations, silica, aluminum, and water (Hay, 1966). The cation ratio, Si:Al, and H_2O compositional parameters are affected by changes in salinity and alkalinity. Mariner and Surdam (1970) demonstrated that the solubility of rhyolitic glass increases with increasing alkalinity. They also suggested that the Si:Al ratio of the zeolites formed by the hydration and solution of glass is a function of the pH of the alkaline solution. The activity of the alkaline earths

decreases rapidly with increasing alkalinity (Surdam, 1977); the activity of H_2O decreases with increasing salinity.

The paragenesis of the DSV zeolite deposit is similar to that recognized in other deposits of altered lacustrine tuffs, but does not exhibit the complete zeolite paragenetic sequence. A model of zeolitization for the DSV deposit must, therefore, explain why the paragenetic sequences of fresh glass ---> chabazite, and fresh glass ---> montmorillonite (and possibly mixed-layer illite/smectite) ---> chabazite observed, generally have not proceeded past the stage of chabazite authigenesis. Although clinoptilolite and erionite have also been detected, their occurrence is too rare to ascertain their paragenetic relations with confidence. Further, the chemical and mineralogical similarities of the altered tuffs suggest similar chemical conditions were prevalent in the lake throughout the time of tuff deposition.

Kinetic and chemical factors may be equally responsible for the mineral paragenesis at DSV. The overall topographic gradient of the valley decreases from northwest to southeast, and widespread erosion has removed large portions of the tuffs. Thus, the present zeolitic tuffs are erosional remnants which were previously of much larger areal extent. The tuffs could conceivably have had a concentric zonation with a potassium feldspar facies surrounded by an analcimic facies, which in turn, was surrounded by a nonanalcimic facies, most of this signature having been destroyed by erosion. Similarly, in areas where the tuffs have not been

eroded at the southeast end of the basin, they are covered by alluvium. Additionally, exploratory drilling has not been conducted at the southeasternmost end of the basin.

Surdam and Eugster (1976) and Surdam (1977) suggest wide playa flats are necessary to produce a well-developed lateral zonation of zeolites. At DSV, wide playa flats existed on the north and northeast sides of the depositional basin, but the lacustrine sediments directly abut the flanks of the steep-walled Dripping Springs Mountains to the south, southwest, and southeast. Although saline, alkaline conditions conducive to the formation of analcime or potassium feldspar may have existed towards the southeast end of the basin, the lack of extensive playa flats there could also have led to widespread encroachment of "fresher" groundwater upon the lake, inhibiting the formation of these minerals.

At DSV, chabazite precipitated under moderately saline, alkaline conditions shortly after deposition of the ash-fall tuffs, when the H^+:alkali ion ratio of the pore water had decreased below the level for montmorillonite formation. Chabazite formation is favored, over other zeolites and feldspar, by a comparatively silica-poor environment (Coombs and others, 1959) with a high activity of H_2O and low $K^+:Na^+ + Ca^{+2} + Mg^{+2}$ activity ratio. Although SiO_2 activity increased from the hydrolysis of the ash, it remained at low enough levels so that the DSV chabazite could form. Furthermore, neither free quartz/opal nor authigenic quartz is associated with the tuffs. Traces of the comparatively more siliceous clinoptilolite and erionite probably began to

crystallize when silica activity became sufficiently high; a condition not long maintained.

The reaction necessary for an alkalic, silicic zeolite, such as chabazite, to form analcime is favored by a low H^+:Na^+ ratio and relatively low activity of SiO_2 ,Si:Al ratio, and activity of H_2O in the pore fluid (Surdam, 1977). A significant increase in the salinity and alkalinity of the pore fluid in the DSV tuffs would have produced chemical conditions favoring analcime by reducing the activity of water, reducing the Si:Al ratio, and decreasing the H^+:Na^+ ratio.

Authigenic potassium feldspar is commonly found in highly saline, alkaline chemical environments. Alkalic, silicic zeolites or analcime may react with pore fluids to crystallize potassium feldspar. The activities of cations, silica, and water are the controlling parameters of such reactions (Surdam, 1977). The primary changes resulting from the reactions are a gain of potassium and losses of sodium and water. Potassium concentration of brines reaches a maximum in the most saline and alkaline brines (Eugster, 1970). A high-pH pore fluid with a high potassium content would have a relatively high K^+:H^+ ratio conducive to the crystallization of potassium feldspar. Further, such a solution might also have a relatively high K^+:Na^++Ca^{2+}+Mg^{2+} activity ratio which would favor the stabilization of potassium feldspar relative to alkalic, silicic zeolites or analcime. A relatively high salinity would reduce the activity

of water and favor the formation of anhydrous potassium feldspar over hydrous zeolites, including chabazite and analcime (Surdam, 1977).

To summarize, assuming that the DSV tuffs were essentially monomineralically altered to chabazite, and never contained an analcime or potassium feldspar facies, only moderately saline and alkaline conditions prevailed in the connate and lake waters throughout deposition of the ash-fall tuffs. The steepness of the flank of the Dripping Springs Mountains may have carried extensive surficial "fresh" water runoff into the lake, inhibiting the development of relatively high saline and alkaline lake waters.

COMPARISON OF SELECTED CLOSED-BASIN ZEOLITE DEPOSITS IN THE SOUTHERN BASIN AND RANGE PROVINCE OF ARIZONA AND NEW MEXICO

Sedimentological and Structural Characteristics of Southern Basin and Range Province Valleys and Basins

The southern Basin and Range province is an area of regionally-corrugated, angular topography of high relief characterized by evenly-spaced, sub-parallel, north-northwest-trending mountain ranges five to 30 km (3.1 to 18.6 mi) wide, and intervening desert valleys commonly ten to 20 km (6.2 to 12.4 mi) wide. The range flanks consist of wide pediments which slope gently basinward, commonly covered by poorly-sorted material concealing range-bounding faults. Late Cenozoic Basin and Range tectonism has produced grabens, which underlie only a small portion of the total valley surface area (Aiken, 1978), between these pediments.

In southeast Arizona, the northeast-southwest-directed extensional regime of the Basin and Range disturbance resulted in volumetrically-minor, alkali-basaltic volcanism (Suneson and Lucchitta, 1983) and large-scale, deep, pervasive fracturing. This tectonism disrupted broad basins created by earlier extensional regimes, and formed a network of deeply subsiding (approximately 18.3 to 182.8 m [60-600 ft]/m.y. relative to the ranges; Damon and Shafiqullah, 1973), closed, more sharply defined basins, in which thick sequences of fluvial, lacustrine, and evaporite sediments accumulated. Lacustrine beds of exactly the same age were deposited in several contemporaneously dammed, subjacent basins. This suggests contemporaneous block faulting was

occurring in the region (Scarborough, 1975). The basins were linked by a series of spillways over bedrock shoulders. Intermittent streams deposited mudstone, siltstone, and minor evaporite sequences along valley segments between spillways.

Tectonic and climatic changes have influenced the evolution of the closed, regional paleodrainage system into the modern, moderately well integrated, exterior system (Hollander, 1960; Martin and Mehringer, 1965; Long, 1966; Scarborough, 1975; Schreiber, 1978). Upwarping, subsidence, and sedimentation continued into the Pliocene (Eaton, 1979; Nations and others, 1982) or Pleistocene (Scarborough and Peirce, 1978) when tectonism and volcanism diminished, allowing establishment of through-flowing drainage (Melton, 1960) and stream incision in the more elevated basins.

The "basin-fill" deposited in basins created by the Basin and Range disturbance and earlier extensional tectonic regimes are exposed in areas of deep dissection or uplift. The deposits are in fault contact with, or unconformably underlie, the Plio-Pleistocene integrated stream and pediment deposits of Heindl (1954). The basin-fill are characterized by: 1) texture and composition that suggest deposition in basins different from the structural troughs of the existing topography, 2) local deformation by thrusting or more complex normal faulting, and 3) occasional intrusion and mineralization (Heindl, 1954). Reliable stratigraphic correlations of units within and between troughs is difficult due to a paucity of age significant fossils. According

to Scarborough and Peirce (1978) the basin-fill is differentiated sedimentologically and structurally from older deposits in that it: 1) tends to retain original depositional dips, 2) contains facies relationships relatively consistent with modern valley configurations, 3) is tectonically deformed only locally, and 4) unconformably overlies rocks as young as early to middle Miocene within areas close to the mountain-piedmont interface.

The typical lithologic facies zonation of basin-fill within the southern Basin and Range province consists of a coarser-grained piedmont facies, in fault and/or depositional contact against range blocks, which grades, often imperceptibly, into a finer-grained basin-center facies. The coarse phase generally consists of bedded, subangular to subrounded cobble fanglomerate with lenses and channel-fill pods of fluvial sand and unsorted, unbedded debris flows (Scarborough and Peirce, 1978). Depositional dips are gentle, usually no more than a few degrees. The basin-center facies consists of either fluvial overbank or lacustrine deposits. Scarborough and Peirce (1978) note the fluvial overbank facies is an assemblage of poor- to well-bedded sandy silt and silty sand which are horizontally bedded cross-valley but dip down-valley subparallel to present stream gradients; they contain lenticular admixtures of thin clay-rich beds, local gypsum beds, and local clay and zeolitically altered ash-fall tuff beds. They also contain local ponded deposits of subeconomic diatomite. The lacus-

trine facies contains more extensive beds of marly limestone, often unconsolidated green- and red-colored silty clay, evaporites, and vitric-silicic ash-fall tuff. Although large volumes of water were required for deposition of the thicker evaporite sequences, the overall depths of the lakes were probably not great, as suggested by scattered occurrences of large mammal footprints and fossils concentrated throughout the lakebeds (Lance, 1960; Seff, 1960; Nations, 1974; Scarborough and Peirce, 1978; Eyde, 1982).

Zeolite Deposits in SE Arizona and SW New Mexico

Volcanic ash deposited in the basins of the southern Basin and Range province was altered to zeolites and associated silicate minerals upon reaction with saline, alkaline-connate and lake waters. Potentially commercial zeolite deposits are located at DSV, Tonto Basin, Bear Springs, and near Bowie, Arizona, and near Buckhorn, New Mexico. The sedimentologic and mineralogic characteristics of these deposits are summarized in Table 5. Numerous other zeolite occurrences and potentially zeolitized ash beds have been reported in saline, alkaline-lake environments in the southern Basin and Range province that will not be discussed in this report. See Hay (1966), Long (1966), Olson (1975), Scarborough (1975), Hawley and others (1976), Arizona Department of Mineral Resources (1978), Janders (1978), Krieger (1979), and Sheppard and Gude (1982) for more information on these occurrences.

Examination of published descriptions and of Table 5

Table 5. Sedimentologic and mineralogic characteristics of five potentially economic zeolite deposits in saline, alkaline-lacustrine systems in the southern Basin and Range province. cs = claystone, ms = mudstone, sls = siltstone, ss = sandstone, ls = limestone, cgl = conglomerate, Tmz = main zeolite tuff horizon, Tuz = upper zeolite tuff horizon, th = thick, cb = chabazite, cl = clinoptilolite, er = erionite, ph = phillipsite, he = heulandite, an = analcime, i = illite, i/sm = mixed-layer illite/smectite, sm = smectite, chl = chlorite, kao = kaolinite, qtz = quartz, calc = calcite, gyp = gypsum, kspar = potassium feldspar, plag = plagioclase, dolo = dolomite, hal = halite, fld = feldspar, hbl = hornblende, bio = biotite, zr = zircon, amts = amounts, ≈ = approximately, th = thick.

Deposit Characteristic	Dripping Springs Valley, AZ cb deposit	Tonto Basin, AZ cb deposit	Bear Springs, AZ cb deposit	Bowie, AZ cb deposit	Buckhorn, NM cl deposit
Location	Lat. 33°07'N Long. 110°46'W along AZ Rt. 77 about 23 mi S of Globe, Gila Co.	along Greenback Valley Rd. about 2.5 mi E of Punkin Center, Gila Co.	2 occurrences near Bear Springs in sec. 1, T.7S., R.23E., 7 mi SW of Pima and 1 occurrence in sec. 27; T.6S., R.24 E., 3 mi SW of Pima; all 3 in Gila River Valley of Graham Co.	Lat. 32°29'N Long. 109°27'W in several secs. in T. 11 and 12S., R.29 and 30 E. about 10 mi NNE of Bowie, in the San Simon Basin, Graham and Cochise Co.'s.	Lat. 33°01'N Long. 108°42'W along W side of Duck Creek Valley in secs. 3, 4, and 10, T.15S., R.18W. about 1 mi S of Buckhorn, Grant Co.
Age of Host Rocks	Miocene(?)-Pleistocene	late Tertiary-early Quaternary	Plio-Pleistocene	Plio-Pleistocene	Plio-Pleistocene
Host Lithologies	formally unnamed lacustrine reddish-brown cs, sls, ss, and ls beds that are nearly flat-lying but dip gently basinward	Gila Cgl—typical lacustrine sequence of ms interbedded with ss, cgl and, less commonly, ls and gyp beds	Solomonsville beds—lacustrine brown ms beds interbedded w/ls, ss, and cgl beds	generally flat-lying, epiclastic fluvial and lacustrine sediments including brown and green clay, and silt, sand, gravel, caliche and cgl representing younger stream deposits (150'th), lake deposits (350' th), and older stream deposits (750' th)	Cactus Flat beds of the upper part of the Gila Cgl—lacustrine green and brown ms and cs
	may be correlative with Miocene Big Dome Fm of Gila River Valley	nearly flat-lying lakebeds dip gently toward center of basin	nearly flat-lying lakebeds dip gently toward center of the Gila River Valley	may be correlative w/ Solomonsville beds in Safford area 25 mi N of this deposit	the deposit is correlative with diatomite deposits ≈ 3 mi N of Buckhorn

Table 5 (cont'd)

Deposit Characteristic	Dripping Springs Valley, AZ cb deposit	Tonto Basin, AZ cb deposit	Bear Springs, AZ cb deposit	Bowie, AZ cb deposit	Buckhorn, NM cl deposit
Zeolite Horizon Descriptions	2 potentially commercial zeolitically altered ash-fall tuffs: Tmz-0.5 to 1.74' th; consists of 3 distinct lithologies (see text) Tuz-up to 5.5' th; consists of 3 distinct lithologies (see text)	informally referred to as Haystack Butte ash bed; up to 12' th; basal foot very pure, remainder of unit is less pure and displays thin horizontal- and cross-bedding from 3 to 6 distinct lithologies recognized in quarry outcrop	lower bed near Bear Springs consists of 2 lithologies: a lower bed 0.5' th and an upper massive bed 1' th upper bed near Bear Springs consists of 2 massive beds each 0.5' th separated by a thin clay parting zeolite bed SW of Pima is about 100' stratigraphically lower than the 2 beds at Bear Springs	2 separate zeolitic-tuff horizons: 1) the marker-tuff horizon consists of 2 lithologies: a lower massive or high grade bed 4-10" th, overlain by a thin-bedded or low grade bed 8-47" th, 2) the lower horizon is 77' below marker-tuff horizon, is up to 26" th, and is platy in the lower few inches and massive above this	2 horizons separated by ≈ 20' of green and brown ms lower horizon-zeolitically altered tuff 3-5' th. upper horizon-massive zeolitically altered tuff 1' th. tuffs were originally probably of rhyodacitic composition
Mineralogy of the Deposit	Tmz-clean, unaltered vitric ash at N end and up to 90% cb at S end of deposit—lesser qtz, calc, gyp, kspar, plag, clay minerals—rare cl, er Tuz-middle massive bed averages 67% cb w/lesser qtz, calc, gyp, dolo, hal, kspar, plag, clay minerals cs- i, i/sm, chl, sm, kao	all lithologic units of ash bed contain cb and cl	lower bed near Bear Springs averages ≈ 45% cb upper bed near Bear Springs averages ≈ 50% cb zeolite bed SW of Pima contains ≈ 80% cb all 3 beds also contain er and trace qtz, fld, mica, and ph	marker-tuff horizon: high grade bed—60-90% cb, trace to 15% er, w/lesser cl, an, thenardite, hal, gyp, clay minerals, qtz, calc, sodic plag, hbl, clinopyroxene, zr. low grade bed— ≈ 40% cb and significant amts. of er and cl lower horizon: mineralogy similar to that of marker-tuff horizon	ms contains sm, zeolites, qtz, calc, and minor to trace i, plag, and secondary gyp. lower horizon-averages 70-90% cl -a lower 0.5' th bed contains ≈ 40% cb and equal amts. of cl upper horizon-over 60% cl and trace er the horizons also contain he, an intermediate phase between cl and he, an, magadiite-type chert, qtz, calc, i/sm, plag, fluorite, hbl and bio.

Characteristic	AZ cb deposit	cb deposit	Bear Springs, AZ cb deposit	Bowie, AZ cb deposit	Buckhorn, NM cl deposit
Paragenetic Sequence of Authigenic Mineralization	glass —> sm (i/sm), cb glass —> cb			glass —> sm and overlapping cb —> er, cl —> an —> sm	hydrolysis of ash => minor clay with overlapping he-group mineralization => er, an => magadiite => inversion of magadiite to chert => possible formation of a second generation of an => caliche formed by cation exchange reactions between zeolites and later solutions
Exploratory Drill Holes	over 150 drilled by Anaconda Minerals Co.	none reported	none reported	over 3,000 drilled by the USGS	none reported
Nature of Exposures and Extent of Deposit	only 3 exposures of Tmz Tmz underlies area of ≈ 1 mi^2 Tuz exposures abundant Tuz underlies area of ≈ 3 mi^2	Haystack Butte ash bed is an important marker bed exposed in the N half of Tonto Basin	lower bed near Bear Springs traceable for ≈ 1 mi along strike upper bed near Bear Springs traceable for ≈ 0.5 mi along strike zeolite bed SW of Pima traceable for ≈ 500' along strike	marker-tuff horizon underlies an area of 25 mi^2 and crops out for 7 mi along strike, mostly on the SW side of San Simon Valley reserves estimated at several million tons of high-grade cb	lower and upper horizon traceable for over 1 mi along strike
Characteristics of Depositional Basin	NW-trending basin, deeper at the SE end saline, alkaline-lake environment	saline, alkaline-lake environment	saline, alkaline-lake environment	NW-trending basin, deeper at the SE end saline, alkaline-lake environment	4 distinct depositional environments in the deposit: 1) soil horizon probably developed on alluvial fan, 2) intermittent stream channel and overbank deposits, 3) interchannel flood-plain deposits, 4) lacustrine or ponded deposits.
References	This report AZ Dept. Mineral Resources (1978) Eyde (1982) Sheppard and Gude (1982)	Royse and others (1971) AZ Dept. Mineral Resources (1978)	AZ Dept. Mineral Resources (1978) Eyde (1982)	Sand and Regis (1967) Edson (1977) AZ Dept. Mineral Resources (1978) Eyde (1978, 1982) Sheppard and others (1978) Sheppard and Gude (1982)	Olander (1979) Eyde (1982) Sheppard and Gude (1982) Sheppard and Mumpton (1984)

reveals several sedimentologic and mineralogic similarities among the zeolite deposits: 1) they are young (Miocene[?]-Pleistocene), 2) they have undergone shallow burial and, consequently, have remained under near-surface conditions of temperature and pressure, 3) they are interbedded with epiclastic fluvial and lacustrine sediments, 4) they were formed in a series of shallow lakes which had variable water levels and variable alkalinity, and in which sedimentation was active concurrently with ash deposition, 5) they are generally flat-lying and, 6) they are lenticular, ranging from a few inches to several feet thick, and are widespread but have been locally removed by erosion. In general, more than one zeolitic-tuff horizon occurs at each deposit. Only one zeolite bed crops out at the Tonto Basin locality, but several other zeolitic-tuff beds, each apparently at different stratigraphic horizons, crop out nearby in the Salt River-Tonto Creek drainage area above Roosevelt Dam (Arizona Department of Mineral Resources, 1978).

The zeolitic tuffs within these five deposits exhibit varying degrees of alteration; they range from highly vitric ash beds, to sandy, clastic tuffs containing a high percentage of lithic material and little vitric ash, to high purity, zeolitically altered tuffs. The original vitroclastic texture of the ashes is preserved. The altered tuffs are extremely fine grained, of low density, and are colored white, gray, and various pastel shades. They vary from massive to thinly bedded. The microcrystallinity of the constituent authigenic mineral assemblage makes estimation

of the relative percentage of each mineral difficult with XRD methods. Scanning electron microscopy is often used to aid this determination and to measure crystal size. The size of individual chabazite crystals at the DSV, Bear Springs, and Bowie deposits averages much less than one micrometer and is typically less than 0.2 micrometers (Edson, 1977; Eyde, 1978; Sheppard and others, 1978). At the Bowie deposit, clinoptilolite crystals are typically two to 32 micrometers long, erionite bundles range from ten to 60 micrometers long, and the maximum dimension of analcime trapezohedra-shaped crystals is 40 micrometers (Sheppard and others, 1978).

The mineralogy of the five zeolite deposits described in Table 5 is quite similar except that the deposits exhibit varying stages of zeolite authigenesis. The zeolitic tuffs have either been essentially monomineralically altered or altered to an assemblage of zeolites, clay minerals, and locally to potassium feldspar or saline minerals. For those deposits in which the mineralogy of the host claystones is known, mixed-layer illite/smectite, discrete illite, chlorite, and lesser smectite and kaolinite dominate the mineral assemblage.

All five deposits contain tuffs which have been at least locally altered to chabazite. Constraints imposed by moderately high salinity and alkalinity of pore fluids in the DSV tuffs inhibited formation of more siliceous zeolites (such as clinoptilolite, erionite, and phillipsite) or anal-

cime, whereas slightly higher salinities and alkalinities of pore fluids in tuffs of the other four zeolite deposits have induced precipitation of these minerals. The Haystack Butte ash bed in the Tonto Basin contains both chabazite and clinoptilolite. The three zeolitic-tuff beds of the Bear Springs deposit contain chabazite and erionite, and trace phillipsite. No paragenetic sequence of zeolite precipitation has been reported for the Tonto Basin or Bear Springs deposits but the more siliceous zeolites probably precipitated at the expense of fresh glass, smectite, and/or chabazite.

Increasing salinity and alkalinity basinward caused lateral zonation of zeolite authigenesis at the Bowie deposit. The high grade bed of the marker-tuff horizon contains abundant chabazite with minor erionite, clinoptilolite, and analcime. The low grade bed contains approximately 40% chabazite and significant erionite and clinoptilolite. The mineralogy of the lower zeolite horizon is similar to that of the marker-tuff horizon. The paragenetic sequence observed at the Bowie deposit is typical of zeolite authigenesis in saline, alkaline-lake environments. Smectite and chabazite were the first minerals to crystallize upon hydrolysis of the fresh glass. Erionite and clinoptilolite crystallized later under more saline and alkaline conditions. Analcime precipitated later at the expense of the alkalic, silicic zeolites under even higher saline and alkaline conditions.

The mineralogy of the Buckhorn deposit is dissimilar to

that of the other four deposits, owing to a vastly different basin-water chemistry and possibly to a different parent ash composition. Olander (1979) speculates that the Buckhorn ash was originally of rhyodacitic composition. In contrast, the DSV and Bowie tuffs were probably originally of rhyolitic composition.

Interstitial solutions passing through the Buckhorn tuff were slightly concentrated, probably with a composition approaching that of Magadi-type $Na\text{-}HCO_3\text{-}CO_3$ brines, or resembling Magadi spring waters (Olander, 1979). Olander states that these solutions were probably moving with a basinward component during most of the zeolitization, inhibiting extensive development of authigenic potassium feldspar or zeolites with relatively low Si:Al ratios, such as chabazite. Hydrolysis of the ash initially resulted in minor clay with overlapping heulandite-group (including clinoptilolite) mineralization. Erionite and analcime were precipitated later through reactions involving localized, concentrated, alkaline solutions. These minerals locally replaced earlier siliceous zeolites. The lower horizon averages 70 to 90% clinoptilolite and the upper horizon averages over 60% clinoptilolite. Both horizons also contain lesser heulandite, a phase intermediate between clinoptilolite and heulandite, erionite, analcime, magadiite, quartz, calcite, mixed-layer illite/smectite, and fluorite. Magadiite may have precipitated close to a fault system tapping deeper-circulating, H_4SiO_4-rich solutions (Olander,

1979).

Regional uplift in the southern Basin and Range province in late Cenozoic time established through-flowing drainage, allowing downcutting of the more elevated basins. Deformation of the basin-fill was minor, although some tilting and faulting did occur. The zeolitic tuffs of the DSV, Tonto Basin, Bear Springs, Bowie, and Buckhorn deposits were extensively eroded and channeled.

Provenance of Zeolitic Ash in SE Arizona and SW New Mexico

Source areas for zeolitized ashes in southeast Arizona and southwest New Mexico have not yet been pinpointed. Several volcanic fields have been proposed as source areas on the basis of constraints imposed by time of deposition, and distance between source area and depositional site.

Scarborough (1975) dated several vitric ashes in southeast Arizona and concluded they were deposited between two and six million years ago, therefore, during the Pliocene. Consequently, only volcanic sites active during that time can be considered as possible source areas of the ashes. The zeolitized ashes in DSV, Tonto Basin, and in the San Simon and Gila River Valleys near Bear Springs, Bowie, and Buckhorn were probably deposited in Plio-Pleistocene time.

The size of vitric ash particles is inversely proportional to the distance from the source. A close source area would be expected to deposit relatively thick ash layers containing coarse glass shards, with pumice fragments and abundant primary mineral grains. Alternately, a distant

source would most likely produce relatively thin beds of fine glass shards with sparse primary grains of very small size. In addition, the smaller the particle size, the larger the surface area (for a given volume of ash) of vitric ash available for reaction with the saline, alkaline-lake water.

Eyde (1982) believes the zeolitized ashes of the San Simon and Gila River Valleys may have been generated by volcanic activity farther west. The source volcanoes could be related to the rifting in the Gulf of California (Scarborough, 1975). The ash was carried eastward by the prevailing winds and deposited in the saline, alkaline-lakes in these valleys. Ash transport over 700 km (435 mi) is not unrealistic. Scarborough (1975), for example, shows that the relative thinness of the ash beds, the sparseness of primary mineral grains, and the maximum grain-sizes (slightly over 0.70 mm) of ashes in southeast Arizona indicate source volcanoes up to 800 km (497 mi) distant. The zeolite deposits of the San Simon and Gila River Valleys are significantly thinner, their individual crystal size is smaller, and they are of higher purity than genetically similar deposits in California, Oregon, and Nevada (Eyde, 1982). This may be because the deposits in the San Simon and Gila River Valleys are farther from the same source of the volcanic ash, assuming these deposits are correlative with those to the west.

Grain size data for vitric ashes in southeast Arizona and southwest New Mexico is sparse. The ashes are generally

very fine- to fine-grained sand size. Within this region, there does not appear to be an areal pattern of grain size distribution which is indicative of a unique direction of ash transport.

The Hopi Buttes volcanic field of northeast Arizona was active during the Pliocene. Scarborough (1975) believes this volcanic field is a possible source for the rhyolitic vitric ashes of the Lower San Pedro Valley. It may have also supplied ash to adjacent valleys in southeast Arizona.

Scarborough (1975) lists a few volcanic sequences which, with further study, may provide additional information as to the source of ashes in southeast Arizona. Included are numerous volcanic deposits in central and west-central Arizona, many of which were deposited in Plio-Pleistocene time.

The extensive Datil-Mogollon volcanic field of Arizona and New Mexico is composed of intrusive, extrusive, and pyroclastic rocks, with compositions ranging from rhyolitic to basaltic. Olander (1979) postulates the zeolitized ash of the Buckhorn clinoptilolite deposit was originally of rhyodacitic composition and was derived from the Datil-Mogollon field. This volcanic field may have also provided the ash precursor for other zeolite occurrences in Arizona and New Mexico.

CONCLUSIONS

The Basin and Range disturbance extensional regime created a series of northwest-trending, closed basins in southeast Arizona and southwest New Mexico which accumulated epiclastic-fluvial and lacustrine sediment. Zeolitization of air-fall tuffs resulted from reaction of vitric ash with saline, alkaline-lake waters in this system. The DSV, Tonto Basin, Bear Springs, and Bowie, Arizona chabazite deposits and the Buckhorn, New Mexico clinoptilolite deposit are potentially economic zeolite prospects formed in this system.

These five deposits have several similarities: 1) they are young (Miocene[?]-Pleistocene); 2) they have formed under near-surface conditions of temperature and pressure; 3) they are interbedded with epiclastic-fluvial and lacustrine sediments. The typical lithologic zonation of basin-fill in the southern Basin and Range province consists of a coarser-grained piedmont facies which laterally grades into a finer-grained basin-center facies. The basin-center facies often contains lacustrine sequences of silty clay, marly limestone, evaporites, and vitric-silicic ash-fall tuffs; 4) they were formed in a series of shallow lakes in which sedimentation and reworking were active concurrently with ash deposition; 5) the zeolitic tuffs are generally flat-lying and lenticular; 6) more than one ash-fall tuff was zeolitically altered at each deposit; and 7) the zeolites are microcrystalline.

Beginning in Plio-Pleistocene time, regional uplift of the southern Basin and Range province established through-flowing drainage, allowing stream incision of the more elevated basins. Paleochannels have eroded large portions of the lakebeds and tuffs.

At least ten ash-fall tuffs are interbedded with lacustrine claystone in DSV. At least five of these have been zeolitically altered. Chabazite is the predominant zeolite but the tuffs also contain rare clinoptilolite and erionite. XRD analysis indicates that the main zeolite tuff ranges from clean, unaltered vitric tuff at the north end of the deposit to 90% chabazite at the south end. Chabazite occurs in each zeolitized tuff as "cubes" or "rhombs" usually much less than one micrometer but up to two micrometers on a side. The crystals are isolated or occur as intergrown clusters or radial stringers. The tuffs also contain trace to abundant fresh glass, quartz, calcite, dolomite, potassium and plagioclase feldspar, evaporite minerals, clay minerals, magnetite, and pyrite. XRD data reveal there is an inverse correlation between the abundance of chabazite and fresh glass in the main zeolite tuff. The chabazite content increases basinward where moderately saline, alkaline waters were present, while the fresh glass content increases towards the basin margins, where there was a greater freshwater influx.

XRD analyses of the less-than-two micron size fraction of the DSV lacustrine and alluvial facies indicate that they contain discrete illite, illite/smectite, chlorite, sodium

smectite, and kaolinite, in decreasing order of abundance. This clay mineral assemblage is typical of saline, alkaline-lake deposits in the southern Basin and Range province. The clays of DSV are predominantly detrital but some discrete illite, illite/smectite, and sodium smectite formed authigenically via reaction of moderately saline and alkaline pore fluids with the volcanic glass and/or precursor clay minerals.

All the tuffs of DSV presumably are of rhyolitic parentage. XRF spectrometry of DSV bulk, zeolitic-tuff samples indicates that zeolitization of fresh rhyolitic tuff produced an enrichment of Al_2O_3, MgO, CaO, TiO_2, P_2O_5, and H_2O, and a loss of SiO_2, K_2O, and MnO. Na_2O became enriched in some tuffs but depleted in others.

Scanning electron microscopy of selected DSV zeolitic tuffs reveals paragenetic sequences of fresh glass --> chabazite, and fresh glass --> smectite (and/or illite/smectite) --> chabazite. Clinoptilolite and erionite are too rare to ascertain their paragenetic relationships with confidence. The complete basinward paragenetic sequence of fresh glass --> alkalic, silicic zeolites --> analcime --> potassium feldspar observed in many closed-hydrographic basin zeolite deposits probably never completely developed in DSV due to kinetic as well as chemical factors. Chabazite precipitated via solution of the rhyolitic glass by moderately saline and alkaline pore solutions when the H^+:alkali ion activity ratio decreased below the

level for montmorillonite crystallization. Chabazite authigenesis was also favored by the relatively silica-poor environment in which the activity of H_2O was high and the K^+:Na^+ + Ca^{+2} + Mg^{+2} activity ratio was low.

The southeast end of the basin probably contained the most saline, alkaline-lake waters. Surficial freshwater runoff from the Dripping Springs Mountains at this end of the basin, may have encroached upon the lake. This could have inhibited the development of even higher saline and alkaline conditions, which favor the crystallization of the more siliceous zeolites clinoptilolite and erionite, in addition to analcime and potassium feldspar. These conditions would have kept the activity of H_2O, the Si:Al ratio, and the H^+:Na^+ activity ratio relatively low. The similar mineralogic assemblages of all the DSV tuffs suggests the moderately saline and alkaline chemical environment persisted throughout their deposition.

APPENDIX I

Detailed lithologic descriptions of the rock units of DSV. The descriptions are derived from field and laboratory observations and from Banks and Krieger (1977) and Cornwall and Krieger (1978).

Q_{al} - **RECENT ALLUVIUM** - Gravel, sand, silt and clay deposits in stream channels and on young low-lying terraces along streams.

Q_t - **TALUS** - "Accumulations of large to small angular blocks at or near base of cliffs and steep slopes (Cornwall and Krieger, 1978)."

Q_p - **SOIL AND GRAVEL VENEER** (0-8.05 m [26.4 ft]) - Unconsolidated reddish-brown soil and gravel with subangular to subrounded pebble to boulder clasts from older rock. The unit covers gently sloping pediment (terrace) surfaces of several ages and is developed largely on older gravel (Q_{og}), lakebeds (T_{uc}, T_{uz}, T_{mc}, T_{mz}, T_{lc}), and conglomerate units (T_g, T_{gc}). Limestone clasts are rare even where deposits overlie carbonate rock or limestone conglomerates.

Q_{og} - **OLDER GRAVELS AND SECONDARY CARBONATES** (0-15.1 m [49.5 ft]) - Reddish clay, silt and sand, and grayish- to yellowish-white carbonate (calcite)-cemented gravels, caliche (?), and conglomerate deposited along but at higher levels than present channels, streams, and washes; in local isolated patches covering older rocks and which, in places, has eroded lakebed deposits; very poorly to moderately well sorted, subangular to rounded, sometimes bedded and graded bedded clasts of older rocks exposed along adjacent drainages; includes deposits of several ages; contains rootlets and root casts; poorly indurated talus slope former; imbrication directions difficult to determine; unit includes a consolidated silt- to boulder-sized, angular to rounded, very poorly to poorly sorted, very well- to well-indurated, ridgecapping, white, calcite-cemented conglomerate (up to about 6.1 m [20 ft] thick) which weathers buff to light brown. Imbrication directions of this conglomerate also difficult to determine; abundant clasts of generally flat, elliptical, very fossiliferous, bluish-gray, neritic limestone (Naco Limestone?); some zeolitized tuff clasts; extensive buildup of white mineral (calcite?) on fracture surfaces; white nodular concretions near base of unit; irregular contact with underlying units;

cut and fill structures present.

QT_{ls} - **LANDSLIDE DEPOSITS** - "Jumbled angular blocks of Escabrosa Limestone and some Martin Limestone have broken from ledges and slid a short distance down the dip slope of these formations (Cornwall and Krieger, 1978)."

T_{gv} - **VOLCANICLASTIC CONGLOMERATE** (0->150 m [492 ft]) - "Facies dominated by angular to subangular, pebble- to boulder-size clasts of Williamson Canyon Volcanics and Cretaceous and Tertiary intrusive rocks. Matrix is greenish-gray, sand size, and composed mainly of decomposed volcanic and intrusive rocks. Induration is poor to slight (Banks and Krieger, 1977)."

T_{gc} - **LIMESTONE-DOLOMITE CONGLOMERATE** (0-200 m [656 ft]) - "An alluvial conglomerate with predominant pebbles, cobbles, and boulders of gray limestone and dolomite; mostly Escabrosa Limestone, but partly Martin Limestone and Naco Limestone. Medium-light-gray, well cemented matrix of finer material consists of comminuted limestone, shale, sandstone, chert, and igneous material. This conglomerate occurs adjacent to the Paleozoic carbonate rocks from which it was largely derived and locally fills deep channels in these rocks (Cornwall and Krieger, 1978)." The unit weathers to large blocks. XRD indicates the matrix consists predominately of quartz and calcite with minor illite/smectite, kaolinite, and chlorite.

T_g - **CONGLOMERATE** (0->460 m [1509 ft]) - "Alluvial conglomerate and a little sand composed of subangular to subrounded clasts representing all pre-Miocene rocks in proportions and size that vary with proximity to and composition of the adjacent bedrock exposures. Matrix of silt- to small-pebble-size material (varying with composition of the adjacent bedrock) is well cemented, particularly near bedrock and is light-olive gray to light tans and browns. Poorly sorted and bedded near bedrock; moderately well sorted and bedded in transitional facies with lakebed facies (Banks and Krieger, 1977)." XRD indicates the matrix consists of abundant quartz, calcite, potassium feldspar, and albite, with lesser dolomite, gypsum, magnetite, pyrite, and clay minerals. "This conglomerate and the other Tertiary alluvial and lakebed deposits in DSV are similar to and tentatively correlated with the Big Dome Formation (Krieger and others, 1974) in the Gila River Valley southwest of the Dripping Springs Mountains; thus the age is probably middle to late Miocene (Cornwall and Krieger,

1978)."

T_{lu} - **LAKEBEDS UNDIFFERENTIATED** (0-unknown but at least 572 m [1875 ft]) - Lakebed facies; interbedded clay, silt, fine sand and limestone. The unit is informally divided into the lower, middle, and upper red claystones where the main zeolite tuff horizon (T_{mz}) and upper zeolite tuff horizon (T_{uz}) are exposed. "Near the center of the basin in sec. 35, T. 3 S., R. 15 E., are orangish-pink to light-brown claystone and siltstone with lenses and veins of gypsum, which outward toward the northeast and southwest margins of the basin, grade into gray beds containing progressively more silt, then progressively more sand, granules, and pebbles; beds of conglomeratic limestone (up to 1.5 m [4.9 ft]) are present and become increasigly abundant on the east side of the basin. A marginal transition zone between the lakebeds and alluvial conglomerates has been included in the map unit. Interbedded air-fall tuffs (<three m [9.8 ft]) are best exposed north of Dripping Springs Wash; alteration of the tuffs is variable; glass shards in one tuff have a refractive index slightly greater than 1.495, indicative of a rhyolitic parentage (Banks and Krieger, 1977)."

T_{uc} - **UPPER RED CLAYSTONE** (0-172 m [565 ft]) - Uppermost informal unit of lakebed facies which itself is divisible into three subunits: 1) a pale yellowish-brown (10 YR6/2) to pale- brown (5 YR6/2), silty to arenaceous claystone and very light-gray (N8), very fine-grained siltstone overlying, and in gradational contact with, 2) a pale reddish-brown (10 R5/4), pale yellowish-brown, very light-gray (N8), light grayish-gray (5 GY8/1), to white (N9) arenaceous claystone, sometimes carbonate-cemented; commonly with lenses (up to 1.2 m [4 ft] thick) of gravels which include reworked, altered zeolitic tuff, overlying and in sharp contact with, 3) a brown arenaceous claystone and very light-gray argillaceous sandstone. Unit as a whole weathers buff to reddish-brown with a "popcorn" surface coating several inches thick and locally with a nodular (elliptical nodules with long axis up to about 25 cm [10 in]), "exfoliating" pattern. Induration is poor; slope former; bedding not readily visible in outcrop; contains rootcasts; manganese oxide staining on fracture surfaces; trace detrital black mafic mineral (biotite, hornblende?), gold-colored mineral (pyrite, amphiboles?), red mineral (iron oxides?), and green mineral (chlorite?) grains are present. Presence of gypsum clusters and lenses (forming terrace-like outcrops) are indicative of saline

basin conditions. White authigenic minerals (calcite, gypsum, chabazite?) have grown along fractures and round, white authigenic mineral clusters are exposed on bedding surfaces. Clay mineral constituents include a predominance of illite and illite/smectite with lesser smectite, chlorite and kaolinite. The unit may be indistinguishable from the middle and lower red claystone units where it is not separated by ash-fall tuffs. The unit has a gradational contact with the upper zeolite tuff. The unit is locally coarser grained near the contacts with the tuff horizon, indicating sedimentation was active, and mixing occurred, upon deposition of the tuffs.

T_{bm} - **MEGABRECCIA, MARTIN LIMESTONE** - "Landslide breccia block 1-5 m(3.3-16.4 ft) thick, of Martin Limestone, overlies flat-lying alluvial conglomerate (T_{gc}) and older megabreccia (T_{bu}); extends south for 0.8 km (0.5 mi) from source on El Capitan Mountain. Breccia consists of angular fragments of limestone and dolomite with little matrix (Cornwall and Krieger, 1978)."

T_{bu} - **MEGABRECCIA UNDIVIDED** - "Landslide breccia block 5-12 m (16.4-39.4 ft) thick, of Escabrosa Limestone locally underlain by several meters of Martin Limestone, conformably interbedded in the upper part of the flat-lying Tertiary alluvial conglomerate (T_{gc}) and lakebeds (T_{uc}, T_{uz}, T_{mc}, T_{mz}, T_{lc}, T_{lu}). The breccia consists in part of closely fitting angular fragments with little matrix; elsewhere the breccia has angular to rounded limestone, dolomite, and minor shale fragments, partly rotated in a finely comminuted matrix of the same material. The flat-lying megabreccia, probably originally one huge slab but now dissected by washes, extends southwest from the source on El Capitan Mountain for 4 km (2.5 mi) toward DSV and is 1.6 km (0.99 mi) wide at its south end. Similar megabreccias are interbedded in Tertiary conglomerates in the Kearny quadrangle southwest of this area (Cornwall and Krieger, 1978)." XRD indicates the matrix material consists predominantly of quartz, calcite, dolomite, and minor illite/smectite, and albite(?).

T_{rt} - **RHYOLITIC TUFF** (up to 0.91 m [3 ft]) - "This rhyolitic tuff is exposed below a megabreccia (T_{bu}) in the northern end of the basin. It is a light- to medium-gray and brownish-gray, fine-grained, partly reworked and waterlaid ash with common to predominant fresh glass shards (refractive index 1.496; Cornwall and Krieger, 1978), rare dark lithic fragments, and minor to abundant quartz,

plagioclase, potassium feldspar, magnetite, biotite, and hornblende. The tuff is locally altered to chabazite (Cornwall and Krieger, 1978)." It also contains minor calcite, gypsum, and clay minerals. The unit consists of three lithologies: a lower, thin-bedded to platy bed up to 12.7 cm (5 in) thick, a middle massive bed up to 0.64 m (2.1 ft) thick, and an upper thin-bedded to platy bed up to 12.7 cm (5 in) thick. The tuff is horizontally bedded and contains some clay laminae. It has a sugary, vitroclastic texture. The unit is well indurated, weathers blockily in outcrop, and is a ledge-former.

$T_{af\ 1-7}$ - **ASH-FALL TUFFS ONE THROUGH SEVEN** - Seven thin (up to about 0.61 m [2 ft]) ash-fall tuffs interfinger with the upper red claystone (T_{uc}) in the northern portion of the valley. The tuffs are white to tan, fine-grained, glassy ashes with a vitroclastic texture. Most are moderately well indurated and weather blockily in large scale and concoidally or flakily in small scale. They are locally calcified near the basin margins. XRD indicates T_{af-1} and T_{af-2} are locally altered to chabazite. All seven tuffs contain quartz, calcite, plagioclase, and clay minerals. Some contain minor dolomite, halite, gypsum, potassium feldspar, magnetite, and pyrite.

T_{uz} - **UPPER ZEOLITE TUFF** - (up to 1.68 m [5.5 ft]) - Very pale-orange (10 YR8/2), gray orange pink (5 YR7/2), very light-gray (N8) to white (N9), very fine-grained, very well sorted, glassy, ash-fall tuff which includes an upper, thin-bedded to platy (about 12.7-20.3 cm thick) bed, a middle massive (about 17.8-26.7 cm thick) bed, and a lower, thin-bedded to platy bed with sharp contacts between them. Inhomogeneously altered to chabazite; contains irregular, nonzeolitic patches usually vitric or altered to clay minerals; calcified in some areas; tuffaceous, vitroclastic, sugary texture often with glass shards preserved; well indurated; weathers buff to white to gray, flakily in small scale, blockily in large scale, sometimes with concoidal or nodular ("exfoliating") pattern. Relict bedding/laminae, small-scale cross-beds, small folds, ripple marks (locally internal), soft sediment deformation, and burrow marks are infrequently present. Detrital mafic mineral grains (biotite, hornblend?), gold-colored (pyrite, amphiboles?) grains, red (iron oxides?) grains and patches of green (chlorite?) mineral grains are present. Illite, smectite, illite/smectite, chlorite, and kaolinite are present. A fibrous white mineral (chabazite, aragonite?) is exposed on

fracture surfaces. XRD indicates trace to abundant quartz, calcite, dolomite, gypsum, halite, potassium feldspar, and albite are present. Undulatory, gradational contact with middle red claystone.

T_{mc} - **MIDDLE RED CLAYSTONE** (up to 2.90 m [9.5 ft]) - Pale reddish-brown (10 R5/4), pale yellow brown (10 YR6/2), pink gray (5 YR8/1), to white (N9), very well- to well-sorted, silty to arenaceous claystone. Fresh samples are very hard, clumpy, and damp. Weathers reddish-brown to brown; "popcorn" textured; poorly indurated. Permeability is relatively high where fractured or popcorn-textured in weathered exposures, but low where fresh. Bedding not readily visible; tuffaceous near top and base of unit; silty in lower inch; faulted with manganese oxide-stained, slickensided surfaces; detrital mafic mineral (biotite, hornblende?) grains and white authigenic mineral (calcite, aragonite, dolomite, halite?) grains present in clusters or in veinlets. XRD also detects chabazite, clinoptilolite, quartz, gypsum, potassium feldspar, plagioclase, and pyrite. Illite, illite/smectite, smectite, chlorite, and kaolinite present; at least three lenses of gypsiferous claystone forming terrace-like outcrops are present, suggestive of a saline environment. Gradational contact with main zeolite tuff.

T_{mz} - **MAIN ZEOLITE TUFF** (up to 0.53 m [1.74 ft]) - Reddish-orange (10 R6/6), very pale-orange (10 YR8/2), pale yellow brown, pinkish-gray (5 YR8/1), very light-gray to white, dense, very fine-grained to fine-grained, ash-fall tuff. "The unit consists of three distinct lithologies, including a lower bed 0.05-0.27 m [0.15-0.87 ft] thick consisting of zeolitically altered ash and about 10% detrital matter. This bed is overlain by, and in sharp contact with, a bed 0.04-0.06 m [0.14-0.20 ft] thick, consisting of a laminated, thin-bedded, zeolitically altered ash containing a trace of detrital matter in addition to a trace of clay and calcite. Overlying this bed is a massive bed 0.09-0.20 m [0.30-0.67 ft] thick of zeolitically altered ash (Eyde, 1982)." Color intensity commonly increases with depth. Often fining grain size with depth; inhomogeneously altered primarily to chabazite; vitroclastic, sugary texture with glass shards commonly preserved; denser with more glass near base; ash contains laminae of siliceous material, white unidentified powdery material, calcareous material and detrital minerals; ripple marks exposed on laminae partings; soft sediment deformation and slickensided surfaces (faulted)

present. Weathers white to gray in nodular, concoidal fracture pattern. Brittle to very friable to friable upon chipping; hollow ring upon tapping with geologic pick; vertical fractures (some clay filled) throughout unit; small angular vugs irregularly positioned; drill core strongly to weakly broken; possible calcite layer near base in one drill hole; calcite-filled vugs and large blebs of calcite on uppermost surface in one hole; calcite also as thin surface coatings and thin stringers; calcareous root impressions; burrow marks; detrital fraction includes biotite, hornblende, zircon, magnetite, white to brown micaceous minerals, gold-colored mineral (pyrite?) grains, and red mineral (iron oxides?) grains. Manganese oxide staining on fracture surfaces, sometimes with dendritic pattern; trace of manganese oxide as liesegang banding. Yellow mineral (sulfur?) grains present. Authigenic clay (interstitial and dark blebs) present including illite, illite/smectite, smectite, chlorite, and kaolinite, sometimes coating desiccation polygons. Erratic, relatively sharp contact with lower red claystone.

T_{lc} - **LOWER RED CLAYSTONE** (thickness unknown, up to about 396 m [1300 ft] maximum) - Pale reddish-brown, pale yellow brown, very light-gray to white, very well-sorted, silty to arenaceous claystone with the same characteristics as the middle red claystone described above, except that it is locally interfingered with conglomeratic lenses with pebble- to boulder-size clasts. The lenses are up to 0.91 m [3 ft] thick and may indicate faulting along the major normal fault on the southwest side of the valley was active during lacustrine-fill time.

P_n - **LOWER PART OF NACO LIMESTONE** (Middle Pennsylvanian) - "Evenly spaced units of resistant limestone and less resistant shaly or silty limestone; each unit about 1.5 m (4.9 ft) thick. Thin beds of siltstone and shale are scattered through the formation and at the base is 1-3 m (3.3-9.8 ft) of siltstone and shale containing lenses and nodules of limestone and chert. Lenses and nodules of chert are locally prominant elsewhere in the formation, and a few interbeds of coarse-grained limestone were noted. Most of the limestone is aphanitic or fine-grained, thin to thick bedded, and light yellowish-gray. The siltstone beds are laminated, pale red to grayish-red and light-olive gray, weathering to the same colors and also to moderate reddish-orange. Fusulinids, brachiopods, corals, crinoids, bryozoans, and ostracods are present and locally abundant in certain beds

(Cornwall and Krieger, 1978)."

REFERENCES CITED

Aiken, C. L. V., 1978, Gravity and aeromagnetic anomalies of southeast Arizona: New Mexico Geological Society Guidebook, 29th Field Conference, Land of Cochise, p. 301-313.

Arizona Bureau of Mines, 1959, Geologic map of Cochise County, Arizona: Arizona Bureau of Mines, University of Arizona, Tucson, scale 1:375,000.

Arizona Department of Mineral Resources, 1978, Arizona zeolites: Mineral Report No. 1, State of Arizona Department of Mineral Resources, 40 p.

Austin, G. S., and Leininger, R. K., 1976, The effect of heat-treating sedimented mixed-layer illite-smectite as related to quantitative clay mineral determinations: Journal of Sedimentary Petrology, v. 46, p. 206-215.

Banks, N. G., and Krieger, M. H., 1977, Geologic map of the Hayden Quadrangle, Pinal and Gila Counties, Arizona: U.S. Geological Survey Geologic Quadrangle Map GQ-1391, scale 1:24,000.

Barker, J. M., 1983, Preliminary investigation of the origin of the Riley Travertine, Socorro County, New Mexico: New Mexico Geological Society Guidebook, 34th Field Conference, Socorro Region II, p. 269-276.

Bradley, W. H., 1928, Zeolite beds in the Green River Formation: Science, v. 67, p. 73-74.

Bromfield, C. S., and Shride, A. F., 1956, Mineral resources of the San Carlos Indian Reservation, Arizona: U.S.

Geological Survey Bulletin 1027-N, p. 613-689.

Carlisle, D., Merifield, P. M., Orme, A. R., Kohl, M. S., Kolker, O., and Lunt, O. R., 1978, The distribution of calcretes and gypcretes in southwestern United States and their uranium favorability based on deposits in Western Australia and Southwest Africa (Namibia): U.S. Department of Energy Open-file Report GJBX-29(78), 38 p.

Carroll, D., 1970, Clay minerals: a guide to their x-ray identification: U.S. Geological Survey Special Paper 126, 80 p.

Colella, C., Aiello, R., and Porcelli, C., 1978, Hydration as an early stage in the zeolitization of natural glass, in Sand, L. B., and Mumpton, F. A., eds., Natural zeolites: occurrence, properties, use: Oxford, Pergamon Press, p. 345-350.

Coombs, D. S., Ellis, A. D., Fyfe, W. S., and Taylor, A. M., 1959, The zeolite facies, with comments on the interpretation of hydrothermal syntheses: Geochim. et Cosmochim. Acta, v. 17, p. 53.

Cornwall, H. R., 1971, Geologic Map of the Sonora Quadrangle, Pinal and Gila Counties, Arizona: U.S. Geological Survey Geologic Quadrangle Map GQ-1021, scale 1:24,000.

Cornwall, H. R., and Krieger, M. H., 1975, Geologic map of the Kearney Quadrangle, Pinal County, Arizona: U.S. Geological Survey Geologic Quadrangle Map GQ-1188, scale 1:24,000.

_____, 1978, Geologic map of the El Capitan Mountain Quadrangle, Gila and Pinal Counties, Arizona: U.S. Geologic Map GQ-1442, scale 1:24,000.

Creasey, S. C., 1965, Geology of the San Manuel area, Pinal County, Arizona: U.S. Geological Survey Professional Paper 471, 64 p.

Cushman, R. L., and Jones, R. S., 1947, Geology and groundwater resources of the San Simon Basin, Cochise and Graham Counties, Arizona: U.S. Geological Survey Open-file Report, 31 p.

Damon, P. E., and Shafiqullah, M., 1973, Geochronology of block faulting and basin subsidence in Arizona: Geological Society of America Abstracts with Programs, v. 5, p. 590.

Dane, C. H., and Bachman, G. O., 1965, Geologic map of New Mexico: U.S. Geological Survey, scale 1:500,000.

Darton, N. H., 1925, Rèsumè of Arizona geology: Arizona Bureau of Mines Bulletin 119, 298 p.

Deer, W. A., Howie, R. A., and Zussman, J., 1966, An introduction to the rock-forming minerals: London, Longman Group, Ltd, p. 389-408.

Deffeyes, K. S., 1959, Zeolites in sedimentary rocks: Journal of Sedimentary Petrology, v. 29, p. 602-609.

Droste, J. B., 1961a, Clay minerals in the playa sediments of the Mojave Desert, California: California Division of Mines Special Report 69, 21 p.

_____, 1961b, Clay minerals in the sediments of Owens,

China, Searles, Panamint, Bristol, Cadiz, and Danby Lake basins, California: Geological Society of America Bulletin 72, p. 1713-1721.

Eaton, G. P., 1979, A plate-tectonic model for late Cenozoic crustal spreading in the western United States, in Riecker, R. E., ed., Rio Grande rift: tectonics and magmatism, American Geophysical Union, p. 7-32.

Edson, G. M., 1977, Some bedded zeolites, San Simon Basin, southeastern Arizona: unpublished M.S. thesis, University of Arizona, 65 p.

Eugster, H. P., 1970, Chemistry and origin of the brines of Lake Magadi, Kenya: Mineralogical Society of America Special Paper No. 3, p. 215-235.

Eyde, T. H., 1978, Bowie zeolite--an Arizona industrial mineral: Arizona Bureau of Geology and Mineral Technology, Field notes, v. 8, p. 1-5.

_____, 1982, Zeolite deposits in the Gila and San Simon Valleys of Arizona and New Mexico, in Austin, G. S., compiler, Industrial rocks and minerals of the Southwest: New Mexico Bureau of Mines and Mineral Resources, Circular 182, p. 65-71.

Geological Society of America, 1963, Rock Color Chart: New York, Geological Society of America.

Gibbs, R. J., 1965, Error due to segregation in quantitative clay mineral X-ray diffraction mounting techniques: American Mineralogist, v. 50, p. 741-751.

_____, 1968, Clay mineral mounting techniques for X-ray diffraction analysis: A discussion: Journal of Sedimen-

tary Petrology, v. 38, p. 242-243.

Hawley, J. W., Bachman, G. O., and Manley, K., 1976, Quaternary stratigraphy in the Basin and Range and Great Plains Provinces, New Mexico and western Texas, in Mahaney, W. C., ed., Quaternary stratigraphy of North America, Dowden, Hutchinson, and Ross, Inc., p. 235-274.

Hay, R. L., 1963, Stratigraphy and zeolitic diagenesis of the John Day Formation of Oregon: University of California Publ: Geol. Sci., v. 42, p. 199-262.

_____, 1966, Zeolites and zeolitic reactions in sedimentary rocks: Geological Society of America Special Paper 85, 130 p.

_____, 1977, Geology of zeolites in sedimentary rocks, in Mumpton, F. A., ed., Mineralogy and geology of natural zeolites: Mineralogical Society of America, v. 4, p. 53-64.

_____, 1978, Geologic occurrences of zeolites, in Sand, L. B., and Mumpton, F. A., eds., Natural zeolites: occurrence, properties, use: Oxford, Pergamon Press, p. 135-143.

Heindl, L. A., 1954, Cenozoic alluvial deposits in the upper Gila River drainage basin, Arizona and New Mexico: Geological Society of America Bulletin, v. 65, p. 1262.

_____, 1958, Cenozoic alluvial deposits of the upper Gila River area, New Mexico and Arizona: unpublished Ph.D. thesis, University of Arizona, 249 p.

Hollander, J. T., 1960, Geology and aquifer characteristics of the inner-valley alluvium in the Safford Valley, Arizona: Arizona Geological Society Digest, v. 3, p. 133-135.

Hunt, C. B., 1978, Surficial geology of southwest New Mexico: New Mexico Bureau of Mines and Mineral Resources, Geologic Map 42, scale 1:500,000.

Janders, D. J., 1978, Comparative sedimentology, stratigraphy, and economic potential of two Tertiary lacustrine deposits in Arizona: unpublished M.S. thesis, Arizona State University, 140 p.

Johns, W. D., Grim, R. E., and Bradley, W. F., 1954, Quantitative estimations of clay minerals by diffraction methods: Journal of Sedimentary Petrology, v. 24, p. 242-251.

Jones, B. F., and Weir, A. H., 1983, Clay minerals of Lake Abert, an alkaline, saline lake: Clays and Clay Minerals, v. 31, p. 161-172.

Keller, W. D., 1970, Environmental aspects of clay minerals: Journal of Sedimentary Petrology, v. 40, p. 788-813.

Knechtel, M. M., 1938, Geology and ground-water resources of the Valley of Gila River and San Simon Creek, Graham County, Arizona: U.S. Geological Survey Water-Supply Paper 796-F, p. 181-222.

Kossovskaya, A. G., 1975, Genetic types of zeolites in stratified rocks: Lithology and Mineral Resources, v. 10, p. 23-44.

Krieger, M. H., 1979, Zeolitization of Tertiary tuffs in

lacustrine and alluvial deposits in the Ray-San Manuel area, Pinal and Gila Counties, Arizona: U.S. Geological Survey Professional Paper 1124-D, p. D1-D11.

Krieger, M. H., Cornwall, H. R., and Banks, N. G., 1974, The Big Dome Formation and revised Tertiary stratigraphy in the Ray-San Manuel area, Arizona: U.S. Geological Survey Bulletin 1394-A, p. A54-A62.

Lance, J. F., 1960, Stratigraphic and structural position of Cenozoic fossil localities in Arizona: Arizona Geological Society Digest, v. 3, p. 155-159.

Long, A., 1966, Late Pleistocene and Recent chronologies of playa lakes in Arizona and New Mexico, unpublished Ph.D. thesis, University of Arizona, 141 p.

Lowe, O., 1875, Report upon mineralogical, agricultural, and chemical conditions observed in portions of Colorado, New Mexico, and Arizona, in 1873, in Wheeler, G. M., U.S. Geographical and Geological Exploration W. 100th Mer. Report: pt. 6, v. 3, p. 569-661.

Mariner, R. H., and Surdam, R. C., 1970, Alkalinity and formation of zeolites in saline-alkaline lakes: Science, V. 170, p. 977-979.

Martin, P. S., and Mehringer, P. J., 1965, Pleistocene pollen analysis and biogeography of the Southwest, in Wright, H. E., and Frey, D. G., eds., The Quaternary of the United States: Princeton University Press, p. 433-451.

Melton, M. A., 1960, Origin of the drainage of southeastern

Arizona: Arizona Geological Society Digest, v. 3, p. 113-122.

_____, 1965, The geomorphic and paleoclimatic significance of alluvial deposits in southern Arizona: Journal of Geology, v. 73, p. 1-38.

Mumpton, F. A., 1973, Scanning electron microscopy and the origin of sedimentary zeolites, in Uytterhoever, J. B., ed., Molecular Sieves: Proc. 3rd. Int. Conf. Molecular Sieves, Leuven University Press, p. 56-61.

_____, 1975, Commercial utilization of natural zeolites, in Lefond, S. J., ed., Industrial minerals and rocks: New York, American Institute of Mining and Metallurgical Engineers, p. 1262-1283.

_____, 1977, Natural zeolites, in Mumpton, F. A., ed., Mineralogy and geology of natural zeolites: Mineralogical Society of America, v. 4, p. 1-16.

Mumpton, F. A., and Ormsby, W. C., 1978, Morphology of zeolites in sedimentary rocks by scanning electron microscopy, in Sand, L. B., and Mumpton, F. A., eds., Natural zeolites: occurrence, properties, use: Oxford, Pergamon Press, p. 113-132.

Munson, R. A., and Sheppard, R. A., 1974, Natural zeolites: their properties, occurrences, and uses: Mineral Science Engineering, v. 6, p. 19-34.

Nations, J. D., 1974, Paleontology, biostratigraphy, and paleoecology of the Verde Formation of late Cenozoic age, north-central Arizona, in Geology of northern Arizona, part 2: a field guide published to accompany

Geological Society of America Rocky Mountain Section Meeting, Flagstaff, Arizona, p. 611-629.

Nations, J. D., Landye, J. J., and Hevly, R. H., 1982, Location and chronology of Tertiary sedimentary deposits in Arizona: American Association of Petroleum Geologists Bulletin, v. 66, p. 1696.

Olander, P. A., 1979, Authigenic mineral reactions in tuffaceous sedimentary rocks, Buckhorn, New Mexico: unpublished M.S. thesis, University of Wyoming, 82 p.

Olson, R., 1975, Introduction, in Lefond, S. J., ed., Industrial minerals and rocks: New York, American Institute of Mining and Metallurgical Engineers, p. 1235-1242.

Papke, K. G., 1969, Montmorillonite deposits in Nevada: Clays and Clay Minerals, v. 17, p. 211-222.

Peirce, W. H., 1967, Geologic guidebook 2--Highways of Arizona: Arizona Highways 77 and 177: Arizona Bureau of Mines Bulletin 176, 73 p.

Picard, M. D., 1957, Green River and lower Uinta Formations--subsurface stratigraphic changes in central and eastern Uinta Basin, Utah, in Seal, O. G., ed., Guidebook to the geology of the Uinta Basin: Intermountain Association of Petroleum Geologists, p. 116-130.

Picard, M. D., and High, L. R., 1972, Criteria for recognizing lacustrine rocks, in Rigby, J. K., and Hamblin, W. K., eds., Society of Economic Paleontologists and Mineralogists, Special Publication No. 16, p. 108-145.

Pye, W. D., 1959, Marine sedimentation in southern Arizona,

in Heindl, L. A., ed., Southern Arizona guidebook II, Arizona Geological Society: Tucson, p. 5-9.

Ratterman, N. G., and Surdam, R. C., 1981, Zeolite mineral reactions in a tuff in the Laney Member of the Green River Formation, Wyoming: Clays and Clay Minerals, v. 29, p. 365-377.

Ross, C. P., 1928, Sedimentary analcite: American Mineralogist, v. 13, p. 195-197.

Royse, C. F., Sheridan, M. F., and Peirce, H. W., 1971, Geologic guidebook 4--Highways of Arizona, Arizona Highways 87, 88, and 188: Arizona Bureau of Mines Bulletin 184, University of Arizona, Tucson, 66 p.

Sand, L. B. and Regis, A. J., 1967, Mineral distribution in size fractions of Tertiary zeolite ores: Society of Mining Engineers, Preprint number 67-H-317, 14 p.

Scarborough, R. B., 1975, Chemistry and age of late Cenozoic air-fall ashes in southeastern Airzona: unpublished M.S. thesis, University of Arizona, 107 p.

Scarborough, R. B., and Peirce, H. W., 1978, Late Cenozoic basins of Arizona: New Mexico Geological Society Guidebook, 29th Field Conference, Land of Cochise, p. 253-259.

Schreiber, J. F., 1978, Geology of the Willcox playa, Cochise County, Arizona: New Mexico Geological Society Guidebook, 29th Field Conference, Land of Cochise, p. 277-282.

Schwenneson, A. T., 1917, Ground water in San Simon Valley, Arizona and New Mexico: U.S. Geological Survey Water-

Supply Paper 425, p. 1-35.

Seff, P., 1960, Preliminary report of the stratigraphy of the 111 Ranch beds, Graham County, Arizona: Arizona Geological Society Digest, v. 3, p. 137-140.

Shafiqullah, M., Damon, P. E., Lynch, D. J., Kuck, P. H., and Rehrig, W. A., 1978, Mid-Tertiary magmatism in southeastern Arizona: New Mexico Geological Society Guidebook, 29th Field Conference, Land of Cochise, p. 231-241.

Sheppard, R. A., 1971, Clinoptilolite of possible economic value in sedimentary deposits of the conterminous United States: U.S. Geological Survey Bulletin 1332-B, p. B1-B15.

_____, 1973, Zeolites in sedimentary rocks: U.S. Geological Survey Professional Paper 820, p. 689-695.

_____, 1975, Zeolites in sedimentary rocks, in Lefond, S. J., ed., Industrial minerals and rocks: New York, American Institute of Mining and Metallurgical Engineers, p. 1257-1270.

Sheppard, R. A., and Gude, A. J., 3rd, 1964, Reconnaissance of zeolite deposits in tuffaceous rocks of the western Mojave Desert and vicinity, California: U.S. Geological Survey Professional Paper 501-C, p. C114-C116.

_____, 1965, Zeolitic authigenesis of tuffs in the Ricardo Formation, Kern County, southern California: U.S. Geological Survey Professional Paper 525-D, p. D44-D47.

_____, 1968, Distribution and genesis of authigenic silicate

minerals in tuffs of Pleistocene Lake Tecopa, Inyo County, California: U.S. Geological Survey Professional Paper 597, 38 p.

_____, 1969, Diagenesis of tuffs in the Barstow Formation Mud Hills, San Bernardino County, California: U.S. Geological Survey Professional Paper 634, 35 p.

_____, 1973, Zeolites and associated authigenic silicate minerals in tuffaceous rocks of the Big Sandy Formation, Mojave County, Arizona: U.S. Geological Survey Professional Paper 830, 36 p.

_____, 1975, abs., Occurrence, properties, and utilization of chabazite from sedimentary deposits in the United States, in Bailey, S. W., ed., Proc. of the Intl. Clay Conference: Mexico City, Applied Publishing Ltd., p. 565.

_____, 1982, Mineralogy, chemistry, gas adsorption, and NH_4^+--exchange capacity for selected zeolite tuffs from the western United States: U.S. Geological Survey Open-file Report 82-969, 16 p.

Sheppard, R. A., Gude, A. J., 3rd, and Edson, G. M., 1978, Bowie zeolite deposit, Cochise and Graham Counties, Arizona, in Sand, L. B., and Mumpton, F. A., eds., Natural zeolites: occurrence, properties, use: Oxford, Pergamon Press, p. 319-328.

Sheppard, R. A., and Mumpton, F. A., 1984, Sedimentary fluorite in a lacustrine zeolitic tuff of the Gila Conglomerate near Buckhorn, Grant County, New Mexico: Journal of Sedimentary Petrology, v. 54, p. 853-860.

Smith, G. I., 1966, Geology of Searles Lake--a guide to prospecting for buried continental salines, in Rau, J. L., ed., Second Symposium on Salt: Northern Ohio Geological Society, v. 1, p. 167-180.

Srodon, J., 1984, X-ray powder diffraction identification of illitic materials: Clays and Clay Minerals, v. 32, p. 337-349.

Starkey, H. C., and Blackmon, P. D., 1979, Clay mineralogy of Pleistocene Lake Tecopa, Inyo County, California: U.S. Geological Survey Professional Paper 1061, 34 p.

Suneson, N. H., and Lucchitta, I., 1983, Origin of bimodal volcanism, southern Basin and Range province, west-central Arizona: Geological Society of America Bulletin, v. 94, p. 1005-1019.

Surdam, R. C., 1977, Zeolites in closed hydrologic systems, in Mumpton, F. A., ed., Mineralogy and geology of natural zeolites: Mineralogical Society of America, v. 4, p. 65-91.

Surdam, R. C., and Eugster, H. P., 1976, Mineral reactions in the sedimentary deposits of the Lake Magadi region, Kenya: Geological Society of America Bulletin, v. 87, p. 1739-1752.

Surdam, R. C., and Sheppard, R. A., 1978, Zeolites in saline, alkaline-lake deposits, in Sand, L. B., and Mumpton, F. A., eds., Natural zeolites: occurrence, properties, use: Oxford, Pergamon Press, p. 145-172.

Tank, R. W., 1969, Clay mineral composition of the Tipton

Shale Member of the Green River Formation (Eocene) of Wyoming: Journal of Sedimentary Petrology, v. 39, p. 1593-1595.

Van Houten, F. B., 1964, Tertiary geology of the Beaver Rim area, Fremont and Natrona Counties, Wyoming: U.S. Geological Survey Bulletin 1164, 99 p.

_____, 1965, Composition of Triassic Lockatong and associated formations of Newark group, central New Jersey and adjacent Pennsylvania: American Journal of Science, v. 263, p. 825-863.

Willden, R., 1964, Geology of the Christmas Quadrangle, Gila and Pinal Counties, Arizona: U.S. Geological Survey Bulletin 1161-E, p. E1-E64.

Wilson, E. D., and Moore, R. T., 1958, Geologic map of Graham and Greenlee Counties, Arizona: Arizona Bureau of Mines, University of Arizona, Tucson, scale 1:375,000.

_____, 1959, Geologic map of Pinal County, Arizona: Arizona Bureau of Mines, University of Arizona, Tucson, scale 1:375,000.

Wilson, E. D., and Moore, R. T., and Cooper, J. R., 1969, Geologic map of Arizona: U.S. Geological Survey Special Geologic Map, scale 1:500,000.

Wilson, E. D., Moore, R. T., and Peirce, H. W., 1959, Geologic map of Gila County, Arizona : Arizona Bureau of Mines, University of Arizona, Tucson, scale 1:375,000.

Wilson, M. D., and Pittman, E. D., 1977, Authigenic clays in sandstones: Recognition and influence on reservoir

properties and paleoenvironmental analysis: Journal of Sedimentary Petrology, v. 47, p. 3-31.

This thesis is accepted on behalf of the faculty of the Institute by the following committee:

Advisor

May 22, 1985
Date